Computer Simulation of Muscle Series Elastic Element Function in Drop Jumping

DISSERTATION

Zur Erlangung des Grades eines Doktors
der Naturwissenschaften
der Fakultät für Physik
der Eberhard-Karls-Universität zu Tübingen

vorgelegt von
HARALD BÖHM
aus Hildesheim

2002

Tag der mündlichen Prüfung:	21. Januar 2002
Dekan:	Prof. Dr. G. J. Wagner
1. Berichterstatter:	Prof. Dr. G. P. Brüggemann/ Prof. Dr. H. Ruder
2. Berichterstatter:	Prof. Ph.D. Dr. D. Wharam

Acknowledgements

I want to express my gratitude to Professor Ruder for giving me the possibility to graduate in his Institute and for his support whenever it was needed. I would like to thank Professor Brueggemann and his co-workers at the German Sport University Cologne to accept me as a college. I would like to thank Professor. Nigg for giving me the possibility to visit his laboratory and the researchers at the HPL especially Dr. Cole leading me the right way in my research activities. I would like to thank Professor Herzog and Dr. Ait Haddou for the stimulating discussions about muscle mechanics. I thank Dr. Arampatzis for telling me all the secrets about drop jumping and letting me use his experimental data for model validation. The ultrasound measurements were only possible with the help of Gaspar Morey and Gianpiero De Monte. Special thanks to Gaspar Morey, Birgit Laube, Dr. Kersting and Dr. Walsh for the review of the manuscript. Finally I like to thank all my friends coming with me to experience Biomechanics in real life during running, snowboarding and mountainbiking.

Dedication

To my parents
Gudrun and Herbert Böhm

Abstract

The contribution of muscle in-series compliance on the power generation of the muscle tendon complex was investigated with a forward dynamic computer simulation. The model of the human body contains eight Hill-type muscles of the lower extremities. The force distribution problem among the redundant muscle groups was solved for the simulated drop jumps by optimization of the resultant jump height. It is shown that the muscle series elastic energy stored in the downward phase provides a significant contribution of 29 % to the muscle energy in the push-off phase. Further by the return of the stored elastic energy all muscles contractile elements can reduce their shortening velocity during push-off to develop a higher force thanks to their force velocity properties. The additional stretch taken up by the series element allows only m. rectus femoris to work closer to its optimal length due to its force length properties. The function of the SEE in the muscle power generation in drop jumping is beside the storage and return of energy the support of the force producing ability of the contractile elements.

Contents

Chapter 1

Introduction

When a rubber ball bounces its initial kinetic energy is stored as elastic strain energy and is converted back to kinetic energy in the rebound.
A person jumping down from a chair can decide whether to land on the ground or to jump up again. The latter movement is called a drop jump. In drop jumping some of the bodies initial energy is stored as elastic strain energy in the muscles and is recovered during the elastic recoil. The rest of the jumping energy has to be produced through metabolic work.

Many sportive movements involve muscle actions in which the shortening of the muscle (concentric phase) is immediately preceeded by a muscle stretch (eccentric phase), ie. running, throwing and vertical jumping. These muscle actions are called stretch-shortening cycles (SSC). The question whether elastic strain energy stored in the eccentric phase can enhance the work output in the concentric phase was a discussion topic in a whole issue from the Journal of Applied Biomechanics [64]. This shows the importance of the question of elastic energy in movement performance and basic muscle research.

It is well known that tendon and tendinous tissue of the muscles have elastic properties which have been determined in different experiments [79], [63], [25], [40], [29], [51]. From experiments on isolated frog muscles it is known that shortening of muscle fibers is influenced by the muscle elasticity [43]. However, its exact role in different movements of daily life is still unclear. Besides the enhancement of the work output in muscle stretch shortening cycle, other possible functions of elastic tissue could be the prevention of injury, metabolic efficiency and stability of movement control. This study focuses on the performance of the muscles during drop jumping.

Measuring the elastic energy storage in human muscles during sportive movements is difficult, nowadays the only noninvasive method is ultrasonography [45]. In vivo fiber recording with ultrasound is limited to slow movements due to the low recording frequency and scanner fixation problems.
A basic understanding of elastic function in fast movement such as drop jumping can be obtained with the help of computer simulation. The elastic behavior of all muscles implemented as well as mechanical parameters during the movement can be obtained.
Bobbert et al. [8] were one of the first who quantified elastic energy storage during jumping with the help of computer simulation. Bobbert estimated for a vertical jump starting in a squatting position, that the elastic structures of the ankle plantarflexors provide 40 % of the total energy delivered by these muscles. For the same jumping condition Anderson and Pandy [2] calculated the contribution of elastic energy to be 35 % of the muscle concentric energy for all eight muscles included in the model. The similarity in the results of the two simulation studies seems to indicate that there is a considerable amount of energy stored which contributes to the muscle performance at take-off. It is not only the amount of energy stored which is recovered at take-off, the muscle elasticity and the reused energy can also influence the force producing ability of the muscle fibers. The effect of tendon on muscle force in dynamic isometric contractions was simulated by van Soest et al. [73]. They found out that tendon removal has an influence on maximum fiber shortening velocity. However these simulations were validated with animal experiments on single muscles. The effect of muscle elasticity on the fiber performance in real life human movement has not yet been investigated.
The acceptance of such simulation results is only as good as the determination of the input parameters and the agreement with the measured kinetics and kinematics. Therefore a database for the subjects as well as measurements of the movement must be available and agree with the simulation results.
For model validation there is a database of drop jumps under different conditions such as varying drop height and contact time available measured by Arampatzis et al. [3]. Further there is access to some of the 15 subjects participating in this study to determine additional parameters needed for the simulation. Another reason for investigating the function of muscle elasticity in drop jumping is that the muscles carry out an intense stretch-shortening cycle and should give considerably high values for the elastic energy stored. Looking at the take-off velocities in drop jumping measured by Arampatzis et al. the athletes reach the same height in the rebound independent of their dropping height (fig. 1.1). The higher potential energy at greater drop heights could possibly be stored in the elastic elements of the muscles but could not be reused to obtain a greater jump height such as the bouncing

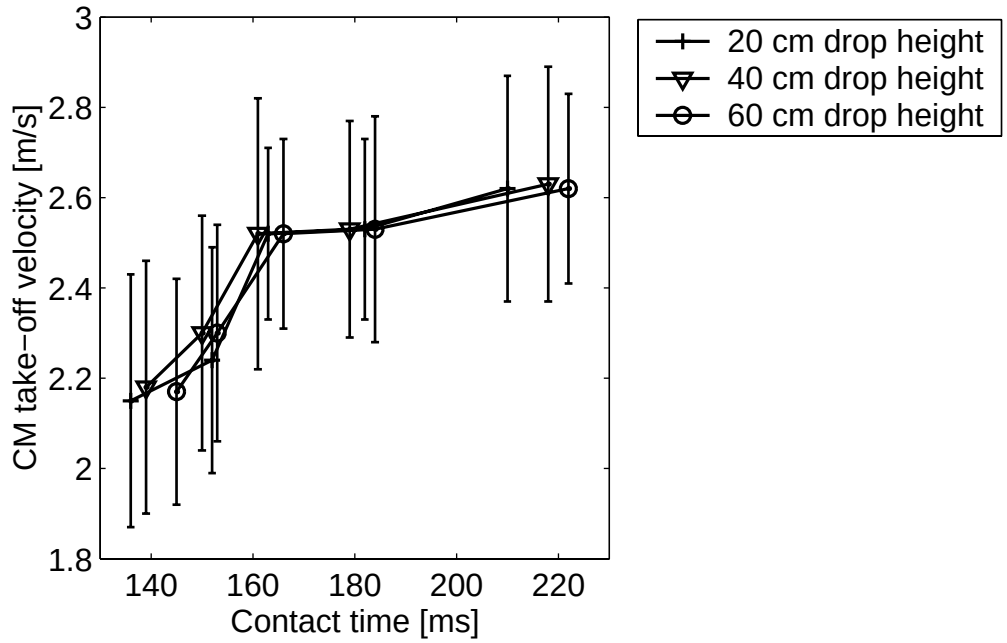

Figure 1.1: *Experimentally determined vertical take-off velocities in drop jumping. The drop height as well as the ground contact time is varied. The data points are averaged values from 15 subjects participating in the study of Arampatzis et al. [3].*

ball which reaches almost the same height from which it was dropped. A valid simulation model should show the same behavior.

To give a more precise formulation of the jumping performance enhancement caused by muscle elastic energy, the muscle tendon unit can be described according to Hill [38] with a passive series elastic component associated with the tendon and aponeurosis and an active contractile element associated with the muscle fibers. The muscle fibers are the only force generating elements in the muscle. The following three statements describe how the muscle elasticity might alter the performance of the contractile element and lead to three hypotheses which will be proven with the help of computer simulation.

A. V. Hill [39] : 'The stored mechanical energy can be used in producing a final velocity greater than that at which the contractile component itself can shorten'.

W. Herzog [24] : 'Tendons and aponeuroses influence the variable contractile

element length and speed, and therefore its force producing ability'.

K. Roeleveld [60] : 'The tendon acts like a stiff force transducer without significantly modifying the muscles performance'.

From the last statement the question arises whether there is any considerable amount of strain energy stored. The statements from Herzog and Hill are describing the effect of series elasticity on the velocity and the length of the contractile element. From the three statements the following hypotheses on the effect of series elasticity can be formulated:

1. A considerable amount of energy can be stored in the muscles series elastic elements.

2. The contractile elements can reduce their shortening velocity to develop a higher force.

3. The contractile elements can work closer to their optimal length.

The purpose of this study is to develop a computer simulation model to first calculate the amount of energy stored in the series elastic element of the muscles in drop jumping (hypothesis 1)and second to show how this stored elastic energy influences the force producing ability of the muscle contractile element (hypotheses 2 and 3).

The study consists of five different steps each associated with a chapter. In chapter two the human body is modeled as an assembly of rigid bodies. In chapter three the muscle model is formulated and the muscle series elasticity used as model input is determined by ultrasonography. Chapter four validates the model, comparing the simulated drop jumps to those measured in the study of Arampatzis et al. [3]. At last step in chapter five the elastic energy stored in the muscles is calculated and the effect of series elasticity on the force producing ability of the contractile elements is investigated.

Chapter 2

Rigid body model

The human body is modeled with an assembly of rigid bodies. The bodies and their constraints as well as the forces acting on the bodies will be described in the following sections.

2.1 Model components

The model should contain enough rigid bodies to provide insight into the force production of the muscles in the lower extremities during drop jumping. The main muscles working against gravity in the movement of interest, are pulling around the hip, knee and ankle joint. The exact modeling of the upper body is not of interest, since drop jumps are a test exercise to quantify jumping performance and the hands are fixed to the hip in the studies carried out by Arampatzis [3]. A model with four segments: trunk with head and arms, thigh, shank and foot linked together with hinge joints (fig. 2.1) is used.

The movement is supposed to be symmetric so that a two dimensional model with half the upper body mass and one leg is modeled. This can be done due to the linearity of the mass in the rigid body equations of motion.
Given the total body mass, the standing height and the sex of a person the segment masses, moments of inertia and geometric dimensions are calculated based on regression equations from a NASA database [53]. The values taken correspond to the average persons participating in the drop jump study carried out by Arampatzis et al. [3]. Modeled is a male subject with body weight and standing height of 78 kg and 183 cm respectively.

In reality the human body is not composed of a set of linked rigid bodies. Each segment represents a composition of a rigid skeletal part and soft components such as skin, muscles, ligaments, organs, fat and other soft tissues. Gruber et al. [32] showed that these structures have a fundamental effect on the impact phase during landing from a vertical jump. The skeletal parts are highly accelerated whereas the soft parts of the body continue to fall during the impact phase. Their function can be simulated using additional wobbling masses.
In the study of Gruber et al. a direct simulation was carried out with a linked four segment model. The net joint moments around the ankle and knee joints were given as time curves. The calculated ground reaction force in the first 20 ms was of much larger magnitude and shape when no wobbling mass was used.
In the simulated drop jumps in this study the net joint moments are not available as constant time curves, they were calculated for a given muscle activation. The muscle forces depend on the activation as well as on the kinematics and the forces applied to the model. Using a rigid body model without wobbling masses, the viscoelastic properties of the muscles would compensate for the wobbling masses. The calculations of the muscle elastic energy would lead to different results. Therefore wobbling masses were included in the model.
The wobbling masses are implemented using an additional rigid body coupled with a nonlinear force to three of the four linked segments of the model. The wobbling masses of the upper body and the upper and the lower leg are shown on the right side in fig. 2.1. The distribution of segment mass to the skeletal part and the wobbling part of the body is done as follows: The bony parts are modeled as a cylinder with the segment length from the NASA database [53] and an assumed radius. The cylinder was filled with a homogenous mass with the density for bone of 1.2 g/cm^3. The mass, inertia and center of mass (CM) of the cylinders are calculated. Together with the wobbling mass the cylindrical bone must have the properties of the overall segment mass obtained from the NASA database. From that condition, mass, inertia and location of the CM for the wobbling mass can be calculated. The masses and inertias used for the model are shown in tab. 2.1, the location of the CM in fig. 2.1.

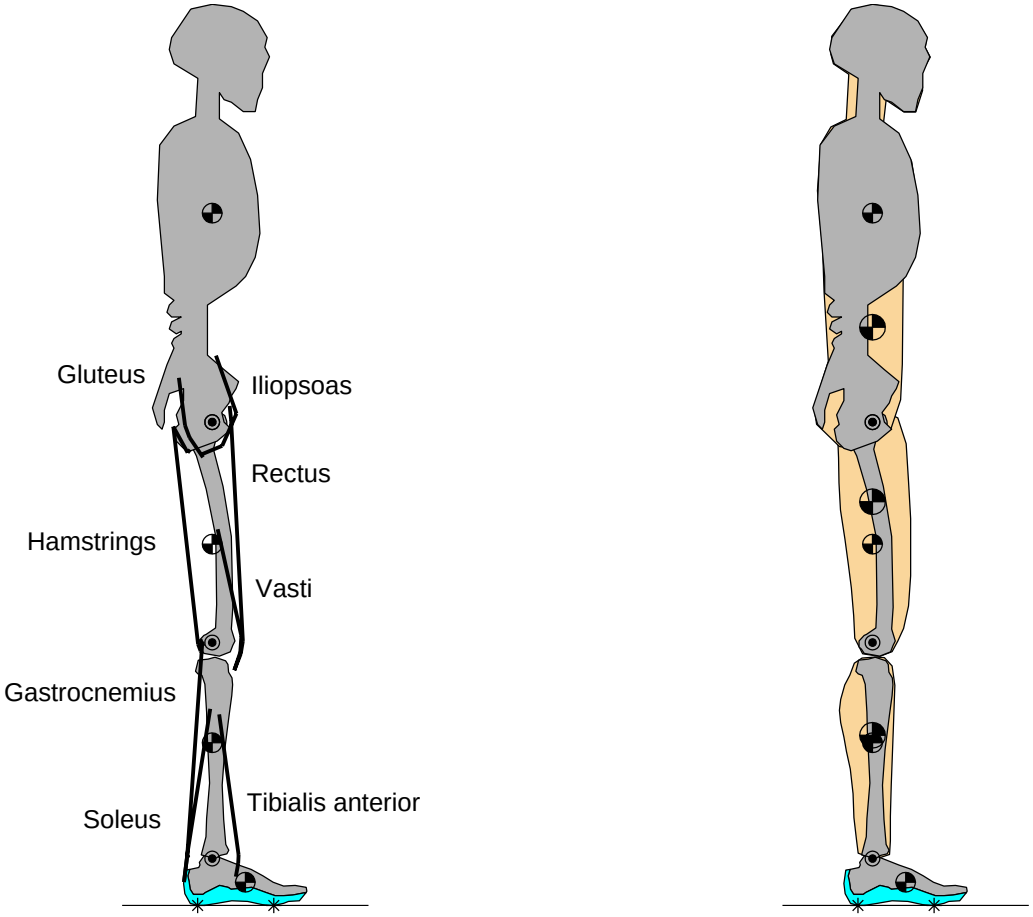

Figure 2.1: *Schematic representation of the musculoskeletal model used to simulate maximum-height drop jumping. The human skeleton on the left side was modeled with a planar four-segment system linked at the hip, ankle and knee with frictionless revolute joints. A total of eight muscle groups transmit forces to the skeleton. The right side shows the skeleton plus the wobbling masses. The stars under the foot show the locations of the ground contact points on the foot.*

2.2 Forces acting on the rigid bodies

In a planar system consisting of rigid bodies each body originally has three degrees of freedom. The four rigid bodies representing the bony parts are constrained by three joints, the three wobbling masses keep their three degrees of freedom. This system of rigid bodies with their inertias, masses and joint locations was implemented in a software package (DADS, LMS

Table 2.1: *Model segment masses and inertias. The segment masses sum up to half of the overall body mass of 78 kg.*

Segments	Bony parts		Wobbling parts	
	mass $[kg]$	inertia $[kg\,m^2]$	mass $[kg]$	inertia $[kg\,m^2]$
Upper body	9.4	0.567	17.0	0.547
Upper leg	2.1	0.042	6.0	0.092
Lower leg	1.2	0.014	2.3	0.030
Foot	1.0	0.004		

international) which automatically generates the equations of motion in a gravitational field. In the case of a human model there is the ground reaction force, the muscle force, the wobbling mass coupling forces and the joint limiting forces which must be implemented by the user via user defined fortran subroutines. In the direct dynamic simulation, at each integration step the subroutines are called and these user defined forces are added up to the equations of motion. A description of these forces can be found in the following sections.

2.2.1 Wobbling mass coupling forces

The coupling forces and moments Qw_{ji} acting between the rigid parts and the wobbling masses are

$$Qw_{ji} = A_j\,(c_i\,\Delta q_i^{bi} + d_i\,\Delta q_i\,\Delta\dot{q}_i). \tag{2.1}$$

A_j is the area of the wobbling mass attached to body j. Δq_i are the relative distance transversal (Δq_1), longitudinal (Δq_2) and the angle (Δq_3) between wobbling mass and skeleton inertial system. The nonlinearity is a result of the nonlinear force deformation curve from tendinous tissue which is mainly responsible for the coupling between skeleton and wobbling mass. The coupling parameters in tab. 2.2 are used in this study. These parameters were chosen such that the maximum relative elongation and rotation is less than two centimeters and three degrees respectively. Further the damping coefficients were varied until the wobbling mass was not oscillating more than two times after touch-down. An additional torque was added to the rigid

$$Tcorr_j = \Delta q_1\,Qw_{j2} - \Delta q_2\,Qw_{j1} \tag{2.2}$$

Table 2.2: *Wobbling mass coupling parameters. The values for b, c and d are normalized to overall body mass used in the simulation. The coefficients A_j are taken from Gruber [32] and are scaled with the respective segment length and mass to the model dimensions.*

Parameter	Value	Units
$b_{1,2}$	3.0	
$c_{1,2}$	$1.6\ 10^8$	$kg/m^4s^2 bodymass$
$d_{1,2}$	$1.0\ 10^5$	$kg/m^3s\ bodymass$
b_3	2.0	
c_3	$1.2\ 10^4$	$kg/s^2rad^2 bodymass$
d_3	$1.0\ 10^3$	$kg/s\ rad^2 bodymass$
A_1 (upper body)	$5.6\ 10^{-2}$	m^2
A_2 (upper leg)	$4.1\ 10^{-2}$	m^2
A_3 (lower leg)	$2.3\ 10^{-2}$	m^2

bodies on which the wobbling mass is attached, to correct the violation of the angular momentum. This violation is caused by the nonlinearity of the coupling forces which do not act on the same line of action and therefore generate an additional angular momentum on the rigid bodies.

2.2.2 Contact forces

The contact between the foot and the ground is modeled by two independent contact elements, one at the heel and the other under the forefoot (fig. 2.1). Each element represents the mechanical properties of the foot, the sole of the shoe and the ground. In the measured drop jumps of Arampatzis et al. [3] the athletes were jumping with sport shoes on force platform built out of steel, so that all the deformation is taken up by the foot and the shoe. A mathematical description of a viscoelastic force vertical and horizontal with respect to the ground is formulated in the equations

$$Fc_{ix} = -Arel_i(c\,\Delta x \mid \Delta x \mid -d \mid \Delta x \mid \dot{x}), \tag{2.3}$$

$$Fc_{iy} = max(Arel_i\,(c\,\Delta y^2 + d\,\Delta y\,\dot{y}), 0). \tag{2.4}$$

The vertical force Fc_y depends on the penetration Δy and the penetration velocity $\dot{y}$ of the contact point i with the surface. In the vertical direction the force is always positive because no sticking to the ground is allowed. The horizontal force is defined for a non sliding foot and depends on Δx and $\dot{x}$.

Δx is defined as the difference between the first horizontal contact point with the ground and the respective contact point on the foot. Arel, c and d are parameters which are obtained simulating an experiment from Aerts et al. [1]. In the study of Aerts et al. impact tests using a pendulum were carried out on the shod heel region of 9 subjects. To get the parameters for the

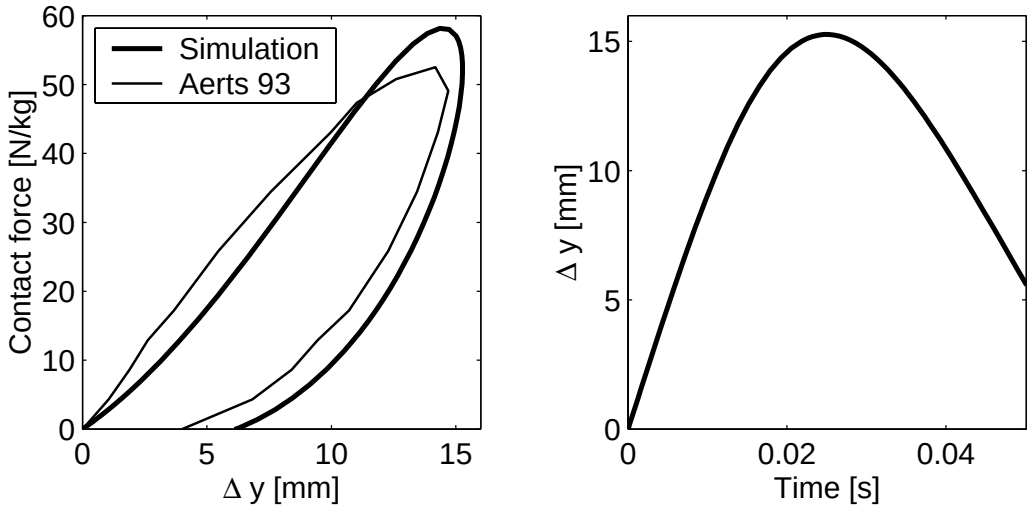

Figure 2.2: *Simulated pendulum experiment, force-penetration (Δy) and penetration-time curve. In the experiment carried out by Aerts et al. [1] maximum penetration was reached at 22.4 ms, on the right plot the simulated penetration of the pendulum shows maximum peak at the same time.*

contact forces the force deformation curve of a pendulum impacting on a soft shoe was simulated and compared to the data measured by Aerts et al.. The equation of motion formulated for the vertical contact force Fc_y acting on a pendulum ($11.615kg$) is integrated. The initial conditions are: $y(0) = 0m$ and $\dot{y} = 0.96\, m/sec$. The integrator ode113 (Matlab 6.0, Mathworks) was used to solve the equations of motion. Keeping $Arel = 1$ the parameters c and d were varied by trial and error to match the experimental curve determined. The velocity term in eq. 2.4 determines the energy loss of the pendulum as well as the time at which maximum pendulum penetration in the shoe is reached. In the study of Aerts et al. the time in which maximum force is reached is 22.4 ms. The best result obtained by trial and error is shown in fig. 2.2. Applying the pendulum experiment to the drop jump impact of the shod foot with the ground, *Arel* is the contact area of the foot with the ground relative to the area of the pendulum. The parameters found for the vertical contact force were also taken for the horizontal force. All parameters used for the contact forces are shown in tab. 2.3.

Table 2.3: *Ground contact parameters.*

Parameter	Value
c	$2.6\ 10^6\ kg\,m/s^2$
d	$3.0\ 10^4\ kg\,m/s$
$Arel_1$ (forefoot)	2.65
$Arel_2$ (rearfoot)	1.29

2.2.3 Muscle forces

In chapter 3 it will be shown that the forces along the muscle line of action $Fm(act, V_{MTU}, L_{MTU})$ can be calculated dependent on the activation, velocity and length of the muscle-tendon-unit. This muscle force described along the line of action of the muscle has to be transformed into the generalized coordinates of the rigid bodies of the model on which they are attached to. The generalized force components along the generalized coordinates q_{ik} of body k are

$$Qm_{ik} = Fm\frac{\partial L_{MTU}}{\partial q_{ik}}. \tag{2.5}$$

The coefficients of the Jakobi matrix $\partial L_{MTU}/\partial q_{ik}$ for the transformation 2.5 are determined numerically. The muscle length $L_{MTU}(\boldsymbol{\varphi})$ can be measured from tendon travel and is obtained from the various literature sources summarized in tab. 2.4. The muscle length $L_{MTU}(\boldsymbol{\varphi})$ depends on the vector of three joint angles:

$$L_{MTU}(\boldsymbol{\varphi}) = \sum_{i=1}^{3}(a2_i\ \varphi_i^2 + a1_i\ \varphi_i) + L_{MTU}(\mathbf{0}) \tag{2.6}$$

The parameters $a1$ and $a2$ describing the change in length of the muscles, $a1$ and $a2$ vary with the joint i and the muscle considered. $L_{MTU}(\mathbf{0})$ is the muscle length at zero joint angle.
To calculate the partial derivatives of the Jakobi matrix, $\boldsymbol{\varphi}$ can be calculated from the four generalized body angles $\boldsymbol{q}_{3k}$, $k\epsilon\{1, 2, 3, 4\}$.

The muscle length for varying joint angles obtained from different subjects in the literature are scaled to the respective segment length of the model. The length at zero joint angle is subtracted and the parameters $a1$ and $a2$ fitted with a second order polynomial. The length at zero joint angle $L_{MTU}(\mathbf{0})$ together with the change in length given by parameters $a1$ and $a2$ determines the absolute muscle length and so the length of the series elastic element.

Table 2.4: *Literature sources for muscle length changes with varying joint angles.*

Muscle	Ankle	Knee	Hip
Soleus	[61]		
Gastrocnemius	[61]	[75]	
Tibialis anterior	[61]		
Vasti		[75]	
Rectus femoris		[75]	[75]
Hamstrings		[75]	[68]
Iliopsoas			estimated
Gluteus			[54]

Table 2.5: *Input parameters for scaling muscle origin and insertion points according to Brand et al. [27].*

Input parameter	Length [cm]
Femoral epicondyle width	9.3
Tibial plateau width	8.6
Distance from lateral malleolus to tibial tubercle	38.5
Perpendicular distance from tibia long axis to tibial tubercle	4.5

Therefore $L_{MTU}(\mathbf{0})$ is important for the amount of energy stored in the muscle. To better match the model segment dimensions, $L_{MTU}(\mathbf{0})$ is not directly taken from the literature, it is calculated as the cable length wrapping around a pulley with the radius of the moment arm from the muscle origin to the insertion point. These points were given by Brand [27] based on anatomical landmarks and segment lengths. The segment lengths were derived from the NASA database. The landmarks were taken on one representative male subject (183 cm 78 kg) and are listed in tab. 2.5.

The coefficients of the Jakobi determinant $\partial L_{MTU}/\partial q_{ik}$ can be denoted as the moment arm of the muscle with respect to the rigid body k. They give an idea on how effective muscle force is transferred to the skeleton. The muscle length and moment arms used in this study are plotted in fig. 2.3.

It has to be noted that the muscle is treated as massless, this can be done because in drop jumping, each single muscle mass is a lot smaller than the total body weight which is accelerated.

Table 2.6: *Joint range angles in flexion and extension, zero joint angle is defined in an upright standing position shown in fig. 2.1.*

Joint	Maximum flexion [deg]	Maximum extension [deg]
Ankle	50	-30
Knee	140	0
Hip	-110	5

2.2.4 Joint range limiting forces

The human joints have a limited range of motion. In the simulated maximum height drop jump (chapter 5), the movement generated by the muscles does not exceed the joint range. In the simulation the muscle forces are not known from the beginning, they are obtained by optimization. Therefore the simulated joint angles could exceed their range of motion during the optimization process when the jump height is not maximal. The muscle lengths are defined for a limited joint range, calculations of muscle length out of this defined joint range may lead to a change of the sign of the moment arm. To avoid this problem a torque Tl_j on the two adjacent rigid bodies in the joint j will be applied when it exceeds its range of motion

$$Tl_j = 400\ \Delta\varphi_j^2 + 40\ \Delta\varphi_j\ \dot{\varphi}_j. \tag{2.7}$$

$\Delta\varphi_j$ is the angle exceeding the range of joint j relative to the maximal or minimal joint angle given in tab. 2.6.

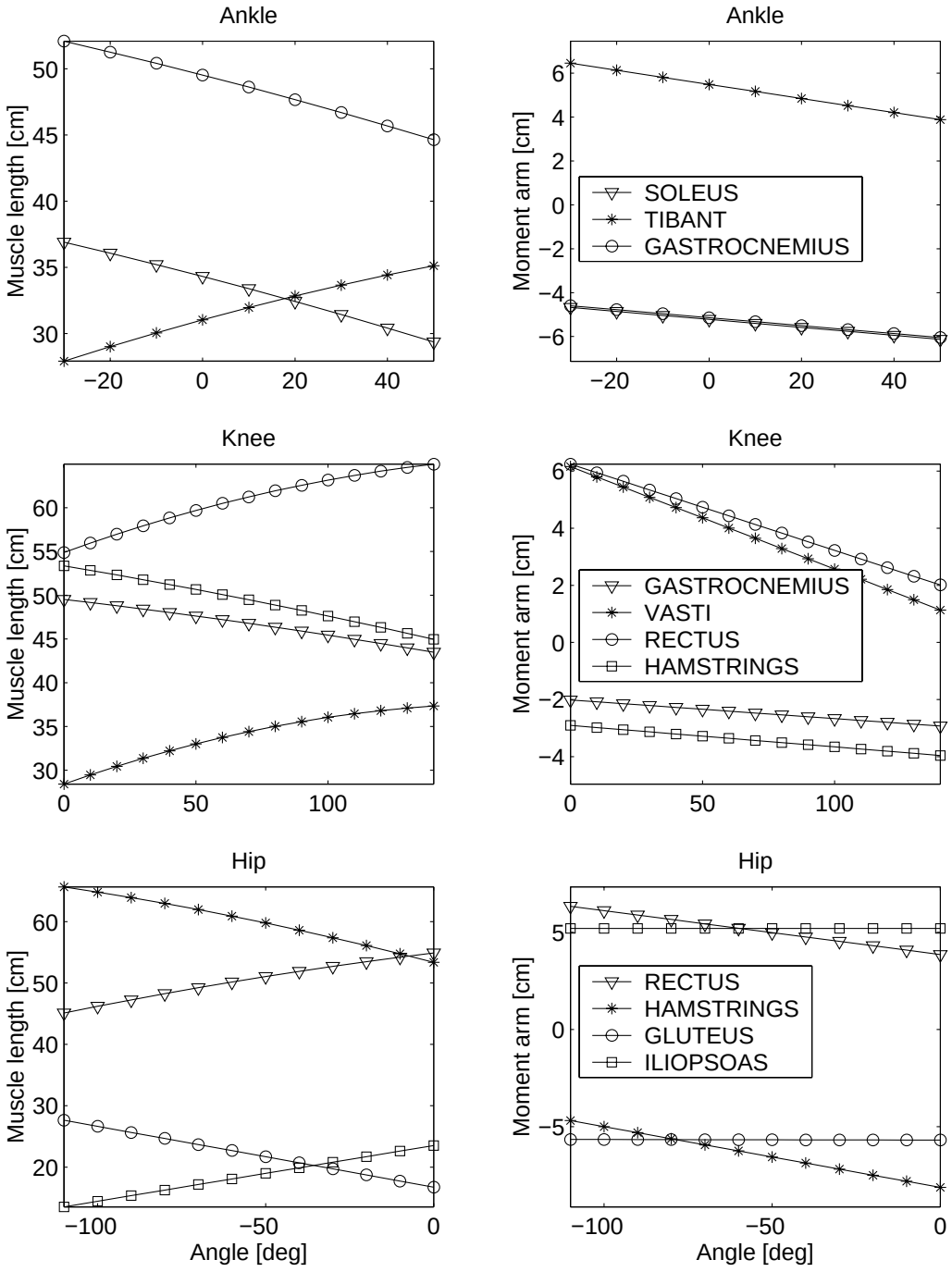

Figure 2.3: *Muscle-tendon length and moment arms versus joint angle. For joint angle definition see tab. 2.6. Differences between the graphs and the literature values can be caused by variation in parameters a1 and L0 varied in the optimization process to obtain the resultant joint torques described in chapter 3.2.1. The sign of the moment arm shows the direction of the torque generated by the muscle.*

Chapter 3

Muscle model

In this chapter an introduction to the muscle structure and force generation is given and a mechanical equivalent, the Hill muscle model is presented. The Hill muscle model consists of various elements whose properties are formulated, so that the muscle force can be calculated in the simulation. The mathematical formulation of the muscle elements is similar to those from van Soest [73]. In addition the force enhancement due to stretch and the activation dependence of the force-velocity relation are also modeled. The parameters for the various elements except the maximal joint-torques and the series elastic strain were taken from the literature. The series elastic strain is essential for the determination of elastic energy storage and was therefore measured with ultrasonography.
In the activation section 3.5 the optimal control problem of the muscles to perform a maximal height drop jump is solved defining an active state function for each muscle. The last part of this chapter connects all muscle properties and gives an outline how muscle force is calculated in the simulation program.

3.1 Introduction to muscle mechanics

In the human body there are muscles of different types depending on the function they fulfill. In this context only skeletal muscles are considered. Skeletal muscles are connecting two bones and can be controlled voluntarily. The primary function of skeletal muscle is to produce force to accelerate body segments.
A lot of different sizes and shapes of skeletal muscles exist depending on their function. In general two basic shapes of muscles can be pointed out:

parallel-fibred and pennate-fibred. In the parallel case the contracting fibers are aligned with the line of action of the muscle. In the pennated case the fibers are tilted at a distinct angle against it. This **angle of pennation** is defined as the angle of the muscle fibers relative to the muscle line of action as shown in the ultrasound image of m. gastrocnemius (fig. 3.1).

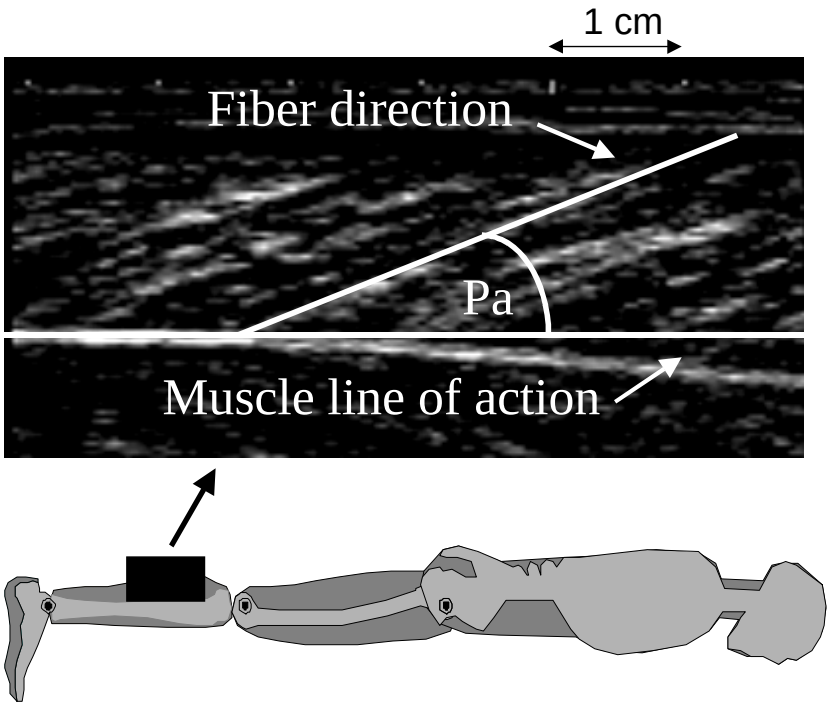

Figure 3.1: *Ultrasound picture of m. gastrocnemius taken from dorsal in the sagittal plane. The angle of pennation (Pa) is 26 degrees with the muscle line of action.*

The length of the muscle-tendon unit L_{MTU} is defined as the whole muscle length from origin to insertion. When the muscle generates force, three different situations depending on the muscle-tendon unit velocity V_{MTU} are defined. In **isometric contractions** V_{MTU} or movements of segments is zero. In **concentric contractions** the muscle is shortened and V_{MTU} is negative. In **eccentric contractions** the muscle is lengthened and V_{MTU} is positive. In the literature the sign of the velocity is reversed so that the shortening of the muscle has a positive velocity. In muscle modeling the muscle length gets smaller while shortening. The length change subtracted from the initial muscle length, therefore for concentric contraction in this study the muscle velocity is defined as negative.

The maximal isometric force a muscle can generate, depends on the number, size and orientation of its fibers. Muscles fibers with an angle of pennation are not pulling along the muscle line of action. The muscle force is then the projection of the fiber direction on the line of action.

$$F_m = F_{fibers}\, cos(Pa) \tag{3.1}$$

This is however a simplification, eq. 3.1 underestimates the actual force for two reasons: first, not all fibers belonging to the same muscle have the same angle of pennation. This can be demonstrated in fig. 3.3 in which the fibers located at the muscle belly have an angle of pennation of 26 degrees and the fibers closer to the tendon insertion are almost horizontally aligned. Second, force transmission perpendicular to the fiber line of action might be possible [41].
As a measure of maximal isometric muscle force the **physiological cross-sectional area (PCSA)** is used. The PCSA is defined as the muscle volume divided by its optimal fiber length. According to that definition keeping the muscle volume constant, muscles with long optimal fiber length have a smaller isometric force. The isometric force is typically calculated from the known PCSA using a proportional factor of $k = 20 - 40N/cm^2$ [24].

$$F_{max} = k\, PCSA \tag{3.2}$$

The formula 3.2 can be explained with a geometrical model shown in fig. 3.2. The ratio in the maximal isometric force of the two muscles with the same

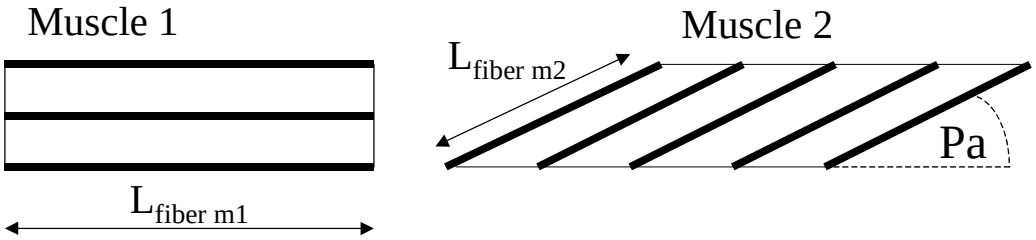

Figure 3.2: *Two muscles having the same volume but different angles of pennation.*

volume and the same force along each fiber is calculated using eq. 3.2 which yields

$$\frac{F_{m1}}{F_{m2}} = \frac{k\, PCSA_{m1}}{k\, PCSA_{m2}} = \frac{Vol./L_{fiberm1}}{Vol./L_{fiberm2}} = 0.65. \tag{3.3}$$

Determining this ratio with geometrical considerations, muscle one having three fibers parallel aligned and muscle two having five fibers tilted with an angle of 30 degrees result in

$$\frac{F_{m1}}{F_{m2}} = \frac{3\,F_{fiber}}{5\,F_{fiber}\,\cos(Pa)} = 0.69. \tag{3.4}$$

The ratio of the muscle forces determined is about the same so that the use of eq. 3.2 to calculate the muscle force is acceptable. Muscle one, with the parallel aligned fibers, has a 0.65 times lower maximal isometric force. This can be explained due to a higher angle of pennation of muscle two. More fibers are aligned in parallel in the same volume. Each fiber is generating the same force so that although the force component along the line of action is calculated with eq. 3.1, muscle two is stronger.
Another effect of the angle of pennation is that for muscles with greater pennation angle a given change in muscle fiber length translates to less muscle shortening along the line of action. This discrepancy can be partly compensated by an increase in angle of pennation during the muscle contraction shown in chapter 3.4.1.

In the previously described, geometrically simplified representation of a muscle, the fibers are described as straight lines, so that analytical expressions for their contractile behavior can be derived. In these geometric models the force-producing-element (the fibers) will be called **contractile element (CE)**. The passive elastic elements which require no metabolic energy, may be in series or parallel to the CE. The in **series elastic elements (SEE)** represent the tendons and aponeuroses of the muscle (fig. 3.3).
For the purpose of this study the modeling of the muscle structure in microscopic detail is not required. A phenomenological model is used to calculate the muscle force when muscle length, velocity and active state are given as input. This model consists of various arrangements of elements, each element can be seen as a 'black box' with a mathematical function describing its mechanical behavior.
Such a muscle model was first presented by A. V. Hill in 1938 [38] to interpret his experimental results. This classic two element model consists of an undamped purely elastic element in series with a contractile element described by the characteristic equation 3.6. The model qualitatively explained several of the mechanical phenomena exhibited by muscle including the rise of isometric tension and the redevelopment of tension after quick release. Adding an extra elastic **element in parallel (PEE)** to the contractile element shown in fig. 3.3, this model has been proven to be very useful in

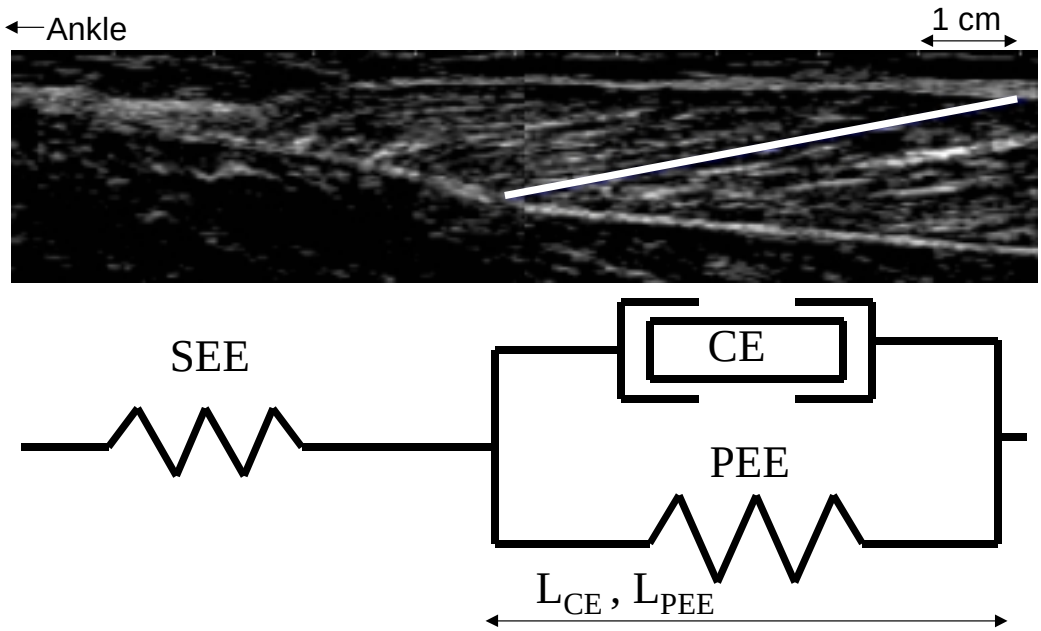

Figure 3.3: *Ultrasound picture of m. gastrocnemius. One fiber bundle marked in white is associated with the force producing CE. This fiber bundle is attached to the aponeurosis, the white structure surrounding the muscle fibers. When the fiber is shortening it pulls at the aponeurosis which transfers the force via the achilles tendon (left side of the picture) to the bones of the foot.*

biomechanics [58], [73], [30], and will be used in this study. In the following sections the mathematical formulations for the CE, PEE and SEE are given.

3.2 Contractile element properties

3.2.1 Force-length properties

The force-length property of a muscle is defined by the maximum isometric force a muscle can exert as a function of its length. When performing isometric maximal knee extensions at different joint angles the maximum measured torque is on average reached at about 60 degrees (fig. 3.5). Each joint angle is associated with a certain muscle length. Even knowing this muscle length and the elasticity of the SEE, the CE force-length properties can still not be determined. It remains to quantify the force sharing between all muscles acting around one joint. For this reason it is difficult to measure the torque-angle properties for intact human muscles. Under the assumption that one and two joint muscles generate their force independent of each other, Herzog et al. determined the torque-angle curve for the two joint muscles m. rectus femoris and m. gastrocnemius at the knee and ankle joint respectively [36], [37]. The authors varied one of the two joint angles so that the length of the two joint muscle changed, while keeping the length of the one joint muscle constant and so the force of the one joint muscle was fixed. These measurements as well as measurements done on isolated animal muscles [35] and fibers [70] show an inverse parabolar force-length curve.

In the model the CE length (L_{CE}) is defined as the projection of the fiber length on the line of action of the muscle (fig. 3.3), it is not the length of the fiber itself. With this definition the length change due to a change in the angle of pennation is included in the CE length change. This simplification is done because we are interested in the behavior of the SEE attached to both endpoints of the fascicle not in the behavior of the fascicles itself.
According to van Soest [73] the active force length relation in isometric contraction is approximated with the parabola

$$F_{len} = c\,(\frac{L_{CE}}{L_{CEopt}})^2 - 2c\,(\frac{L_{CE}}{L_{CEopt}}) + c + 1. \tag{3.5}$$

The factor c is defined as $c = -1/width^2$, the parameter $width$ is the maximum range of the active force in the CE with respect to optimum length (L_{CEopt}) (fig. 3.4). The force-length curve of the muscles generating the same joint movement results in the isometric torque-angle relation. Given the muscle parameters $width$ of the force-length curve, optimal length of the CE (L_{CEopt}), SEE slack-length ($L_{SEEslack}$), the maximum isometric force (F_{max}), the maximal isometric strain of the SEE and the muscle length change

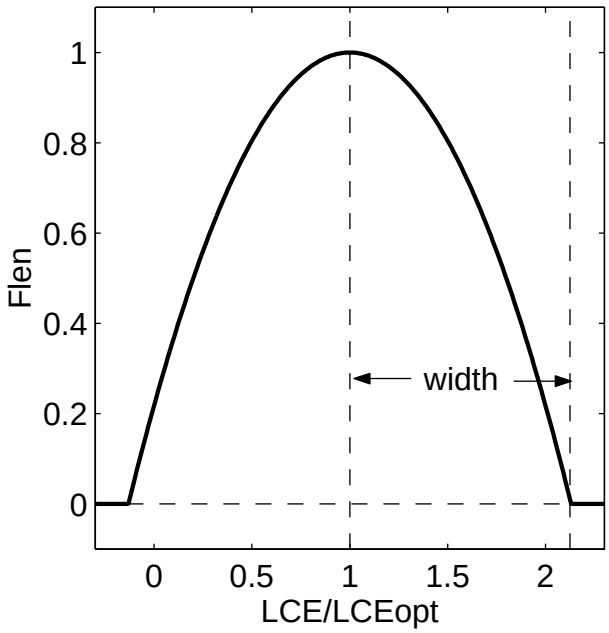

Figure 3.4: *CE force-length curve for m. gastrocnemius described by eq. 3.5.*

with varying joint angles, the resultant joint torque for each maximally activated muscle can be calculated for different joint angles (fig. 3.11). Adding all muscle torques around the same joint the resultant joint torque can be calculated. To test the validity of their musculoskeletal model other authors [58], [21], [7], [30] compare their calculated isometric joint torques with experimental joint torques reported in the literature. Several parameters in the model can be fitted to get a good agreement.
The question arises why it is necessary to compare simulation models used in dynamic situations with static measurements. The reason for it is that the defined parameters in the Hill model are based on the isometric force-length properties of the muscles. The parameter *width* of the force-length curve can not be determined in dynamical situations where the stimulation and velocity are changing over time.
Three main problems that appear when the calculated joint torques are fitted to the measured joint torques from the literature.

1. Joint torques taken from the literature are measured from different research groups using different methods on a number of different populations.

2. A whole group of muscles usually generates the torque around one joint

so we have to solve the force distribution problem among these muscles.

3. The decision must be made which parameter in the model should be optimized to match the experimentally determined resultant joint torques

The first problem is solved best by measuring the resultant joint torque with one method, for a group of comparable subjects used in the simulation study. In this study the maximal isometric force at the ankle, knee and hip joint in the optimal position were measured on four athletes who participated in the drop jump study from Arampatzis et al. [3]. The values measured with (Multi-joint system 3, Biodex, NY) were considerably higher than most of those found in the literature [65], [55], [76] [62], [72], [46]. An exception was the measured isometric plantar flexions by Bobbert et al. [10]. The joint torques measured in their study, also on trained athletes was about $230\,Nm$ which is close to the average of $248\,Nm$ obtained from the four athletes measured in this study. The whole torque-angle relation was not experimentally determined, the torque-angle curves from the literature were normalized on the maximal isometric force and multiplied with the mean maximal isometric force measured on the four athletes. For optimization purposes the data points of the isometric torques were interpolated so that for each joint 10 data points were given in the measured angle range (fig. 3.5 and 3.6).

The force distribution problem among many muscles acting around the same joint, is solved by neglecting the co-contraction and grouping the muscles into one and two joint muscles. For example m. soleus in the model includes the function of all single ankle joint plantar flexors. This reduces the distribution problem on two muscles, m. soleus acting only around the ankle joint and m. gastrocnemius around the ankle and knee joint. The force sharing between those two muscles were according to the ratio of their PCSA.

The procedure of changing muscle parameters to get an agreement with the experimental measured isometric joint torques has been investigated by Bobbert et al. [7]. The sensitivity of the output depends mostly on the parameter $L_{SEEslack}$ followed by the linear coefficient of the moment arm $a1$, F_{max} and L_{CEopt}. The parameter $width$ of the force length curve was not investigated. The parameters optimized in this study are $a1$, L_{CEopt}, $PCSA$, $L_{SEEslack}$, $width$. The parameters $a1$, L_{CEopt}, $PCSA$ are varied within their standard deviation found in the literature. The parameters $width$ and $L_{SEEslack}$ are not taken from the literature. $L_{SEEslack}$ is calculated with a pulley model (chapter 2.2.3) whose standard deviation can not be estimated, the variation is set to 10 %. An initial guess for the parameter $width$ can be found in [30],

it is allowed to vary within 20 % to better match the shape of the resultant joint torques.
The parameters were optimized by minimizing the sum of squared errors using (Matlab 6.0, Mathworks). The best curves for ankle knee and hip joint were shown in fig. 3.5 and fig. 3.6. For the hip joint no flexion data was found, therefore only hip extension was optimized. In the cases two joint muscles were involved and resultant joint torque data was also available for another configuration of the neighboring joint, the parameters were optimized to agree best with both configurations.

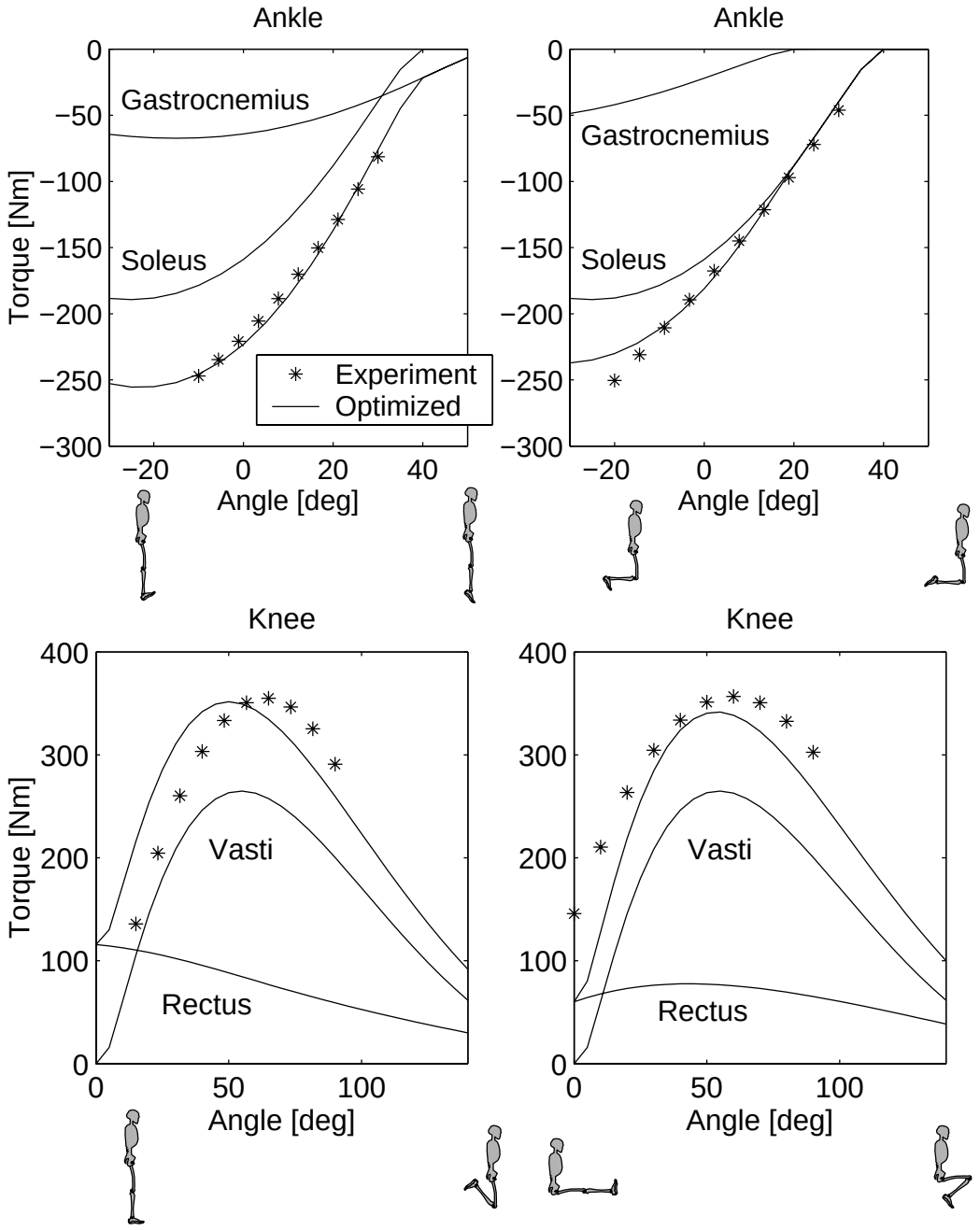

Figure 3.5: *Comparison between measured and optimized ankle plantar flexion and knee extension torque-angle curves. Experimental values for the ankle joint were taken from Sale et al. [62], for the knee joint from Eijden et al. [72] and Lindahl et al. [46]. The experimental data are modified with the method described in the text. The joint angle range is drawn within its limits used in the model. The skeletons below the graph show the joint configuration for minimum and maximum plantar flexion and knee extension.*

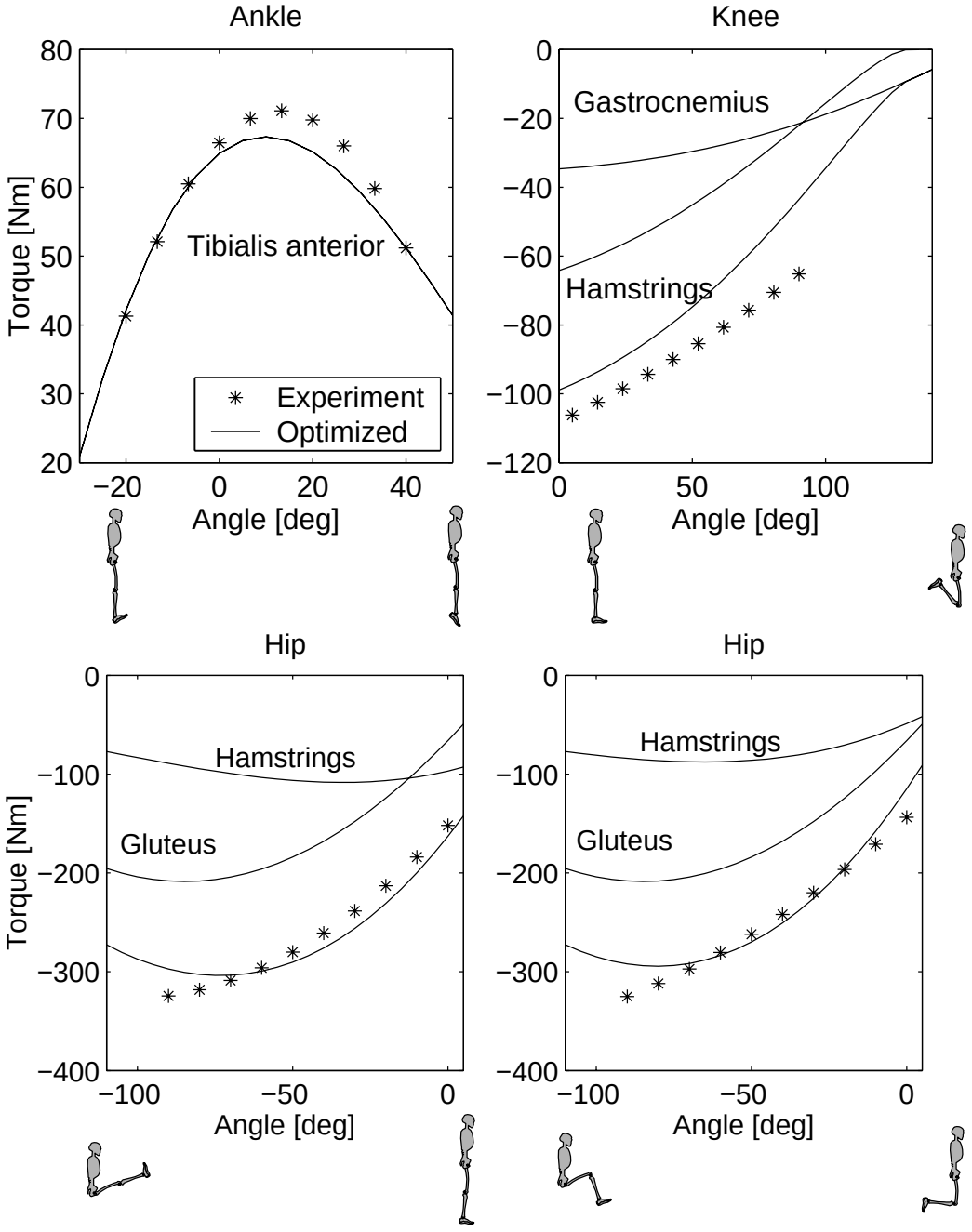

Figure 3.6: *Ankle dorsal flexion, knee flexion and hip extension torque-angle curves. Experimental values were taken from Gerritsen [30] for the ankle, from Smidt [65] for the knee and from Nemeth et al. [55] and Waters et al. [76] for the hip joint.*

3.2.2 Force-velocity properties

When pulling a rubber band apart with maximal effort, the pulling velocity that can be achieved decreases when the stiffness of the rubber band increases. This fundamental property of muscle is known as the force-velocity property. For a given muscle or muscle group and a constant level of activation, the maximal velocity of shortening that can be achieved decreases for contractions against greater resistance. The hyperbolic equation

$$F_{vel} = \frac{F_{max}\, b + a\, V_{CE}}{V_{CE} + b}, \tag{3.6}$$

that appropriately describes the general shape of the force-velocity properties for concentric contractions is known as the Hill equation. This function has the asymptotes $\lim_{F_{vel}\to\infty} = -b$ and $\lim_{V_{CE}\to\infty} = -a$. At zero CE velocity ($V_{CE}$) the force is equal the maximal isometric force F_{max} of the muscle measured. The parameters a and b must be chosen so that the function fits experimental data. Ideally measurements of the CE force-velocity properties should be made at a specified muscle fiber length and activation, while the muscle velocity is constant. In the literature values of $\frac{a}{F_{max}}$ and V_{max} instead of b can be found. By setting F_{vel} in eq. 3.6 equal to 0, V_{max} can be obtained by the following equation

$$V_{max} = b\,\frac{F_{max}}{a}. \tag{3.7}$$

The maximum velocity V_{max} often exceeds the capabilities of the measuring device [69], [26], [71]. Therefore V_{max} is not measured directly, it is extrapolated determining a and b at lower velocities.
Actual values for the parameters in the Hill equation are affected by various physiological conditions, such as angle of pennation, fiber length and fiber type composition.
An important, but not well understood aspect of the force velocity properties deals with the circumstance when the load imposed on the muscle exceeds the maximum isometric force that the muscle is capable of generating. Under this circumstance the muscle is stretched while activated. This is called eccentric contraction. There is no standard equation such as the hyperbolic Hill equation (3.6) to describe the force-velocity properties in eccentric contraction. Qualitatively it can be said that when the muscle is forcibly stretched with a given velocity, the muscle generates a braking force, which becomes greater at greater stretch velocities, up to a limit velocity, beyond which no further increase in resisting force is observed. The absolute value of this limit velocity

is lower than the maximal velocity of shortening [42], [47]. The asymptotic value of the force reached is 1.8 and 2 times F_{max} according to [42] and [47] respectively. There appears to be a discontinuity force-velocity curve across the isometric point. The rise in force in slow stretching is six times larger [42] than the fall in force associated with the corresponding velocity of shortening. In the muscle model the Hill equation 3.6 formulated for concentric contraction is extended to eccentric contraction using another parameter set. The parameters used for eccentric and for concentric contraction are given further on.

Concentric contraction

The relationship between force and velocity for concentric contraction is given by the Hill equation 3.6. In the literature various values can be found for the parameters a and b describing the Hill equation, but only in the study of Chow et al. [15] values of a and b were measured with variation of the activation level. The values were fitted with the parabolas

$$a(act) = -0.0089(act - 94.2)^2 + 59.3 \tag{3.8}$$

$$b(act) = -0.0147(act - 70.3)^2 + 72.0. \tag{3.9}$$

The active state (act) is given in % ($0 \leq act \leq 100$). The force can be calculated knowing a and b with

$$F_{vel} = \frac{act\, b(act) - a(act)\, V_{CE}}{V_{CE} + b(act)} \frac{1}{100}. \tag{3.10}$$

V_{CE} : CE velocity in % of V_{max}, $V_{CE} \leq 0$.
V_{max} : Maximum CE velocity when $act = 100\%$.
F_{vel} : CE force at optimal length normalized to F_{max}.

The eq. 3.10 is used to control the model with the help of an active state function (act(t)), it is plotted for varying activation levels in fig. 3.7.

The eq. 3.10 describes the concentric velocity normalized to the maximum shortening velocity V_{max}. To compute absolute velocities V_{max} needs to be determined. V_{max} varies with muscle architecture, it depends on the fiber length, angle of pennation and fiber type distribution, which is explained in the following three paragraphs.

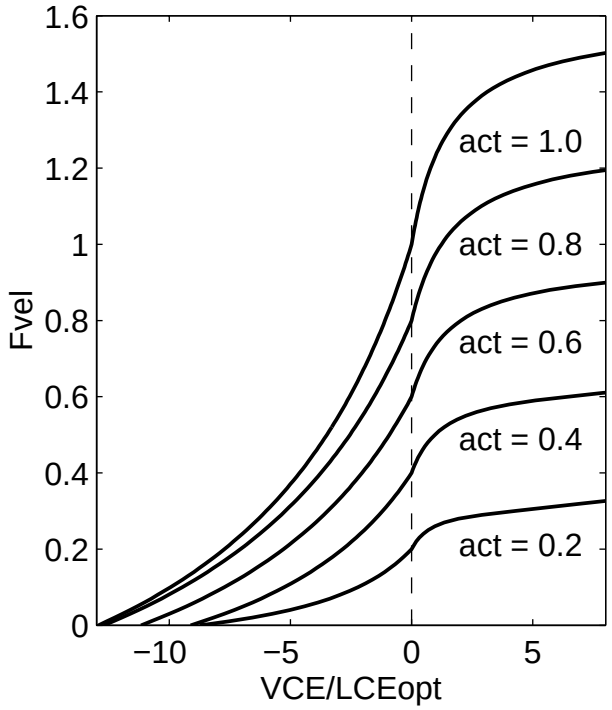

Figure 3.7: *M. gastrocnemius force-velocity property described by eq. 3.10 and eq. 3.12, for activation levels ranging from 0.2 to 1.0.*

Effect of fiber length: Muscle fiber length results from multiplying the number of sarcomeres by the average sarcomere length. The sarcomeres in series are expected to have an average maximum shortening velocity. The velocity of the whole muscle is proportional to the number of sarcomeres shortening and therefore to fiber length.

Effect of pennation angle: The previously described effect that a given muscle fiber length change translates to less muscle shortening for muscles with a greater pennation angle leads also to a slower shortening velocity along the muscle line of action.

Effect of fiber-type distribution: Through muscle biopsy fibers can be classified into slow and fast fibers. Muscles with a high percentage of fast fibers found in the biopsy have a higher maximum shortening velocity [26], [49]. Muscles with a low percentage of fast fibers are better for endurance. Compared to the knee muscles, the ankle muscles m. soleus and m. tibialis anterior have a low percentage of 30 % and 28 % fast fibers respectively (tab.

3.2). Therefore the m. soleus and m. tibialis anterior are well suited for balancing the body during standing for long periods of time.

The maximum shortening velocity has been determined in various experiments described in the literature [15], [69], [71], [26]. Some authors reporting V_{max} in units of rad/s, others in optimal fiber lengths per second. With an assumption of moment arm, optimal fiber length (L_{CEopt}) and angle of pennation (Pa) for the muscles (tab. 3.2), the maximum shortening velocity V_{max} can be calculated along the muscle fiber direction in fiber length per second. A comparison of the various sources is shown in tab. 3.1. Although

Table 3.1: *Maximum shortening velocities and fiber type composition of various muscles and muscle fibers. In Chow et al. [15] the fiber type was not measured* 55 % *fast type fibers was assumed according to [67]. Angle of pennation and optimal fiber length were taken from tab. 3.2. In the case of the quadriceps the mean values from m. vasti and m. rectus were taken. Moment arm is assumed to be 5.8 cm for wrist and 5 cm for quadriceps muscles.*

Muscle, reference	V_{max} $[rad/s]$	Fast fibers [%]	V_{max} $[L_{CEopt}/s]$
Wrist flexors, [15]	8	55	9
Quadriceps, [69]	23	60	15
Quadriceps, [71]	18	61	12
Isolated fiber bundles, [26]	-	100	6

there is a higher amount of slow type fibers in the intact muscles, the V_{max} values are higher than those from Faulkner [26] measured for isolated bundles of only fast twitch fibers. Due to the limitation of only one measurement on isolated human fibers, it can not be distinguished whether the methods used in the single fiber experiments, or the lacking elastic energy storage and release in the intact muscle tendon unit experiments, is the reason for this discrepancy. The fiber velocities in various isolated animal fiber experiments on mouse and rats slow and fast fibers range from 7-13 and 9-24 fiber lengths per second, respectively [16], [17], [48] and [59] and are higher than those measured by Faulkner. The decision was made to use the normalized values from Chow et al. [15] described by eq. 3.8 and eq. 3.9. The absolute fiber velocities of 14 optimal fiber length/s were taken as estimated by Herzog [24] for the knee extensors. This considerably high value accounts for the well trained persons participating in the model validation study.
The fiber type dependency is accounted for in the model by scaling the maximal velocity of the CE with the percentage of fast type fibers (FTF_{muscle}) compared to the average amount of the knee muscle m. vasti and m. rectus

(FTF_{knee}). The higher maximum velocity in muscles of longer fiber length is considered by scaling to the optimal length L_{CEopt} of the muscle to be simulated. The effect of pennation angle on the CE shortening velocity is taken into account by the projection of fiber length with $\cos(Pa)$.

$$V_{max,muscle} = 14 \, \frac{FTF_{muscle}}{FTF_{knee}} \, \frac{L_{opt,muscle}}{L_{opt,knee}} \, \frac{\cos(Pa_{muscle})}{\cos(Pa_{knee})} \tag{3.11}$$

Table 3.2: *Maximum CE velocity (V_{max}) determined by eq. 3.11 using the parameters Pa and L_{CEopt} and FTF. The parameters F_{max}, Pa and L_{CEopt} are originally from Winters [78], they are further optimized, to match resultant joint torques described in section 3.2.1. The parameters for the wrist muscles are not optimized.*

Muscle	$F_{max}[N]$	$L_{CEopt}[cm]$	$FTF[\%]$	$Pa[deg]$	$\boldsymbol{V_{max}}[L_{CEopt}/s]$
Gastroc.	1408	5.2	50	14	12.9
Soleus	4045	4.7	30	24	7.3
Tibialis ant.	1343	8.2	28	7	7.4
Rectus	1917	7.6	55	12	13.7
Vasti	6925	7.7	52	9	14.3
Hamstrings	1680	11.2	50	9	13.2
Gluteus	3683	13.6	50	5	13.3
Iliopsoas	1879	11.0	50	7	13.1
Wrist flexors	168	5.3	55	9	9.1

Eccentric contraction

The Hill equation 3.6 for concentric contraction was also used with a reversed slope 3.12 to describe the force velocity relation in eccentric contraction

$$F_{vel} = \frac{c1 - c2\, V_{CE}}{V_{CE} + c3} \, \frac{1}{100}. \tag{3.12}$$

V_{CE} : CE velocity in % of V_{max}, $V_{CE} > 0$.
F_{vel} : CE force at optimal length normalized to F_{max}.

The new parameters c1, c2 and c3 were determined under the following three conditions for equations 3.10 and 3.12 spanning the whole contractile element velocity range:

1. Both functions are continuous at $V_{CE} = 0$.

2. The slope at $V_{CE} = 0$ increases from positive to negative velocities about a slope factor of 2 (sf = 2). This moderate value compared to slope factor 6 measured from [42] is taken because the force enhancement due to muscle stretch, described in section 3.2.3, also starts to increase CE force when the muscle is stretched while its activated.

3. The asymptote of the force at eccentric velocities is 1.6 times F_{max} (af = 1.6). This factor is lower than the values of about 1.8 to 2 F_{max} from [47] and [42] respectively. Considering an additional force enhancement due to muscle stretch the eccentric force can be higher than 1.6 times the maximum isometric force.

From these three conditions, parameters c1, c2 and c3 can be determined as follows.

$$c2 = -af\ act \tag{3.13}$$

$$c3 = \frac{b}{sf}\frac{act + c2}{act + a} \tag{3.14}$$

$$c1 = act\ c3. \tag{3.15}$$

and were used to calculate the force-velocity properties for positive velocities in fig. 3.7.

3.2.3 Force enhancement following stretch

It is experimentally proven that there is force enhancement following stretch and force depression following shortening of the human skeletal muscle [18], [33], [13]. Depending on the previous situation the actual isometric force is different if the CE was previously stretched or shortened.
The enhancement following a stretch could be up to 1.6 times higher than in a maximum isometric contraction without any previous stretch or shortening [18]. For the simulation of drop jumps all the important muscles acting against gravity are being stretched, in the following isometric and shortening phase the force will be enhanced. Therefore the stretch is an important issue for the simulation and should be included in the model. Simulating drop jumps without force enhancement of the CE, the model can not reach the jump height of the athletes in the study of Arampatzis et al. [3], provided that muscle model parameters V_{max} and F_{max} are not unrealistic high.
The mechanisms underlying force enhancement are not well described in the literature, from experimental observations the following four properties should be contained in a simulation of force enhancement following stretch:

1. Linear increase with the stretch amplitude up to maximal enhancement of 1.6 times the isometric force without stretch [18].

2. Exponential decay of the enhancement (pot), in the isometric hold phase following stretch [18], which can be described by the differential equation
$$\frac{dpot}{dt} = 1.9\, pot \tag{3.16}$$

3. Having a certain amount of potentiation after stretch, a following shortening should reduce the enhancement rapidly because there exists force depression after shortening [24].

4. Herzog suggest in [24] that enhancement is accomplished through an increase in the the average force of a force producing site (cross-bridge) rather than through an increase in the number of force producing sites. This implicitly follows that it is proportional to the number of force producing sites and therefore to the active state of the muscle.

In the following algorithm all of the four properties are included to obtain force enhancement after stretch.

Eccentric contraction ($VCE > 0$) :

$$pot(i) = pot(i-1) + cf\ (\frac{L_{CE}(i)}{L_{CEopt}})\ act(t) - df\ pot(i-1)\ \Delta t. \qquad (3.17)$$

Concentric contraction ($VCE \leq 0$) :

$$pot(i) = max(\ pot(i-1) - cf\ (\frac{L_{CE}(i)}{L_{CEopt}}) - df\ pot(i-1)\ \Delta t\ , 0). \qquad (3.18)$$

pot	: Enhancement factor in eq. 3.20 to calculate the CE force.
cf	: Enhancement factor chosen such that in drop jumping (1+pot) is not higher than (1.6).
df	: Decay factor 1.9 representing data from Cook [18].
i	: Computing time steps $i \in N$. The simulated time is $t = i\ \Delta t$.
Δt	: Time difference between steps i.

The force enhancement due to stretch during drop jumping is highest in m. vasti and is demonstrated in dependence of the active state and the CE length in fig. 3.8

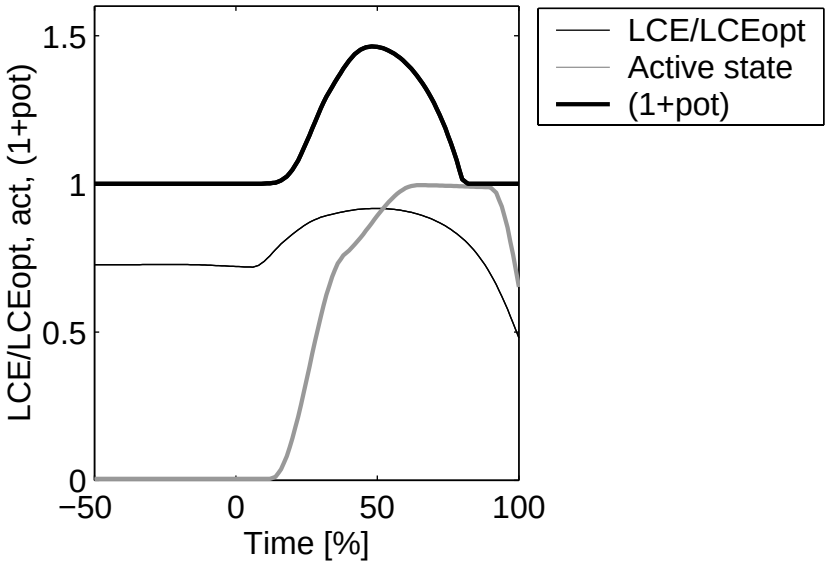

Figure 3.8: *Force enhancement of m. vasti during a drop jump with a contact time of* 200 *ms. The enhancement factor (1+pot) increases with stretch and decreases with shortening.*

3.2.4 Force-length-velocity properties

Ideally, measurements of the force-velocity properties are done at the same fiber length. On the other hand the force-length curve is determined in isometrical condition with a fiber velocity equal to zero. A combination of both effects as it happen in real life movement, can be described according to Bahler et al. [5] by multiplying the force-length function 3.5 with the force-velocity functions 3.10 and 3.12

$$F_{CE}/F_{max} = F_{len}(L_{CE})\, F_{vel}(V_{CE}). \tag{3.19}$$

This yields an area in three dimensions (fig. 3.9).

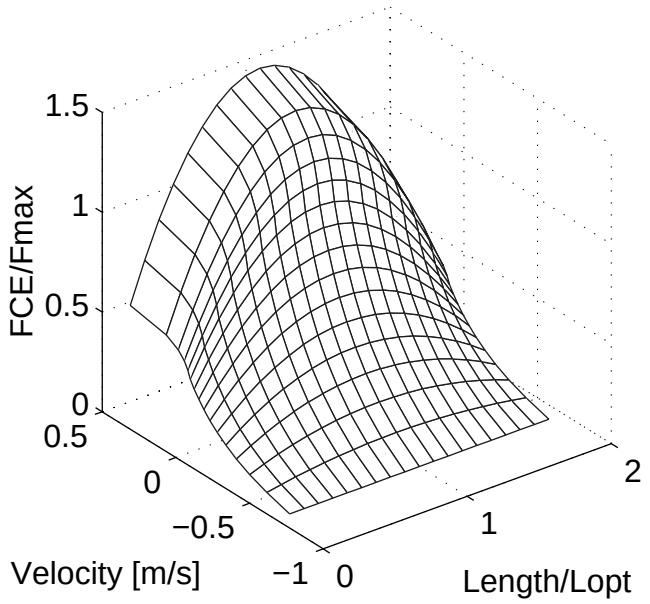

Figure 3.9: *Force-length-velocity property of m. gastrocnemius.*

In the model, the force generated by the CE (F_{CE}) is calculated multiplying the force-length function ($0 \leq F_{len} \leq 1$) with the force-velocity function ($0 \leq F_{vel} \leq 1.6$) which results in eq. 3.20. The force enhancement due to previous stretch is taken into account with the factor $(1 + pot)$ with $(0 \leq pot \leq 0.6)$

$$F_{CE}/F_{max} = (1 + pot(t, L_{CE}))\, F_{len}(L_{CE})\, F_{vel}(V_{CE}, act(t)). \tag{3.20}$$

The maximum isometric force F_{max} is calculated using the physiological cross sectional area (PCSA) values from Winters [78] and an average value of force

per unit area of $43N/cm^2$. The PCSA is scaled from the subjects used in Winters to the segment dimensions of the computer model as follows. The PCSA is defined as the muscle volume divided by the muscle optimal fiber length. The muscle volume is assumed to be proportional to the segment mass (Ms), the fiber length is assumed to be proportional to the segment length (Ls). The scaling formula is therefore

$$F_{max,muscle} = 43\, PCSA_{Winters}\, \frac{Ms_{model}}{Ms_{Winters}}\, \frac{Ls_{Winters}}{Ls_{model}} \tag{3.21}$$

For individual muscles the optimal fiber length could be determined by ultrasonography. With the construction presented in section 3.4.1 this can only be done for m. gastrocnemius, so for model consistency all muscle fiber lengths were taken from Winters [78].

3.3 Parallel elastic element properties

The parallel elastic elements (PEE) are associated with the connective tissue structures surrounding the muscle fibers, fascicles and the entire muscle. For rat skeletal muscle the force development is insignificant except for length exceeding 110 % of the optimal length (Bahler [5]). The author mentioned that the length at which PEE force occurs are often beyond the physiological range. This can be confirmed by the drop jump simulation, the muscles mainly work at the ascending limb of the force length curve and not over 110 % of their optimal lengths (fig. 5.11). Calculating the muscles force-length curves in maximum isometric contractions in their defined joint range which is not completely used in drop jumping, the muscle forces are mainly located at the ascending limb of the force-length curve (fig. 3.11). Another study from Wilkie [77] found the theoretical predicted length at which PEE contributes to the muscle force varies for different frog muscles between 80 and 160 % of L_{CEopt} so that the passive elastic element properties must be determined for each muscle individually.
Due to the force-length relation the muscle force would drop to zero when the muscle is lengthened at the descending limb of the force length curve. This is not true for muscle fiber bundles. The parallel elastic element avoids this instability at the descending limb. From the CE length during drop jumping modelling of the PEE according the measurements from Bahler [5] would not be required. To avoid computational problems at long CE lengths the PEE is modelled the same way as described in van Soest [73]. When the relative CE length increases above 140 % of its optimal length the force increases in a parabola shape so that at 50 % strain the maximum isometric force is reached (fig. 3.10). This is calculated using the following equation

$$F_{PEE} = K_{PEE}\,(max(L_{PEE} - L_{PEEslack}, 0))^2 \tag{3.22}$$

with the constant factor

$$K_{PEE} = \frac{strain_{PEE}\,F_{max}}{L_{CEopt}^2(width + 1 - L_{PEEslack})^2}, \tag{3.23}$$

with $strain_{PEE} = 0.5$ and $L_{PEEslack} = 1.4\,L_{CEopt}$.

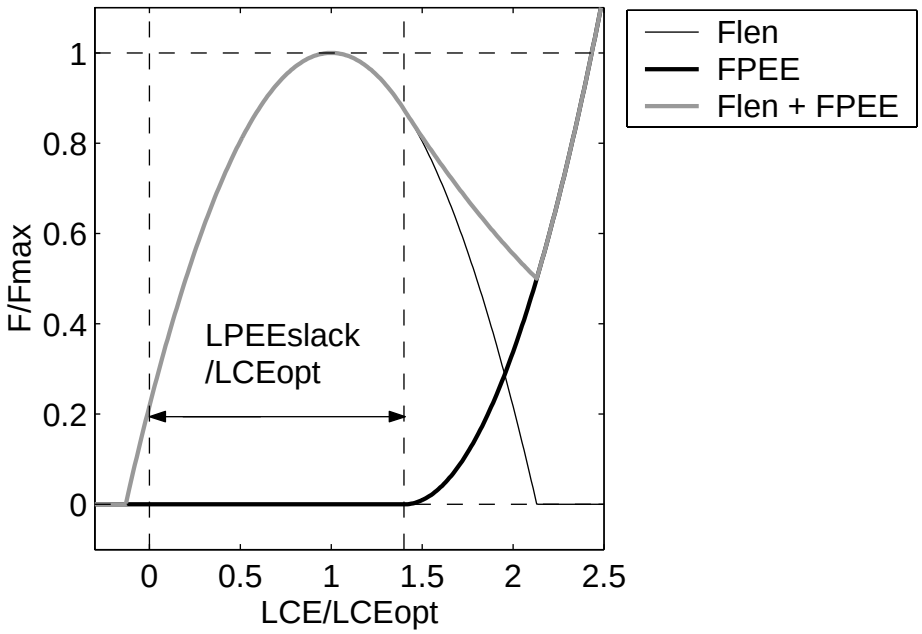

Figure 3.10: *Force-length property, explicitly showing the contribution of the parallel elastic element at the descending limb of the force-length curve.*

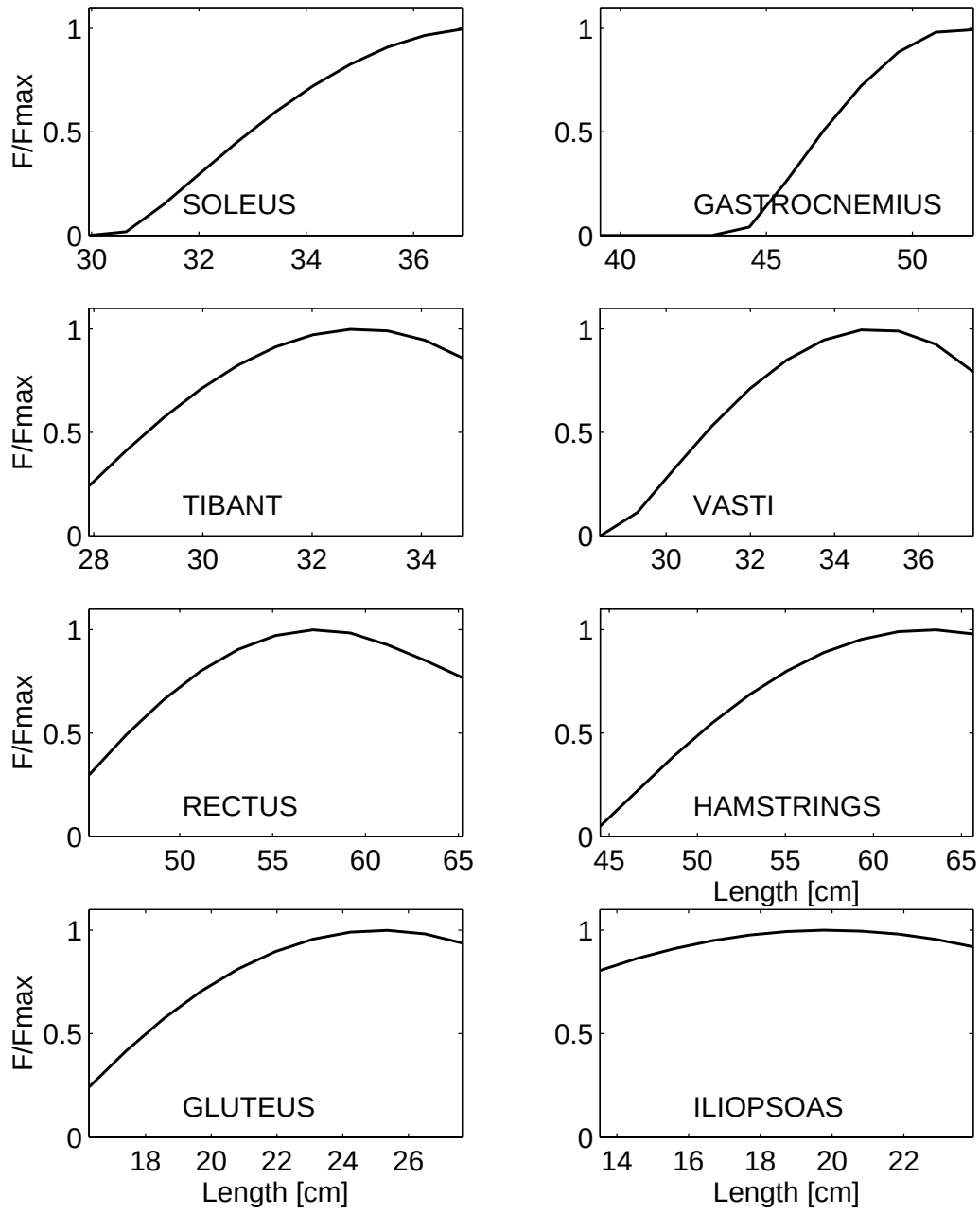

Figure 3.11: *Maximum isometric force-length property for all muscles in the model. The length range is according to the defined joint range of motion. In isometric contractions at these angles the muscles mainly operates at the ascending limb of the force-length curve.*

3.4 Series elastic element properties

The passive SEE transmit the forces from the muscle CE and PEE to the bones with the viscoelastic aponeuroses and tendon. The aponeuroses refers to the tendinous sheets that usually extend along and deep into the belly of a muscle.
The series elasticity of the muscle fiber itself, in the cross-bridges and myofilaments, is assumed to be accounted for in the active properties of the contractile element. Which are validated in experiments for single fibers, which of course include the fiber elasticity.

The compliance of the SEE can be quantified with its static force-length characteristic. Here we are interested in the tendon and aponeurosis compliance not in the elasticity of the muscle fiber itself. The tendon is anatomically easy identifiable. Tendons can be isolated from the muscle-tendon complex and their mechanical properties have been measured in vitro [79], [63]. The ultimate stress at which failure occurs was determined to be 9 to 13 % strain [79]. The mechanical properties of tendons change with sterilization and preservation [66] so that in vivo experiments would lead to more accurate results.
In most of the computer models of the muscle-tendon unit the same strain value is used for tendon and aponeurosis. However there is experimental evidence [25] that the aponeurosis is more compliant than the tendon.
With the method of quick release or the ultrasonography it is possible to quantify in vivo the passive muscle-tendon compliance. Both methods will be explained in the following.

In the quick release experiment done by Hof et al. [40], the decline in torque during the release is measured as a function of joint rotation. Correcting these data for inertia and shortening of the fibers, the muscle elasticity can be described with a torque-angle curve. Those releases must be rather fast so that the force producing fibers do not change their active state during the contraction. Assuming an average plantar flexor series elastic element length of 43 cm and a moment arm of 4.2 cm, 4.3 percent strain at 116 Nm maximum isometric ankle joint torque can be estimated from Hof [40]. This torque-angle curve contains the whole muscle-tendon compliance namely the tendon, aponeurosis and fiber compliance.

In the ultrasonography method the SEE elongation is measured during maximum isometric contractions, by tracking the fiber insertion points into the

aponeurosis [29]. This procedure will be described in detail in section 3.4.1. With ultrasonography the tendon and aponeurosis compliance at different locations on the muscle belly can be measured.
In both, the quick release and the ultrasonography method the SEE compliance can be measured in vivo. The advantage of the ultrasonography method is that for the modelling of SEE only the aponeurosis and tendon compliance are required not the fiber compliance. For both methods measuring a force-length curve for a single muscle is difficult when there is more than one muscle acting around the same joint. Assuming that one of the muscles is activated maximally at its optimal length, maximal isometric SEE elongation for this muscle can be determined. Knowing maximum SEE elongation, the force length curve can be approximated with a second order polynomial (fig. 3.15) which approximates well the shape of the SEE force length curve in isolated animal muscle experiments [25].
In the muscle model the passive SEE force-length curve is described by a second order polynomial

$$F_{SEE} = K_{SEE}\, max(L_{SEE} - L_{SEEslack}, 0)^2 \tag{3.24}$$

with the factor

$$K_{SEE} = \frac{Fmax}{(strain_{SEE}\, L_{SEEslack})^2} \tag{3.25}$$

The SEE force F_{SEE} is defined such that at maximum isometric force (F_{max}) the strain in the SEE is 4.0 % ($strain_{SEE} = 0.04$). This value of 4.0 % is measured in section 3.4.1. Compared to the measurements of Magnusson et al. [51] it seems to be low. Whether this is due to overestimation in the study of Magnusson or underestimations in our own study is not sure. To account for both values the simulation was carried out as well with 4.5 % maximum strain.
The slack-length $L_{SEEslack}$ depends on the muscle and is obtained simulating a maximal isometric contraction at optimal muscle length with the optimal joint configuration for the muscle. The length L_{CEopt} from Winters [78] and 4 % strain are subtracted from the muscle-tendon length to obtain $L_{SEEslack}$. The optimal joint configuration for each muscle is chosen so that the calculated resultant joint torques are already in good agreement with the measured joint torques before $L_{SEEslack}$ and L_{CEopt} are involved in the optimization process described in section 3.2.1.

3.4.1 Measuring muscle series elasticity using ultrasonography

Before introducing the methodology of the measurement, the spatial as well as the time resolution of the ultrasound scanner used in this study are explained. This demonstrates the abilities of ultrasonography in muscle imaging.

Ultrasound scanner resolution

A linear ultrasound scanner consists of 200 or more separate arrays (fig. 3.12). These arrays are closely spaced piezoelectric elements, each with its own electrical connection to the ultrasound instrument. This enables elements to be excited individually or in groups to produce focussed ultrasound beams. Echo signals detected by individual elements are amplified separately before being combined to reconstruct the image.
The images are actually built up from a tissue volume which depends on the slice thickness and the beam width defined in fig. 3.12. Interference from different arrays is focussing the width of the resultant beam. This reduces the slice thickness from 4.3 mm close to the scanner to 1.7 mm in the focus zone (Shimadzu, SDU 350XL 5-7.5 MHz, Jpn.). The beam width is about 1 mm in the focus zone.
Two reflectors in the axial direction can be distinguished if the time-gap between the arrive of the two echo signals is longer than ultrasound pulse duration. Considering a pulse with 5 cycles and a wave frequency of 7.5 MHz the pulse time would be 0.6 μs. With the transmission speed in muscle tissue of 1600 m/s [81] the axial resolution is 1 mm. Spatial resolution improves as the frequency is increased. On the other hand sound beam attenuation also increases when the frequency is increased, so beam penetration decreases. The choice of ultrasound frequency for any examination is the result of a compromise between resolution requirements and the beam penetration to show all the tissue of interest.
When examining m. gastrocnemius which is close to the surface, it is better to use the higher 7.5 MHz frequency instead of 5 MHz.
In conclusion the resolution in the image plane with the setup used in this study is about 1 mm, with the information coming from a depth of 1.7 up to 4.3 mm perpendicular to the image plane.
With the given resolution the question arises what muscle structure can be seen on the ultrasound image of gastrocnemius muscle. The skeletal muscle may be thought of in structural units of decreasing size. The entire muscle is

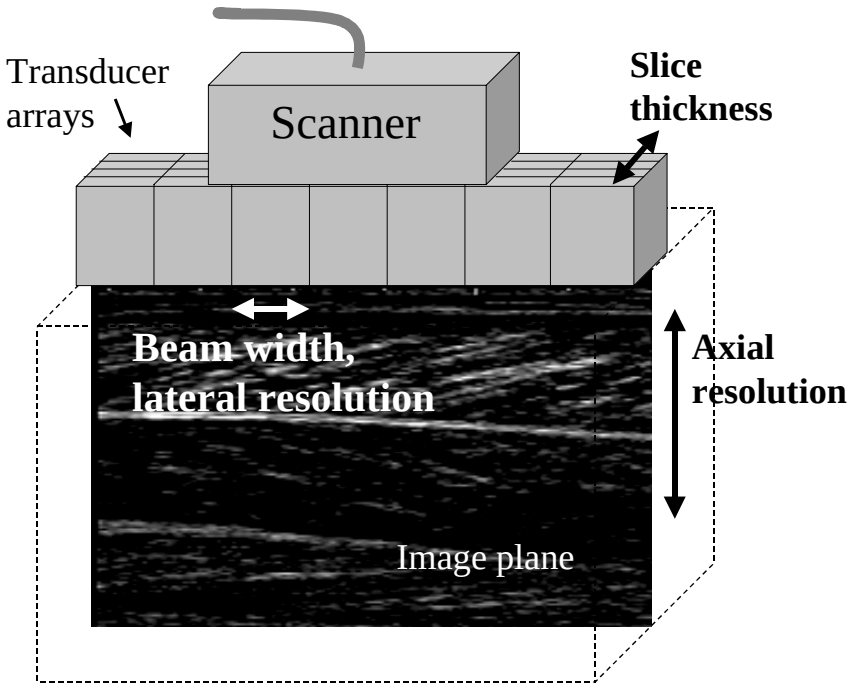

Figure 3.12: *Ultrasound scanner with description of the different resolution directions.*

surrounded by a connective tissue sheath called the epimysium. Fascias are the outermost layer of epimysium around the outside of a whole muscle. Very thick and heavy fasciae are called aponeurosis. The next smaller structure is the muscle bundle or fascicle which consists of a number of muscle fibers surrounded by a connective tissue sheath called the perimysium. The muscle fiber is next, which is an individual muscle cell surrounded by the endomysium, a thin sheath of connective tissue which binds the individual fibers together within a fascicle. The diameter of a fiber is about 10 to 100 μm, the diameter of a fascicle 0.5 to 2 mm [26]. With an resolution of about 1 mm the fascicle structure can be seen. The single fiber surrounded by the endomysium can not be resolved.

Imaging dynamic muscular contractions the time resolution of the scanner used in this study is limited to 20.9 Hz with two focus zones used. Every 40 ms one picture is taken. Filming muscular contraction during drop jumping contact of 160 ms 4 picture can be obtained, this is not enough to discussing the fascicle length change in this situation. In isometric contractions where

the force is built up in about one second 20 pictures are available in which the fiber length change can be determined over time.

Methods

The goal is to perform maximum isometric contractions at m. gastrocnemius optimal length. During the isometric contraction the fiber insertion point P shown in fig. 3.16 is tracked over the ultrasound images obtained from zero force till the force reaches maximum. The strain of the series elastic tissue can be determined when the distance from the muscle origin at the heel up to the fiber insertion point is known.
Four trained male subjects 26-32 years of age participated in the study. The subjects had to perform isometric plantar flexions against a plate lying on the table shown in fig. 3.13.

The ultrasound scanner was positioned on m. gastrocnemius medialis muscle belly at the most distal point where both aponeurosis were still parallel aligned. The scanner was then rigidly fixed to the table. Increasing muscle volume at maximum contraction was compensated with a gel pad of 2 cm thickness between the scanner and the skin (Sonokit soft, Sonogel, Germany). The plantar flexion force was measured with a pressure distribution insole (Pedar, Novel, Germany). Feedback of the plantar pressure was given to the subject, so that for each trial the same maximum force was obtained. M. gastrocnemius is a two joint muscle crossing the ankle as well as the knee joint. To measure the maximum isometric strain at m. gastrocnemius optimal length, the plate under the foot is allowed to change its angle with the center of rotation located at the knee joint. The knee angle was varied and so the length of m. gastrocnemius until the isometric force reached was maximal and so m. gastrocnemius has its optimal length. With this configuration the subjects were asked to build up to a maximal contraction within 2 seconds and maintain that contraction for at least one second. Within the first 2.5 seconds 52 ultrasound pictures were taken. The trials were repeated 10 times for each subject and the five trials in which the fascicles could be best tracked and the plantar pressure was highest were used for the determination of maximum SEE strain. Maximum SEE strain was determined tracking the fascicle insertion point P for all 52 pictures so that the same fascicle can be observed at zero and at maximum isometric force. Due to the fact that m. gastrocnemius is not the only muscle generating the plantar flexion force and force may vary between the muscles during isometric contractions, maximum strain and not the strain at maximum force was taken.

Figure 3.13: *Construction to measure maximum series elastic compliance.*

The length change resulting from heel lift was recorded with a camera and subtracted from the length change of the insertion point P. The strain was then calculated knowing the length L0 (fig. 3.14) from the insertion point at the heel to the scanner at zero force. The resultant force-strain curve is plotted in fig. 3.15.

Results and discussion

The average maximum strain measured in the SEE was 3.97 %. The individual data are shown in tab. 3.3. The correction for the heel lift is essential, it was up to $10\,mm$ so that over 10 % strain would be obtained if this correction was not carried out.
The maximum strain values found in this study are slightly lower than those

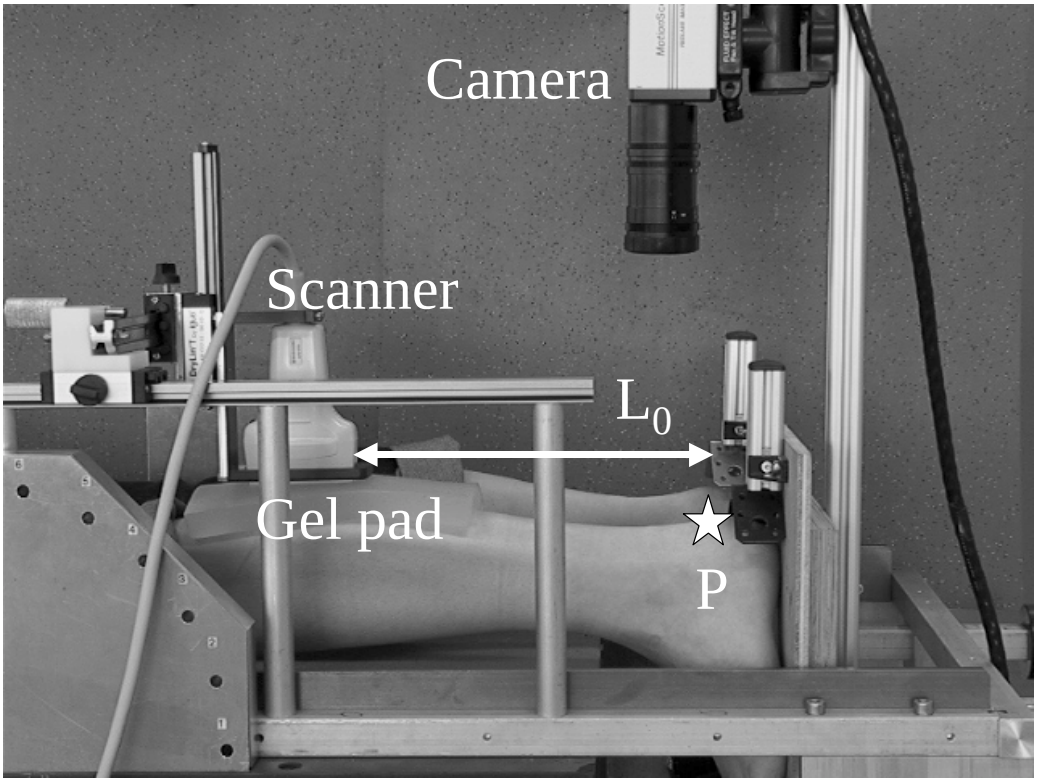

Figure 3.14: *Reference distance L0 from Tendon insertion point at the heel to scanner left image window shown in fig. 3.16.*

Table 3.3: *Subject properties and measured results.*

Subject	Maximum isom. torque [Nm]	Maximum strain [%]
1. (180 cm 78 kg)	221	4.31 ± 0.38
2. (180 cm 70 kg)	192	3.64 ± 0.35
3. (184 cm 82 kg)	232	4.04 ± 0.31
4. (165 cm 65 kg)	210	3.87 ± 0.43
(177 cm 74 kg)	214	**3.97** $\pm$ 0.18

measured with ultrasonography by Magnusson et al. [51]. They reported 4.4 and 5.6 % strain on the most distal and most proximal location on m. gastrocnemius muscle belly respectively. Comparing both methods with each other there are two main differences. First our scanner was positioned in between the two locations measured in their study. Second, their scanner was taped to the skin and relative scanner movement to the skin was neglected. Therefore heel lifting must not be corrected, because the scanner is

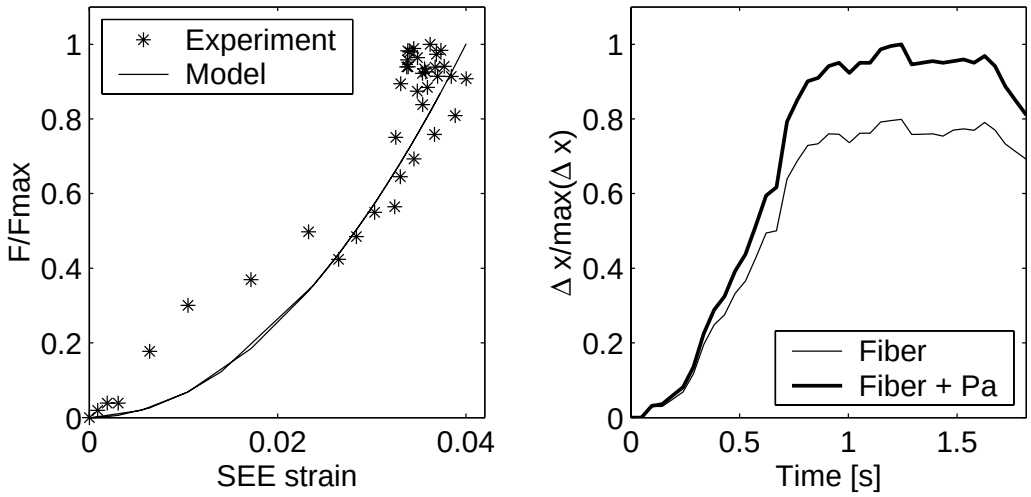

Figure 3.15: *On the left side experimentally determined SEE force-length curve during isometric contraction compared to a second order polynomial. On the right side, the experimentally determined length change along the muscle line of action, compared to projection of the fiber, keeping its initial angle of pennation constant.*

moving when the heel is lifted. Instead a correction for ankle joint rotation was carried out. Ankle joint flexion additionally shortens the muscle length from origin to insertion. The first difference would result in an average strain value of about 5 % between the most distal and the most proximal location on the muscle belly and would be 1 % higher than those found in our study. Their method correcting the joint angle change at high forces could lead to underestimation of the foot deformation and therefore to overestimation of the strain measured. The error from scanner movement can not be systematically analyzed and is dependent on the subjects muscles as well as on the location on the muscle. From our own measurements on trained athletes with a big m. gastrocnemius the scanner was tilted during contraction when it was taped to the skin.
For subject one and three, maximal plantar flexions were also performed in a seated position on a commercial available torque measurement device (Multi-joint system 3, Biodex, NY). Up to 10 % higher torque at the same knee and ankle joint angle is obtained there. The higher joint torques in a seating position is assumed to be caused by a higher comfortability of the subjects having a resistance against the back compared to a resistance at the shoulders. This behavior could lead to underestimation of the maximal isometric strain measured in this study.

Other strain measurements with ultrasonography on m. tibialis anterior were performed by Maganaris et al. [50], they reported 2.5 % strain. This is quite low compared to those on m. gastrocnemius. The lower strain value might be quite reasonable considering the different tasks of both muscles. M. gastrocnemius has to work against gravity and accelerate the body, m. tibialis anterior has to stabilize the ankle joint before and at touch-down, but does not require a lot of energy saving or power generating capacities such as m. gastrocnemius. Comparing the strain measured to the quick release experiments [40], 4.3 % strain estimated in section 3.4 is in good agreement.
With the method chosen it was possible to determine the SEE maximum strain at m. gastrocnemius. Another outcome of the measurements is that the fiber shortening as well as the a change in the angle of pennation is resposible for the shortening of the muscle along its line of action. Calculating the muscle shortening assuming a constant angle of pennation, 80 % of the length change would be due to fiber shortening alone. The remaining 20 % is due to a change in the angle of pennation. Comparing the CE behavior of the computer model to the behavior of isolated muscle fibers measured, an under determination of the length change might be possible.

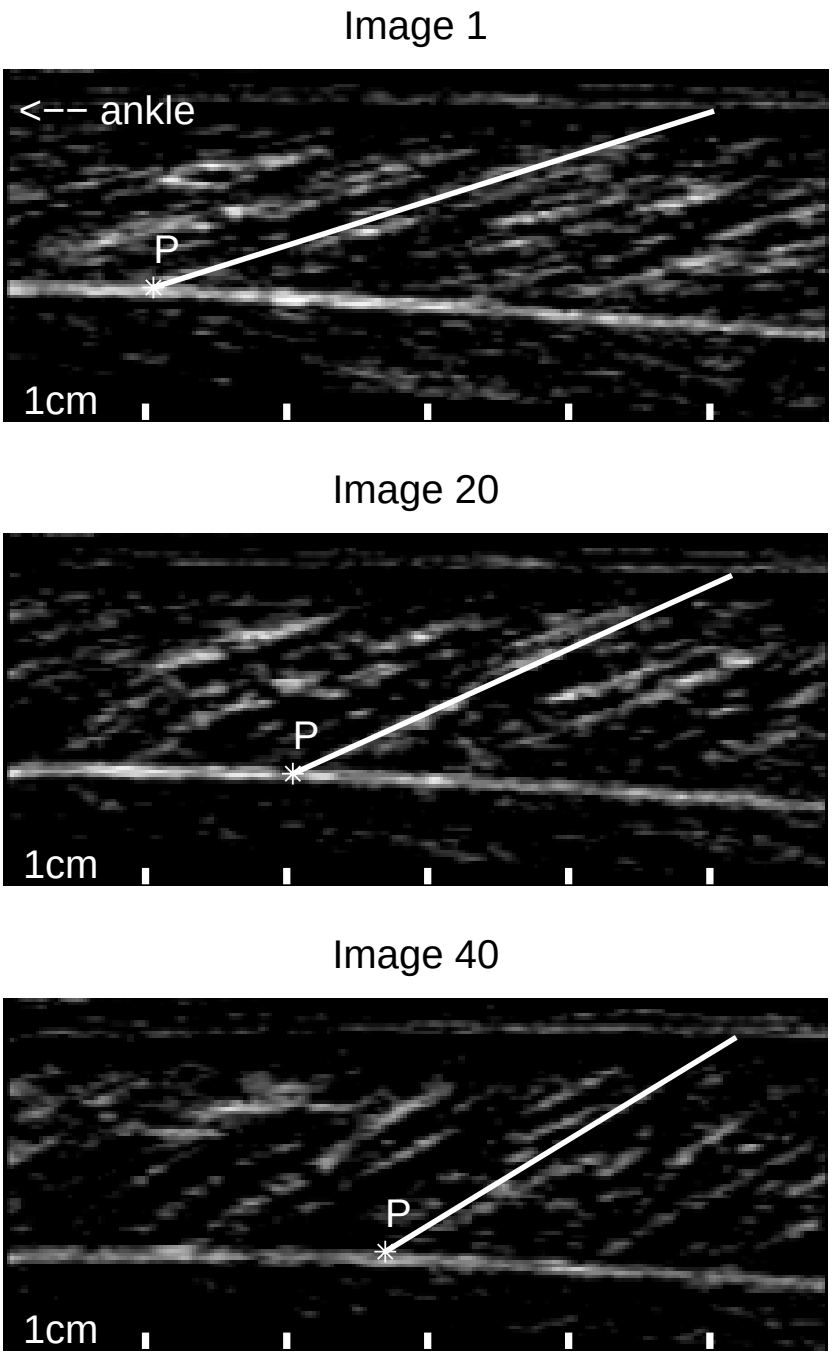

Figure 3.16: *Series elastic strain measured from 40 ultrasound images, shown are the images of subject 4.*

3.5 Activation

The muscle activation is described by an active state function depending on parameters which have to go through an optimization process to make the model jump as high as possible.

3.5.1 Active state function

At a given length of a muscle fiber, the isometric tension developed is proportional to the active state (act) [34]. This state is characterized for a single muscle fiber by the relative amount of Ca^{2+} ions bound to troponin [22]. In the resting muscle fiber act is equal to act_0. When the maximal number of interactive sites in the filaments are exposed by the action of calcium then $act = 1$. The the relative amount of Ca^{2+} ions bound to troponin increases with increasing frequency of stimulation.

During voluntary contractions it is not possible to activate a single muscle fiber. A muscle is organized in so called motor units. A motor unit describes a motor neuron and all the the muscle fibers that are activated by this single neuron. The magnitude of muscle force can be controlled with the number of motor units that are activated and the frequency of stimulation. The rise of muscle force in isometric contraction is first increased by additionally activating more motor units. All the motor units are probably recruited when the force reaches about 50 to 85 % of maximum [23]. The increase of muscle force beyond that is caused by an increase of the stimulation frequency. The shape of the increase in force resembles a sinusoid function shown in fig. 3.17.

In this simulation study an exact knowledge of the chemical processes involved is not required. The active state is the sum of motor recruitment and frequency of stimulation.
The simulation approach from van Soest [74] for vertical jumps from a squatted position uses one parameter for each muscle to control the model. This parameter is the on set of the muscle. When the muscle is switched on the active state is one and remains one till take-off. This approach is successful for jumping from a squatted position. Pandy [2] uses an active state function linearly interpolating between control nodes to account for a more complex activation pattern in a countermovement before jumping. Both approaches did not integrate the equations of motion till maximal height was reached, the simulation was terminated when the body leaves the ground. The authors calculated jump height from the vertical center of mass velocity at take-off.

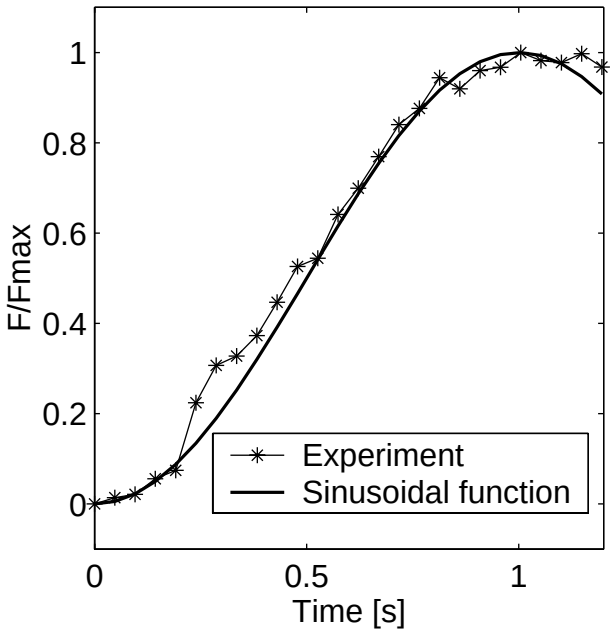

Figure 3.17: *Force at the Achilles tendon, performing an isometric plantar flexion. The experimentally determined increase in force can be fitted well with a sinusoidal function.*

In a first approach drop jumps were simulated until take-off with three parameters per muscle the on off and average stimulation frequency with an activation dynamic described by Hatze [34]. Calculation leads to high rotational accelerations of the segments at time of take-off. Integrating until the maximum height was reached, the high accelerations achieved do not lead to an upright flight position. The control model with three parameters for each muscle was not able to regulate an upright body position, additionally unrealistic high joint limiter torques were the consequence.
The decision was made to use a set of control nodes to account for the more complex control problem during drop jumping. The active state between the control nodes was interpolated with sinusoidal functions (Appendix B) representing the increase of muscle tension. The nodes were equally spaced between the first and last node. The first and last control nodes are set to $act_0 = 0.005$ according to Hatze [34] and are allowed to vary their time in certain boundaries. All other nodes in between the first and last node have an amplitude between a lower and upper boundary within the range zero and one (fig. 3.18). This implementation of the active state implicitly leads to the fact that muscle activation can not increase immediately.

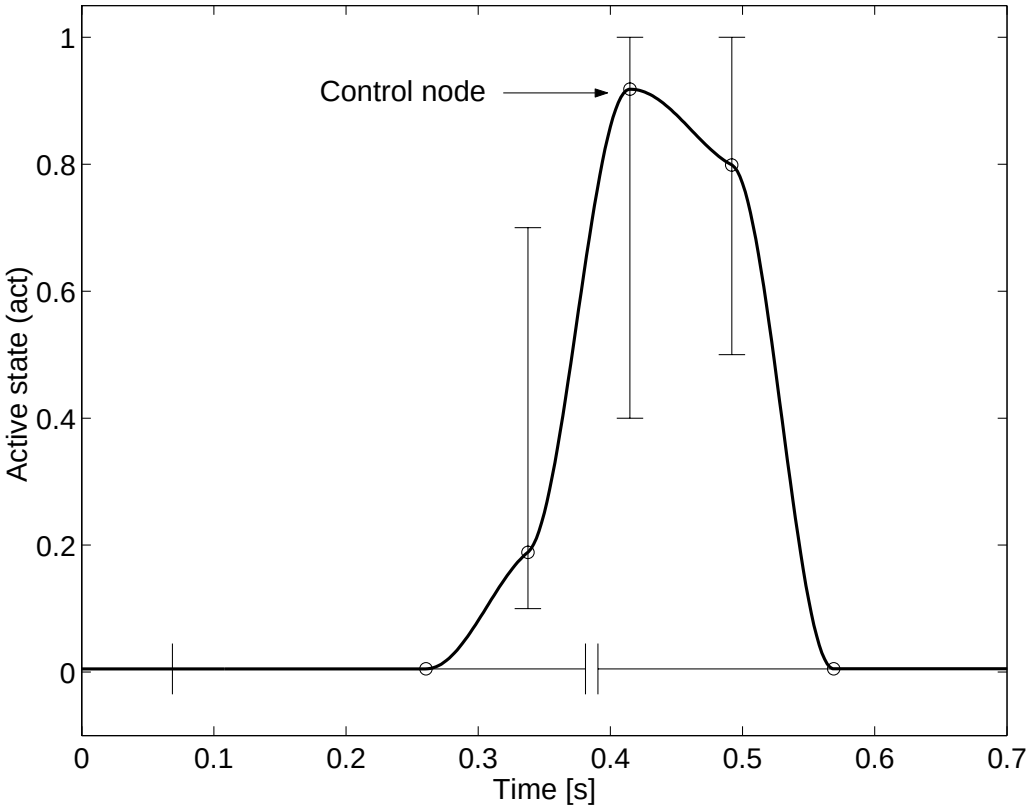

Figure 3.18: *Active state function with 5 control nodes used for m. soleus. The "T" bars indicate the boundaries used in the optimization process.*

The amount of nodes were kept minimal to reduce the optimization parameters and so the computing time. For each muscle the number of nodes and their boundaries were chosen based on EMG on and off times found in the literature and their obvious functional need in the drop jump simulation for each muscle.

3.5.2 Cost function and optimization process

Beside the goal to reach maximum height, the cost function for the optimization of muscle control in drop jumping consists of other aspects such as receptor information for injury prevention and metabolic energy requirements. The latter two influences are not well known and therefore difficult to describe. In this study the cost function is the resultant jump height of the upper body CM to be maximized. This can be done because during a

maximum height drop jump which is repeated only a few times metabolic energy saving processes or fatigue are not important. The injury prevention is first, inhibition of muscle activation at very high force rates, second co-contraction or inhibition preventing the joint going to its limits. The first one is not taken into account, the second one is considered giving a penalty to the cost function when the joint limiter torque reaches more than 4 Nm for each joint separately. The optimization process is shown in fig. 3.19.

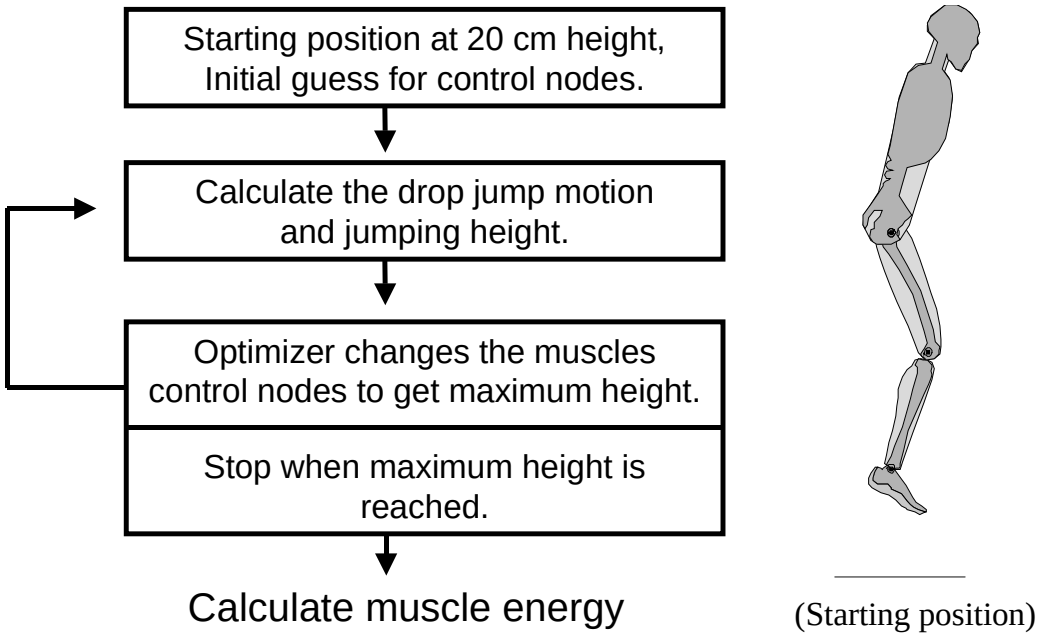

Figure 3.19: *Optimization Process.*

First the optimizing process was carried out so that the total Body CM achieved maximum height. This leads to a backward rotation of the upper body and not to an upright movement as it is in vertical drop jumping. Taking the upper rigid body CM (not the wobbling mass CM) for the height calculation an upright position after take off can be simulated.
This leads to the speculation that it is advantageous to jump backwards to reach a maximum total body CM jump height. This is in agreement with the observation that a summersault can performed easier backwards than forwards because of the greater height of the body CM reached. This behavior confirms the validity of the simulation model.

Plotting the resultant jump height with two varying control nodes for m. vasti keeping all other control nodes fixed, local maxima can be seen. The local maxima cause a gradient based optimizer to detect them as the maximum.

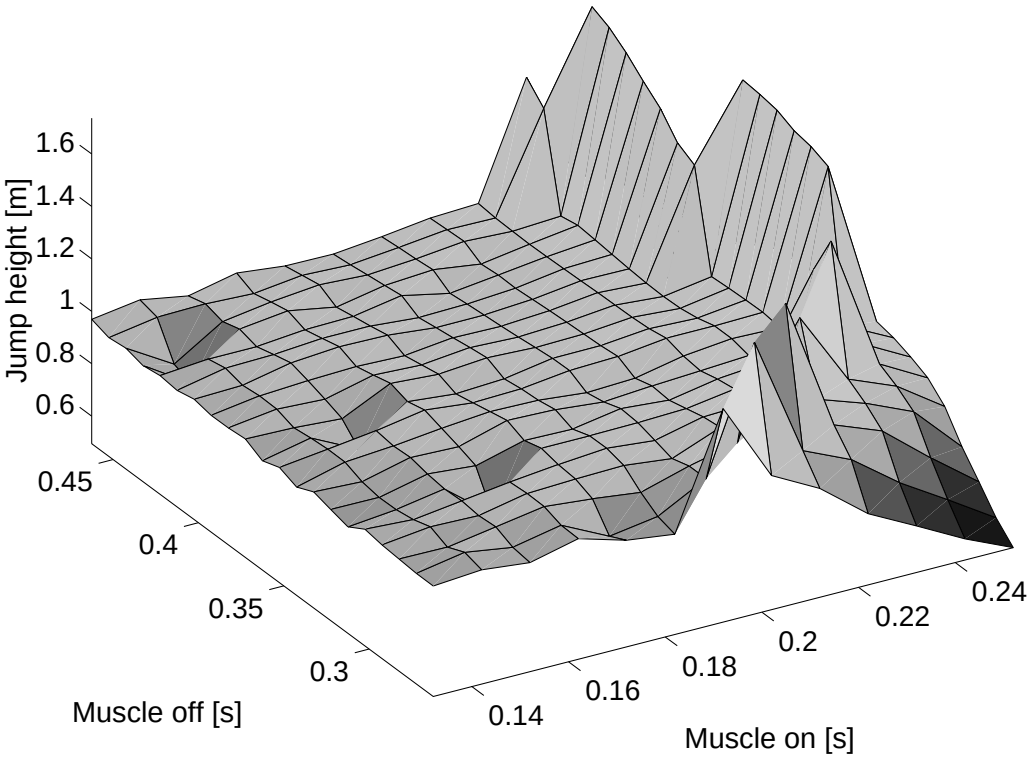

Figure 3.20: *Jump height dependent on the time of the first and last control node of vasti muscle. All other nodes are kept at their fixed values. Dropping height is 20 cm, so ground contact starts at about 0.2 seconds.*

The method of simulated annealing [19] guarantees to find the global optimum. Simulated annealing was applied by other authors to solve their muscle optimization problem [80], [56]. The method of simulated annealing with about 41 design variables would requires 1.6 million function calls to reach the global optimum, for a problem with only 10 design parameters [19]. With an average time of one second to integrate the rigid body equations of motions using (DADS, LMS international) on a computer (PC, Pentium III , 800 MHz), 1.6 million calls would require 18 days and is computational too inefficient.
The optimization was performed using a constrained gradient based method

(Matlab 6.0, Mathworks). To avoid local minima the gradient based method was used with 100 calls randomly disturbing the initial node configuration. This method takes about 12 hours to obtain an optimal solution. There is no guarantee that it is the optimal one. From fig. 3.20, if we can conclude from one muscle to all others, there is a broad range for the first and last control node for the two absolute maxima, so they should be found varying 100 times the initial node configuration.

3.6 Computation of muscle force

So far the properties of CE, PEE and SEE components of the Hill muscle model are formulated. For the arrangement of the CE and PEE in series with the elastic element the state equation, a relation between V_{CE}, L_{CE} and L_{MTU} is derived in symbolic form. This state equation has to be solved to calculate the muscle force used as input for the rigid body model in eq. 2.5.

Neglecting the muscle mass, the sum of PEE and CE forces connected in parallel equals the SEE force

$$F_{SEE} = F_{CE} + F_{PEE}. \tag{3.26}$$

Due to the arrangement of the CE and the SEE in series the length of the muscle L_{MTU} is the sum of the CE length and the SEE length

$$L_{MTU} = L_{CE} + L_{SEE}. \tag{3.27}$$

The SEE force from eq. 3.24 depends on L_{CE} and L_{MTU}

$$F_{SEE} = f_1(L_{CE}(t), L_{MTU}(t)) \tag{3.28}$$

Since the SEE has no elements parallel to it, F_{SEE} is the the force exerted by the muscle on the rigid bodies which needs to be determined.
To calculate F_{SEE} an equation relating V_{CE} to L_{CE} and L_{MTU} has to be derived. From eq. 3.20 F_{CE} is a function of $V_{CE}(t)$, $L_{CE}(t)$ and act(t),

$$F_{CE} = f_2(V_{CE}(t), L_{CE}(t), act(t)), \tag{3.29}$$

and F_{PEE} depends only on $L_{CE}(t)$

$$F_{PEE} = f_3(L_{CE}(t)), \tag{3.30}$$

so that equation 3.26 can be expressed as

$$f_1(V_{CE}(t), L_{CE}(t), act(t)) = f_2(V_{CE}(t), L_{CE}(t), act(t)) + f_3(L_{CE}(t)). \tag{3.31}$$

due to the formulation of all functions involved, eq. 3.31 can be solved for V_{CE} (Appendix C) yielding the state equation

$$V_{CE}(t) = f_4(L_{CE}(t), L_{MTU}(t), act(t)). \tag{3.32}$$

This state equation can be integrated numerically, given starting values for L_{CE} for a given act and L_{MTU} as a function of time.

Chapter 4

Model validation

Model validation is important to document the accuracy of the simulation results. In this chapter it will be shown that the simplified human model is able to reproduce the measured parameters within a certain range of drop jump heights and ground contact times.

4.1 Inverse versus direct dynamics method

The question arises whether it would be more appropriate to use inverse dynamics rather than direct dynamics to calculate the effect of SEE energy in drop jumping. In the inverse dynamics method all the external forces are measured and the segment accelerations are calculated from video data. In the next step from the equations of motion internal forces and resultant joint torques can be calculated.
In the direct dynamics method the rigid bodies are started in an initial position and dependent on the muscle and contact forces implemented in the simulation program, the rigid bodies change their trajectories at each integration step. In the direct dynamics method the muscles need an activation function to let the model jump as high as possible. In the case of a maximum height drop jump the muscles activation functions are optimized so that the model jumps as high as possible. In the direct dynamics approach all muscle forces are known. In the case of inverse dynamics only the resultant joint torques are known, the force sharing between muscles to give the resultant joint torques needs still to be solved. Having additional information such as EMG data gives an estimation of the force sharing of certain muscle groups, but no direct relationship between EMG and muscle force production has been documented yet [31], [57]. Another solution to solve the force sharing

problem in inverse dynamics would be to apply an optimization criteria such as minimizing the joint forces [20]. Inverse dynamic calculation of resultant joint torques itself has its difficulties when the model setup does not match the kinematic data measured, ie. when the model joint axes are fixed but the real joint axes such as the knee joint are allowed to move, high forces occur [11]. A very elegant method to solve this problem and the problem of muscle force sharing together was carried out by Wright et al. [80]. The rigid body model with muscles was forward simulated, optimizing the muscles active state by minimizing the difference between the forward simulated and the measured kinematic data. This method is very elegant because it also solves the problem of applying real life kinematic data to a rigid body model.
The aim of this study is to investigate the function of series elasticity in drop jumping performance. Having the jump height already given in the inverse dynamics method, the effect of varying series elasticity on jump height can not be investigated. Therefore the direct dynamics method was chosen.

4.2 Validation strategy

For model validation the vertical sinking of the body CM from touch-down to its lowest height Δs and the vertical CM take-off velocity are chosen. CM take-off velocity is closely related to jump height and represents the performance of the jump. The joint kinetics and muscle energetics in the downward movement are represented by Δs. Both parameters are calculated for varying ground contact times and drop heights.
The model is considered to be valid when the calculated jump height and Δs are in the range of the standard deviation found in the measurements of Arampatzis et al. [3].
No direct relationship has yet been documented between measured EMG and active state of the muscle [31], [57]. On the other hand the electrical signal causes the muscle to be in an active state. Good agreement between the calculated active state and the EMG amplitudes underly the validity of the activation model.
The sensitivity of the model to varying initial conditions and muscle parameters was tested to show the model stability, in other words to what extent small changes in the initial conditions or muscle parameters leads to completely different model behavior.
In addition to the model and model parameter validation, errors in the formulation of the equation of motion and the numerical accuracy of the integrator to solve the equations of motion can be tested when Newton's second law is

maintained within numerical tolerances during the whole simulation time.

4.3 Jumping performance

In the study from Arampatzis et al. [3] drop jumps from 20, 40 and 60 cm height were measured. The athlete was given the command to jump as high as possible. Additionally for each jump height the subjects performed jumps with varying contact times. The drop jumps for each person were grouped into five groups according to their ground contact times. The ground contact times for the five groups averaged over 15 subjects jumping from 20 cm can be seen in fig. 4.1. The CM take-off velocity has almost the same value of

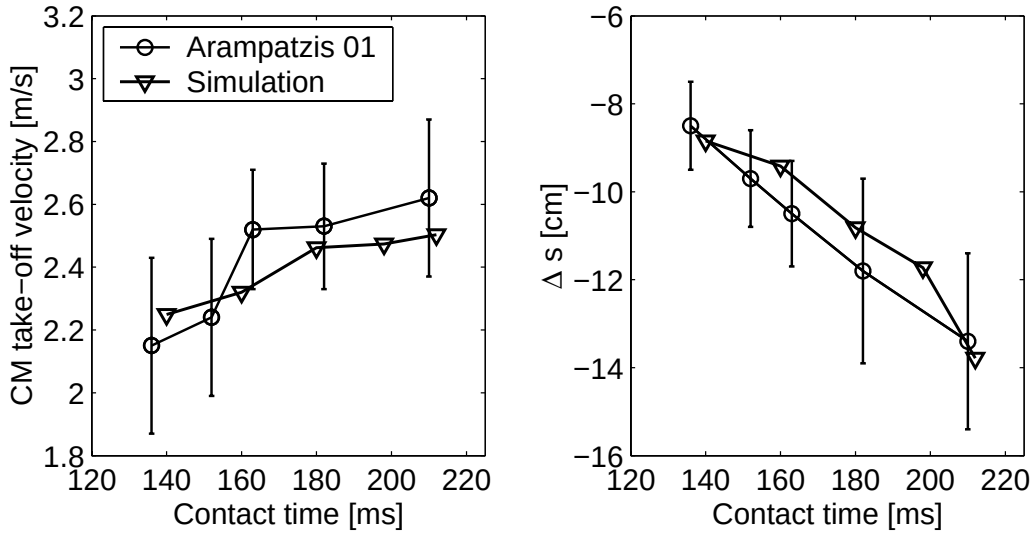

Figure 4.1: *Comparison between simulation results and measured drop jumps from Arampatzis et al. [3]. with different contact times. The CM take-off velocity and the maximum vertical sinking of the CM Δs are shown for five different ground contact times.*

2.5 m/s for contact times from 210 down to 162 ms, and gets smaller with a further reduced contact time. Five drop jumps from 20 cm height were simulated. The model was forced to choose a certain ground contact time, giving a penalty to the cost function when the contact time was not in the range specified. The ranges for the five simulations were 120-140 ms, 140-160 ms, 160-180 ms, 180-200 ms, 200-220 ms. Except for the longer contact times the optimizing process results in a contact time as long as possible in the given

interval. This is reasonable for the contact times slower than 180 ms because in these cases take-off velocity increases considerably with increasing contact time. Comparing the simulated CM take-off velocities with the measured ones in fig. 4.1 the same behavior can be seen. The three longer contact times have almost the same CM take-off velocity and it decreases for the two shorter contact times. However the decrease of the shortest contact time was not as big as in the measurements.
All simulated CM take-off velocities are in the range of the standard deviation measured. Taking into account the general behaviour of the measured mean values, the shortest simulated contact time should yield a smaller take-off velocity compared to the longer contact times. Considering the high force rate in all muscles which goes along with a short contact time there must be some receptory inhibition preventing the muscle from being damaged [23]. No receptory inhibition was included in the model. Although the take-off velocity is within the standard deviation, for the shortest contact time the model was found to be not valid. The drop jump with the shortest contact time is therefore excluded in the result chapter, discussing the SEE energy of the muscles.
With increasing contact time the body CM sinks lower after touch-down (fig. 4.1). The simulated vertical sinking of the CM is within the standard deviation measured.

Jumping from 20, 40 and 60 cm height, with a contact time about 180 ms, the vertical take-off velocity measured by Arampatzis et al. [3] remained constant (fig. 4.2). Bobbert et al. [9] also reported no variation of jumping performance with moderate drop heights up to 60 cm. Other studies investigated drop heights over 60 cm [4], [12], [44]. They found that jump height varies with drop height and that an optimum exists. The decrease of jump height above optimal drop height is assumed by Komi and Bosco [44] to be caused by inhibitory reflexes, because muscle-tendon receptors are triggered by excessively high muscle forces.
The simulated take-off velocities and Δs are within the standard deviation measured by Arampatzis et al. The CM take-off velocities increase and Δs decrease with greater drop heights. The reason for the increase in take-off velocities is the lower vertical sinking (Δs), which manifest in a greater muscle stretch and therefore in a higher force enhancement explained in section 3.2.3. The increase in drop height up to 60 cm is in accordance with the observation made by [4], [12], [44] that an optimal height exists, however the simulated jump height would increase with increasing drop heights above 60 cm, since there is no muscle inhibition included in the model.

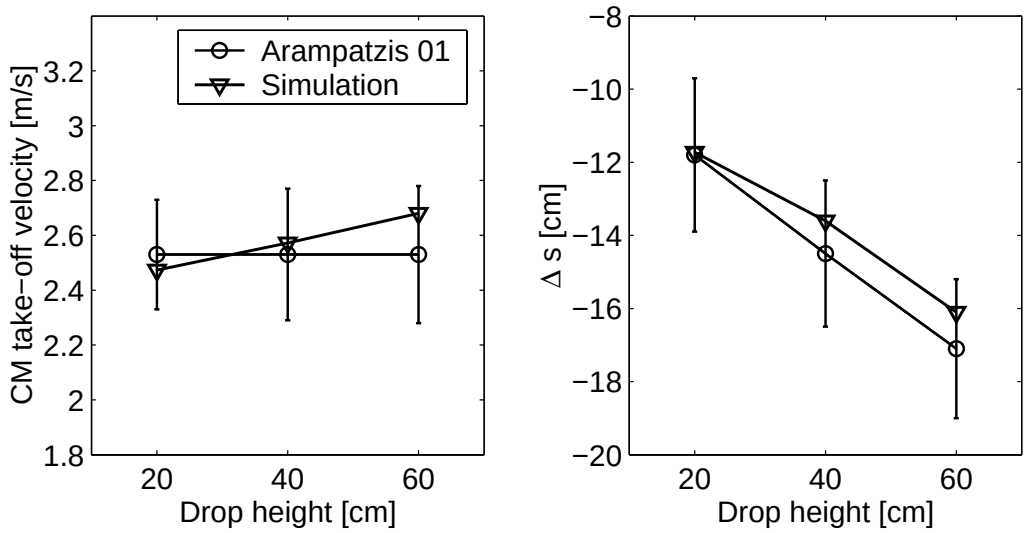

Figure 4.2: *Comparison between simulation results and measured drop jumps from Arampatzis et al. [3]. CM take-off velocity and maximum vertical sinking Δs of the CM are shown for different drop heights, with ground contact times of about 180 ms.*

In conclusion all the simulation results are in the standard deviation measured. The general behavior of the model compared to the measurement indicates that for drop jumping at the shortest contact time and from greater heights the inhibition of muscle activation due to injury prevention mechanisms are missing in the model. Therefore in chapter 5 the effect of muscle elasticity on four drop jumps from a drop height of 20 cm with ground contact times ranging from 160 up to 212 ms is discussed. The model is found to be valid for these four jumping conditions.

4.4 Active state compared with measured electromyogram

In the drop jump study of Arampatzis et al. [3] the EMG signals of five muscles (m. gastrocnemius medialis, m. gastrocnemius lateralis, m. tibialis anterior m. vastus lateralis and hamstrings muscles) were available. The recorded EMG signals were rectified and smoothed and the filtered data were normalized using the maximum EMG data from the trial with the highest leg stiffness as the reference value. Compared are the filtered EMG data

with the calculated active state predicted by the model (fig. 4.3). Shown are two drop jumps with 160 and 212 ms simulated contact times which are compared with 153 and 210 ms measured contact times. The muscles m. gastrocnemius medialis as well as m. vasti medialis are compared to the muscles m. gastrocnemius and m. vasti in the model containing the medial as well as the lateral part. Shifting the active state time curves shown in fig. 4.3 about 50 ms to the left, the measured muscle activity agree qualitatively well with the active state calculated. Remembering that the active state is proportional to muscle force, where as the EMG signal has to travel along the muscle and causes chemical reactions to happen so that the muscle force increases. This electromechanical delay from EMG to force takes about 30 to 100 ms [14] and agrees well with the delay between active state and measured EMG observed for the m. gastrocnemius m. vasti and the hamstrings muscles. For m. tibialis anterior no delay can be seen but in the shorter $160\,ms$ jump the activation in the beginning as well as in the end of the shorter jump is in good agreement.
In conclusion the optimized active state agrees qualitatively well with the measured EMG and indicates that the modeled active state function, as well as the optimization process leads to realistic muscle activation patterns.

4.5 Sensitivity of muscle parameters

There are too many muscle input parameters involved, to test all of them systematically with regard to their influence on jumping performance. It is obvious that higher maximum isometric muscle force (F_{max}) and maximum shortening velocity (V_{max}) increase jump height. Important for the validity of the simulation results is, that small changes in some of the muscle parameters ie. SEE slack length or moment arms would lead to a completely different model behavior. To test the sensitivity, the series elastic compliance was changed from 4.0 to 4.5 % strain at maximum isometric force. The model was re-assembled and the muscle parameters were re-optimized to match the resultant joint torques. This procedure causes small changes in all muscle parameters involved in the optimization process described in section 3.2.1.
The jumping performance increases slightly for the more compliant tendon (fig. 4.4) where as the general characteristic, a decrease with shorter contact times remained the same.

4.6 Sensitivity of initial ankle joint angle

The same person performing a variety of drop jumps at their preferred contact time must be able to compensate for small differences in their joint configuration during the flight phase before touch-down. The sensitivity of varying joint angles has been investigated by van Soest and Bobbert [74]. The authors compared a rigid body simulation including Hill type muscles with a model driven by joint actuator torques. They found that the Hill muscles are able to compensate perturbations in the joint angle so that the movement can still be performed. In the case of the torque driven model the movement could not be performed successfully.
Drop jumps from 20 cm with contact times ranging from $180ms$ up to $200ms$ were simulated, increasing the plantar flexion angle about 5 and 10 degrees. Without changing the stimulation pattern the drop jump could still reach 90 % of its height at original joint angle (tab. 4.1).

Table 4.1: *Variation of initial ankle angle and jump height reached with the same active state function as with unchanged ankle angle and with a re-optimized active state function.*

$\Delta\phi$	Jump height [%], same active state	Jump height [%], re-optimized active state
+0	100	100
+5	98	100
+10	90	99

This leads to the conclusion that the viscoelastic properties of the Hill muscles itself can well compensate for perturbations in the ankle angle without changing the active state. This finding agrees well with the results from van Soest and Bobbert. Re-optimization of the active state with the criteria to jump as high as possible leads to almost the same jump height. Therefore the model is not sensitive to small variations in the initial ankle joint angle.

4.7 Validity of the model calculations

Newton's second law, that the CM acted upon by a force moves so that the external force vector is equal to the time rate of change of the linear momentum vector is tested. It can be formulated for the linear as well as for the angular momentum P and L, respectively

$$\dot{\boldsymbol{P}} = \sum_i \boldsymbol{F}_i^{(ex)} \tag{4.1}$$

$$\dot{\boldsymbol{L}} = \sum_i \boldsymbol{T}_i^{(ex)}. \tag{4.2}$$

$\boldsymbol{F}_i^{(ex)}$: external force.
$\boldsymbol{T}_i^{(ex)}$: external angular momentum.

The linear momentum P is defined as the overall body mass (M) times the second derivative of the CM vector ($\boldsymbol{R}$). For the practical application equation 4.1 and 4.2 are integrated which is demonstrated for the linear momentum

$$\int_0^t M\ddot{\boldsymbol{R}} = \int_0^t \sum_i \boldsymbol{F}_i^{(ex)} \tag{4.3}$$

$$M\dot{\boldsymbol{R}}(\boldsymbol{t}) - M\dot{\boldsymbol{R}}(\boldsymbol{0}) = \int_0^t \sum_i \boldsymbol{F}_i^{(ex)}. \tag{4.4}$$

The definition and integration of angular momentum can be found in [11]. To demonstrate that eq. 4.1 and 4.2 are true during the simulation process the left side of eq. 4.4, the momentum difference, is compared with the right side, the integrated external forces (fig. 4.5).

The differences between the integrated forces and torques and the momentum change are maximally 0.04. The maximum differences are found at the time of ground contact or take-off where numerical difficulties occur. The reason for those errors are first in the integration of the equations of motion with the simulation program (DADS, LMS international), and second in the integration of the external forces and torques. The errors were found to decrease with increasing accuracy specified in the simulation program. The errors of the simulation program can be reduced by lowering the maximum integration step size and the solution and integration tolerance. Changing this values is going along with high computational cost so the errors observed here are accepted.

The results indicate that Newton's second law is maintained within numerical accuracy and no systematic errors violating the equations 4.1 and 4.2 by programming the model and its muscle, wobbling mass, joint limiter and contact forces were observed.

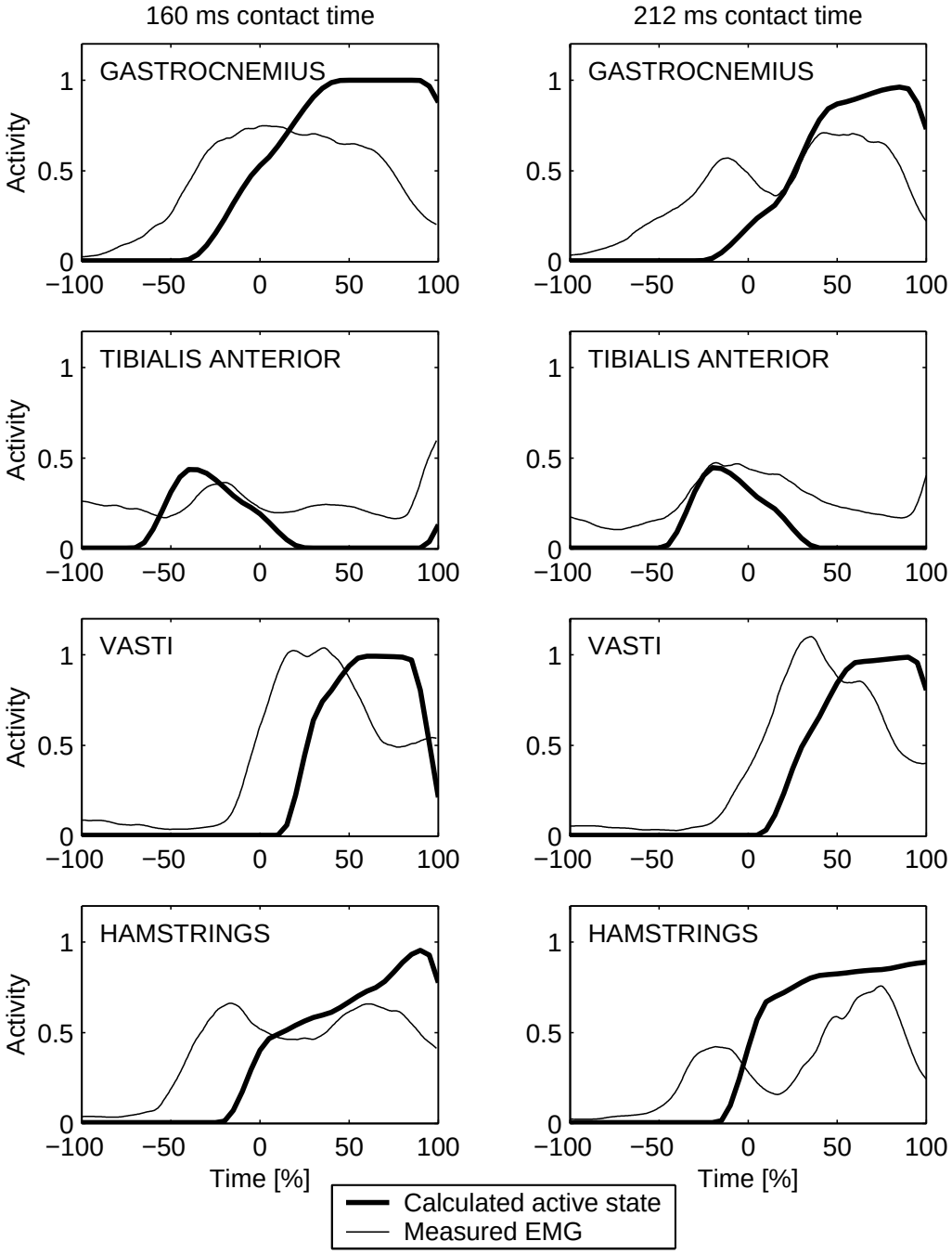

Figure 4.3: *Comparison between measured EMG from Arampatzis et al. [3] and optimized active state. Measured data of four different muscles were available: Gastrocnemius medialis, vastus medialis hamstrings and tibialis anterior. The simulated jumps with 160 and 212 ms contact time were compared with those measured at 153 and 210 ms contact time. The drop height for both jumps was 20 cm.*

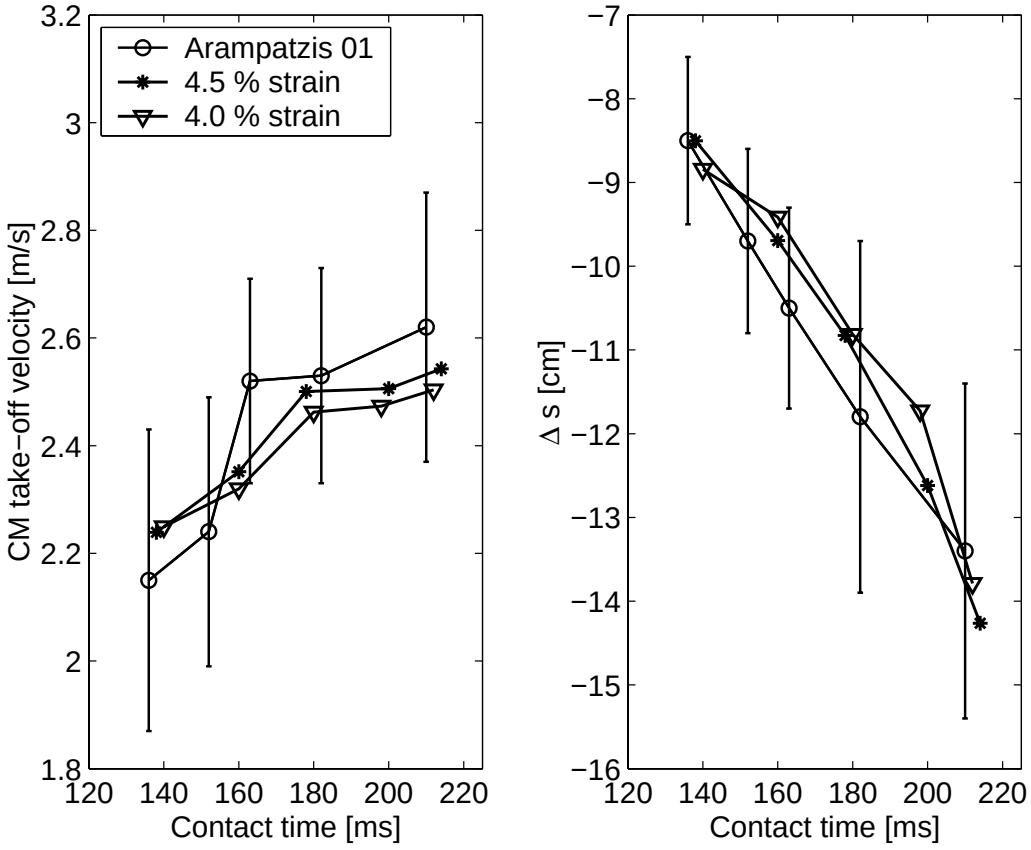

Figure 4.4: *Comparison of two simulation results, one with* 4.0 % *the other with* 4.5 % *strain of the SEE at maximum isometric force. The CM take-off velocity and the maximum vertical sinking of the CM* Δs *are shown for five different ground contact times. Both drop jump simulations were optimized to jump as high as possible.*

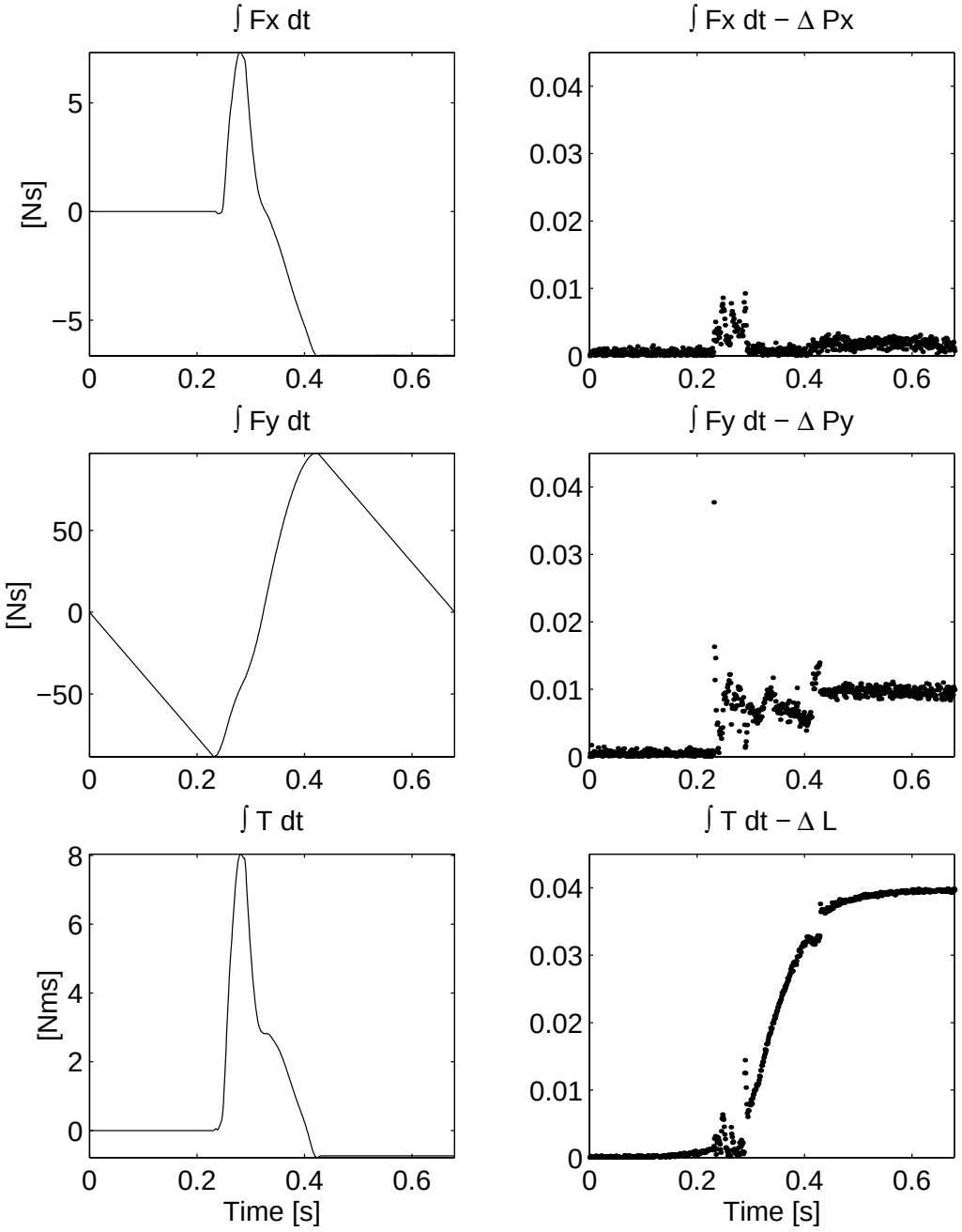

Figure 4.5: *On the left side the integrated external forces in horizontal (Fx) and vertical direction(Fy) and the integrated external torques acting on the rigid bodies in drop jumping are shown. The basic equations 4.1 and 4.2 are true when the linear and angular momentum difference is equal to the integrated external forces and torques respectively. Errors during the simulation are demonstrated by subtracting the linear and angular momentum difference from the integrated external forces and torques which is shown on the right side. The contact time for the drop jump shown is 200 ms.*

Chapter 5

Simulation results and discussion

In this chapter the three hypotheses about the function of series elasticity formulated in the introduction are investigated. The three hypotheses are demonstrated on four drop jumps from 20 cm drop height with contact times ranging from 212 ms (jump 1) down to 160 ms (jump 4). In the first section drop jump energetics for the rigid bodies as well as for the muscles are explained in general. In the next section the energetics for different muscles are compared, and the sum of the SEE energy of all muscles is calculated and set into relation to the overall muscle energy as well as to the energy of the rigid bodies. The energy values are given as mean values over the four drop jumps considered. The four jumps were simulated with different tendon compliance as well, which lead to different muscle energies. The sections 5.3 and 5.4 show the effect of SEE on the CE force generating ability.

5.1 Simulated drop jumping

The drop jump is separated in two phases, the downward movement until the potential energy of the body reaches its minimum and the upward movement where the potential energy increases until it is greater than the initial potential energy (fig. 5.1). During ground contact the muscles generate forces to decelerate the body CM during the downward movement and to accelerate the body CM during the upward movement. The muscles acting against gravity in the model are m. soleus and m. gastrocnemius at the ankle joint, m. vasti and m. rectus at the knee joint, m. gluteus and the hamstrings muscles at the hip joint. All these muscles acting against gravity perform

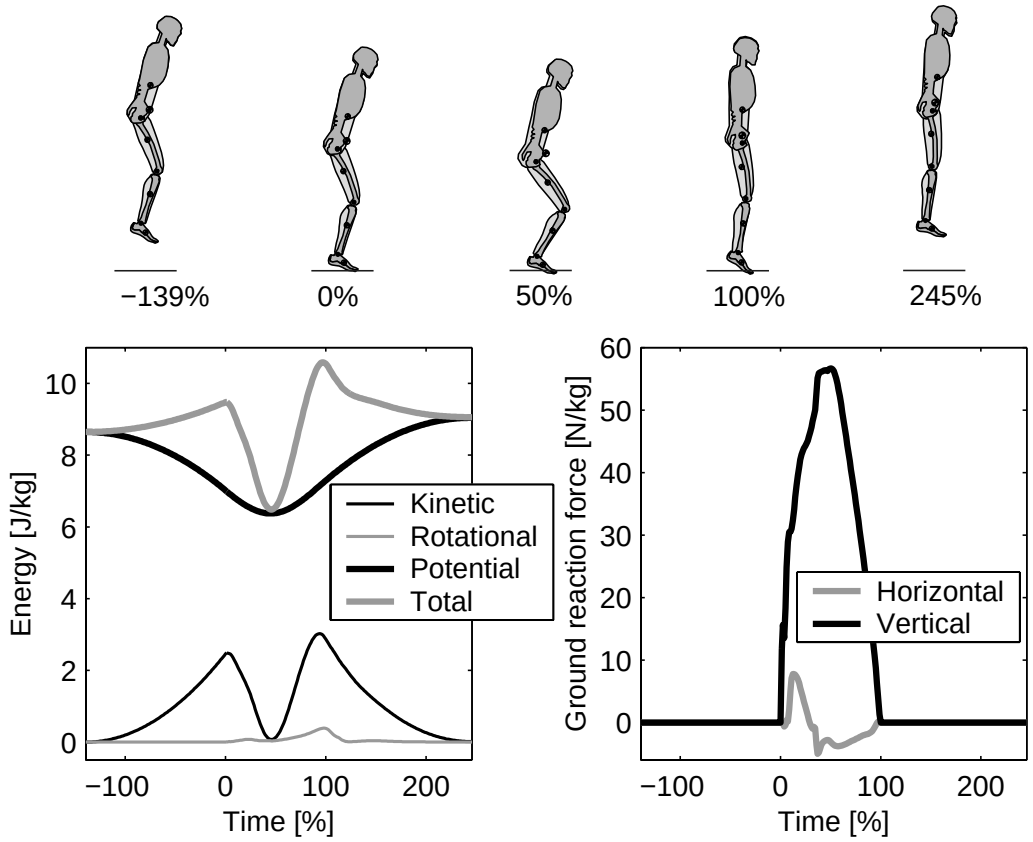

Figure 5.1: *Pictures, energies and ground reaction forces in simulated drop jumping. The model starts from 20 cm foot height. The maximum jump height is reached at* 145 % *ground contact time after take-off. The absolute ground contact time for this jump is* 160 *ms*

a so called stretch-shortening cycle. First during the downward movement the muscle-tendon-unit (MTU) is stretched and then shortened during the upward movement, the MTU and CE length for m. vasti are shown in fig. 5.2. In the eccentric phase, when the MTU or the CE is stretched, its power output is positive. In the concentric phase when the MTU or the CE is shortened its power output is negative. In fig. 5.2 the CE elements do not follow the same stretch as the MTU, part of it is taken up by the SEE. When the muscle is not activated the change in length of the CE and the MTU is the same. With increasing activation the CE tries to shorten, the SEE is stretched and elastic energy is stored. When the CE is stretched while its activated mechanical energy is dissipated. When the MTU is shortened, the

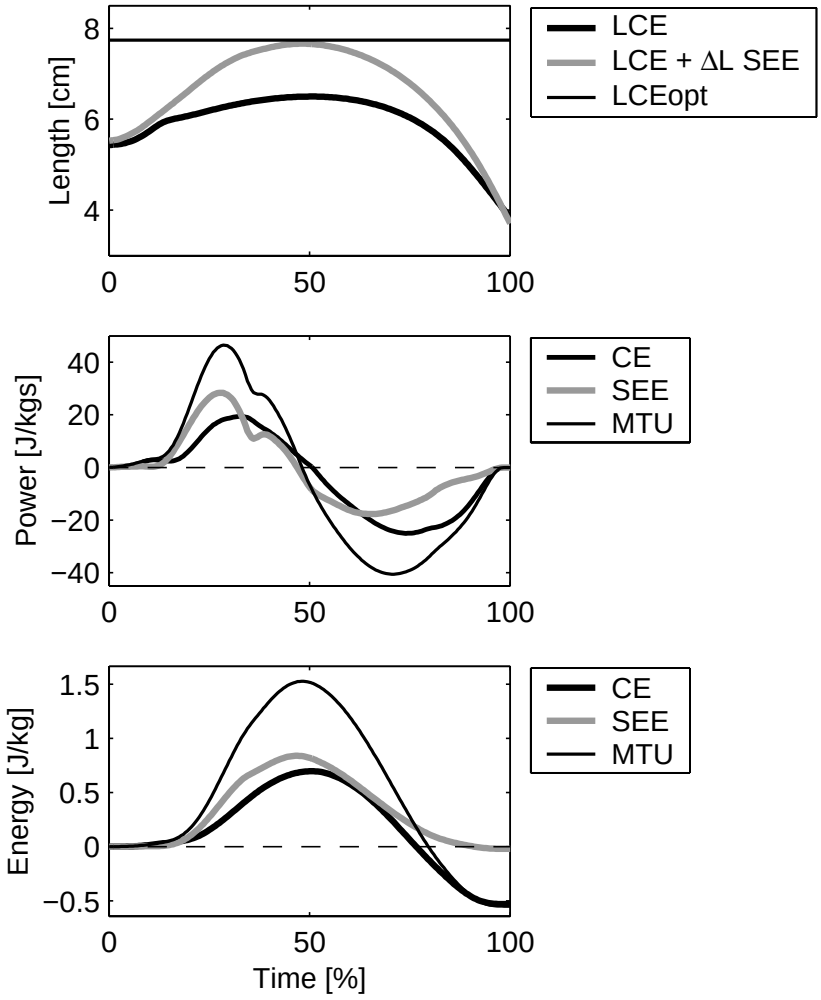

Figure 5.2: *Muscle length, power and energy of m. vasti during drop jumping from 20 cm with 160 ms contact time.*

elastic strain energy is returned and contributes to the overall muscle power output in the concentric phase (fig. 5.2). The SEE is ideally elastic therefore no energy is dissipated, most of its energy is returned at the end of the stretch shortening cycle. A small amount of about 6 % strain energy remains at the end of ground contact (fig. 5.8), because the muscle force does not drop to zero at take-off. In the drop jump shown in fig. 5.2 in which the jump height is higher than the drop height, the mechanical energy of the CE and the MTU is lower than in the beginning of the jump. That means that during the drop jump the CE generated more energy than it dissipated.

5.2 Muscles mechanical energies

In the following sections only the six muscles acting against gravity m. soleus, m. gastrocnemius, m. vasti, m. rectus m. hamstrings and m. gluteus are considered. These six muscles are performing a stretch-shortening cycle during ground contact. Even though m. tibialis anterior and m. iliopsoas are not considered during the contact phase they can not be removed from the model, they are important in the flight phase after ground contact. The muscles acting against gravity produce high body segment accelerations at take-off, which would cause the joints to reach their range of motion limits. The consequences of excluding tibialis anterior and m. iliopsoas would be unrealistic high joint limiter forces. Co-contraction of m. tibialis anterior and m. iliopsoas prevent that from happening at the ankle and hip joint respectively. Additionally m. tibialis anterior is also activated before ground contact (fig. 4.3) to make the ankle stiffer without changing its touch-down angle too much. To demonstrate the function of tibialis anterior all muscle torques acting around the ankle joint during drop jumping are shown in fig. 5.3.

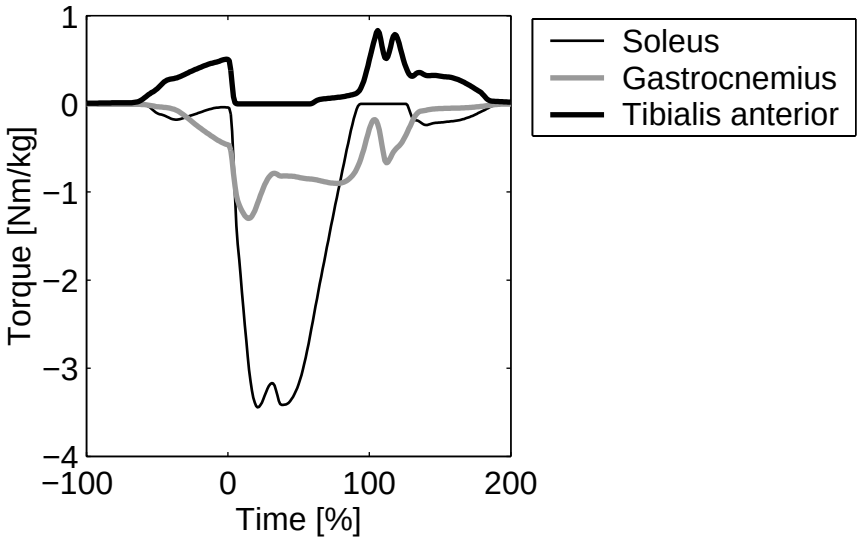

Figure 5.3: *Muscle torques around the ankle joint for a drop jump from 20 cm with 160 ms ground contact time. M. tibialis anterior generates torque against the plantarflexor muscles m. soleus and m. gastrocnemius before and at the end of ground contact to stabilize the ankle angle.*

Regarding the CE and SEE energies during ground contact for different mus-

cles, a difference can be distinguished between the muscles crossing one and the muscles crossing two joints. According to the data from Winters [78] the one joint muscles are able to produce a higher maximum isometric force than the two joint muscles crossing the same joint (fig. 5.4 B). On the other hand

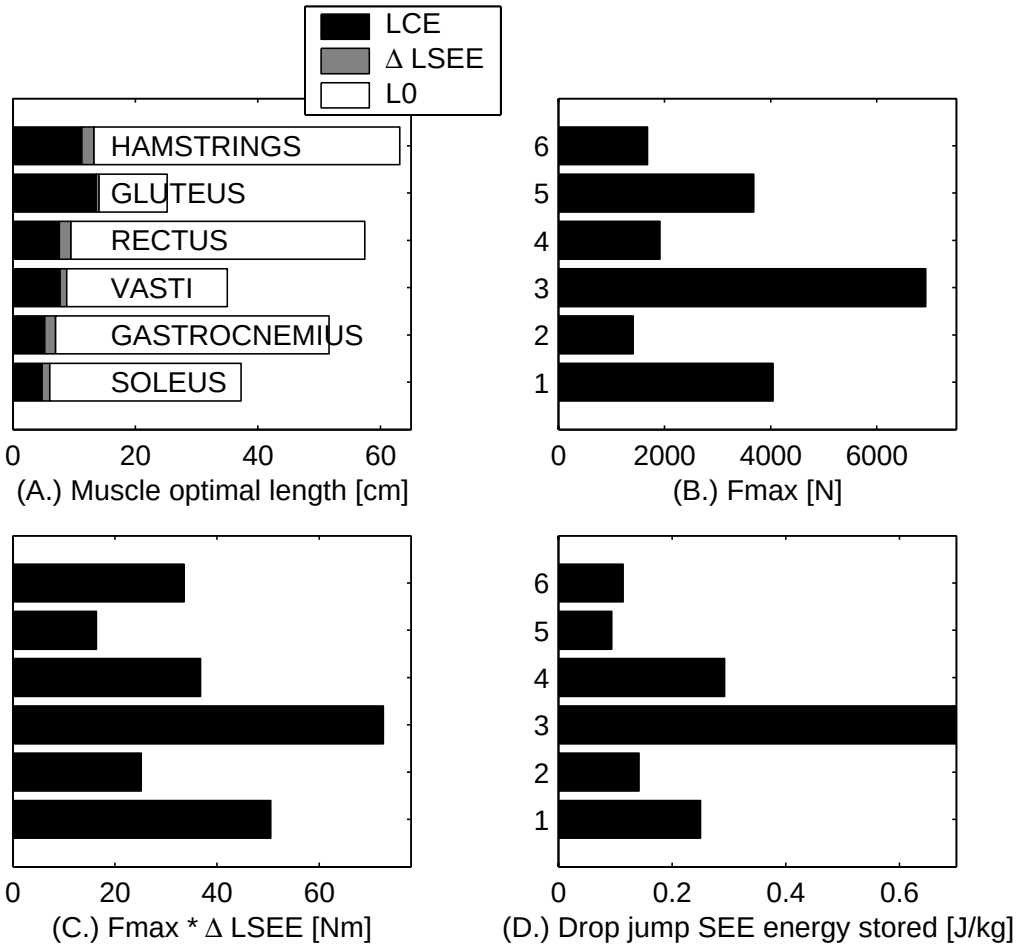

Figure 5.4: *(A.): Muscle component lengths at maximum isometric contraction at optimal joint angles for each muscle. LCE is the CE length Δ LSEE is the stretch of the SEE due to the isometric force. L0 is the SEE length when no force is produced by the muscles. (B.): Maximum isometric muscle forces. (C.): Muscles abilities for SEE energy storage. (D.): Maximum energy stored in the muscles averaged over four drop jumps with contact times from 160 up to 212 ms.*

the two joint muscles have a longer series elastic element (fig. 5.4 A). Since the series elastic energy is defined as force times stretch, a high maximum

force as well as a long SEE length together result in a high potential for energy storage shown in fig. 5.4 C. The amount of energy stored shown in fig. 5.4 D. results from averaging the maximum stored energy for each muscle over four drop jumps with contact times ranging from 160 to 210 ms. Comparing the potential of energy storage in fig. 5.4 C with the actual amount of energy stored in fig. 5.4 D, both graphs are closely related. Adding up the one and two joint muscles acting around the same joint the most energy is stored in the muscles acting around the knee joint and least in the hip joint.

At the ankle joint m. soleus and m. gastrocnemius together store 0.38 J/kg elastic energy. The amount of energy for one muscle is normalized to half of the total body weight of 78 kg. Measurements of Fukashiro et al. [28] at the achilles tendon determined 0.47 J/kg and 0.21 J/kg SEE storage in hopping and squat jumping respectively. The amount of energy calculated in this study for drop jumping is within the values for squat jumping and hopping, normalized also to half of the bodyweight of the subject participating in the study of Fukashiro et al.. The higher value found in hopping compared to drop jumping is reasonable because in hopping the knees do not contribute much to the overall movement, the plantarflexors are mainly responsible for moving the body CM. The lower values in squat jump are due to the lower muscle stretch because the body starts from a squatting position and has no potential energy to decelerate it compared to a 20 cm drop jump.

Regarding the CE and SEE energies over time for a maximum height drop jump with a contact time of 160 ms, the one and two joint muscles show a different behavior (fig. 5.5).

In the two joint muscles the energy is returned later during ground contact and the amount of dissipated CE energy is less. For m. rectus there is even no CE stretch seen during ground contact and therefore no energy is dissipated.

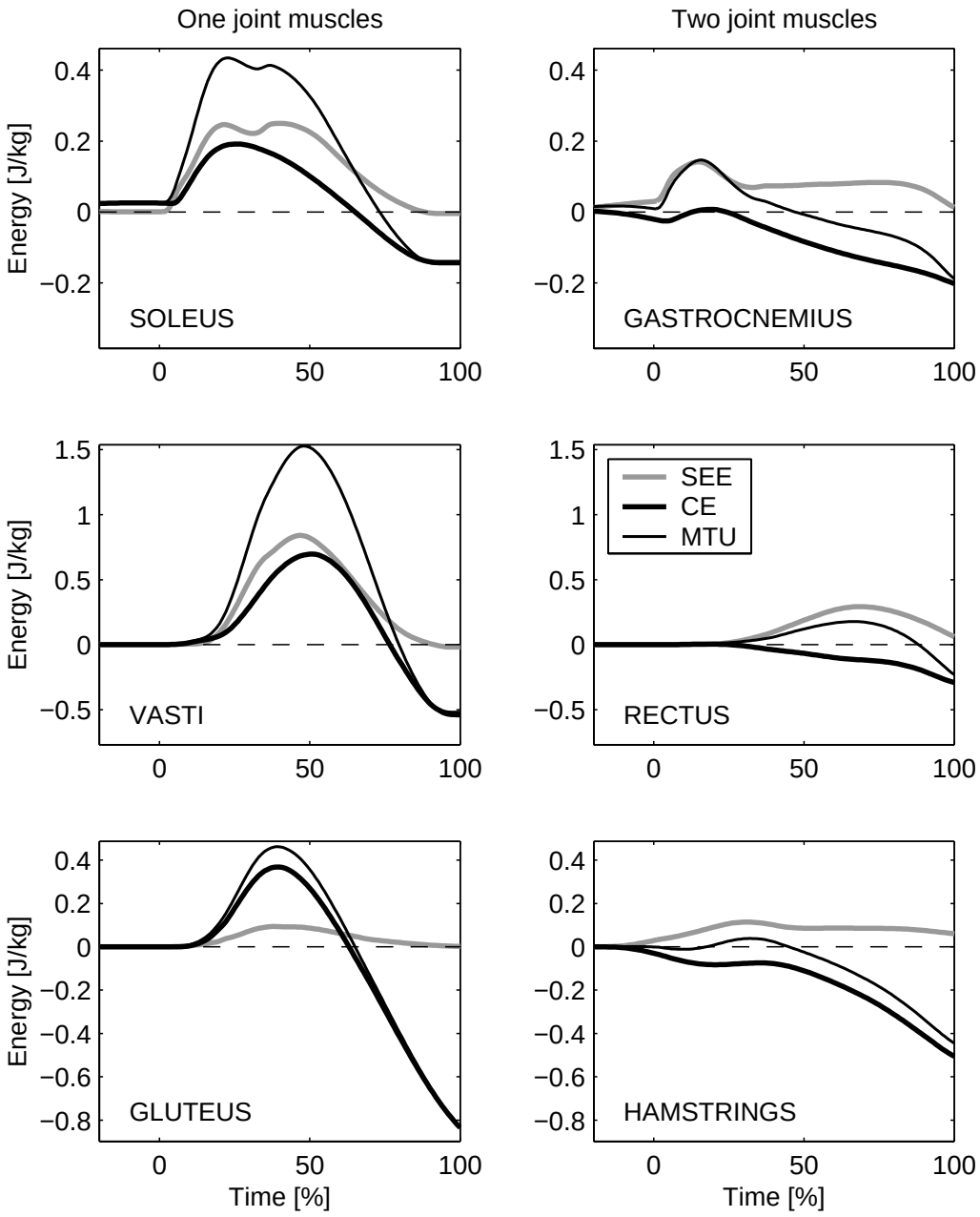

Figure 5.5: *Muscle energies for a 20 cm drop jump with 160 ms contact time. The energy is obtained by integrating the negative and the positive muscle power over time.*

Having discussed the energetics of individual muscles in drop jumping the hypotheses to prove is, whether or not the stored SEE energy contributes considerably to the muscle energy during drop jumping. To show the contribution of the SEE energy, the CE, SEE and MTU energy for all muscles acting against gravity is calculated from the start of the jump to take-off. The following flight phase is not considered. The sum of the stored SEE energy for all muscles is compared to the energy generated by the CE. The energy is calculated by integrating the power over time. The integration was completed for the positive and negative power separately which is equivalent with the eccentric and the concentric phase respectively. In the eccentric phase shown in fig. 5.6, the energy dissipated in the CE's is about the same

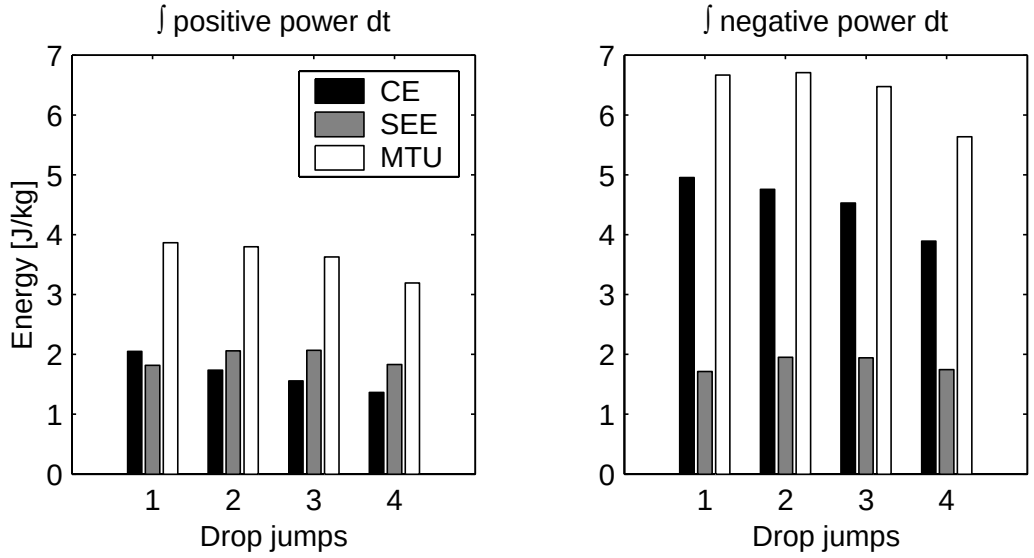

Figure 5.6: *Muscle energies of four drop jumps with contact times from 212 ms (drop jump 1) down to 160 ms (drop jump 4). The energy is obtained by integrating the negative and the positive muscle power over time. Negative power means that the muscle is shortened during force production. This is mostly the case for the upward movement.*

as the energy stored in the muscles SEE's. In the concentric phase the average stored SEE energy of 1.8 J/kg contributes to 29 % of the MTU average concentric energy of 6.4 J/kg. Anderson and Pandy [2] calculated the contribution of SEE for countermovement and squat jumps. The contribution of SEE energy determined by these authors was 35 % of the MTU concentric energy. Counter movement and squat jumps did not show big differences in the amount of series elastic energy stored. The contribution of SEE energy

is 6 % higher than those found in this drop jump study. The reason for the higher contribution of the strain energy in the study of Anderson and Pandy might be the higher maximal strain value in their model, which is up to 6 % depending on the muscles, compared to a strain of 4 % in the drop jump model.
Summarized there is a considerable amount of 29 % series elastic energy contributing to the concentric muscle energy in drop jumping.

In the next paragraph the muscle energy is compared to the potential energy of the body CM and the wobbling mass coupling energy. In fig. 5.7, 151 %

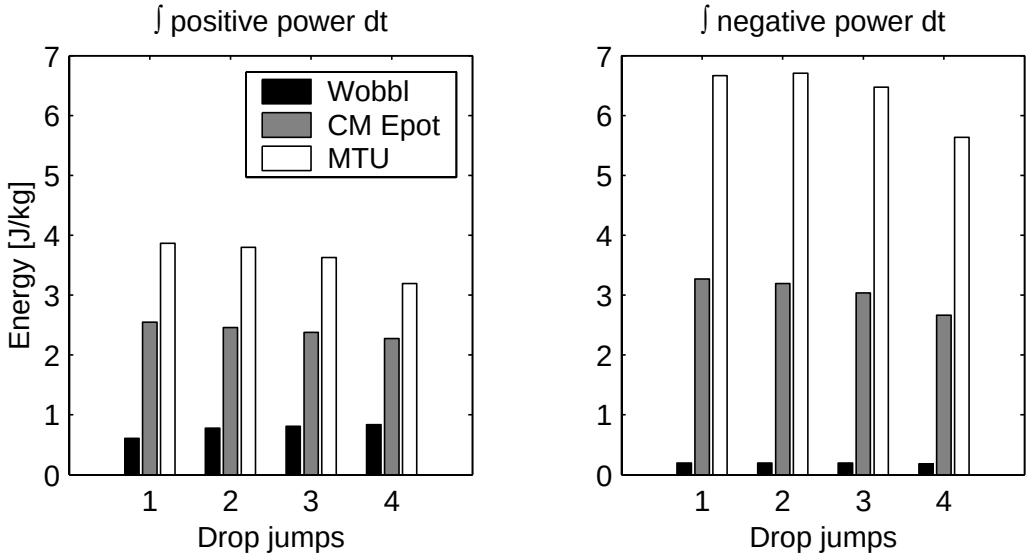

Figure 5.7: *Muscle energies (MTU) and wobbling mass energies (Wobbl) compared to the energy used to decelerate and to raise the body CM potential energy (CM Epot). Four drop jumps with different contact times ranging from 212 ms (drop jump 1) down to 160 ms (drop jump 4) are shown.*

of the energy to decelerate the CM from its initial drop height to the lowest position is generated by the muscles, 31 % is done by the wobbling masses. In the concentric phase even 209 % of the potential energy to lift the body CM is generated by the muscles. Only 6 % is contributed by the wobbling masses. It is mechanically quite ineffective to raise the CM potential energy with double the amount of muscle energy. Part of the high energy waste can be explained from the muscle coordination to generate mechanical work during the upward movement. This is demonstrated for the knee extension in the following. M. gastrocnemius is on the one hand a plantar flexor muscle

extending the ankle joint. On the other hand it is attached to the knee and acts there against knee extension. The hamstring muscles are hip extensors but work as well as knee flexors and therefore against the muscles extending the knee at push off. Having these muscles working against each other increases the overall muscle mechanical work to raise the body CM.
The calculations done here are purely mechanical and do not consider metabolic energy. The SEE energy return does not require any metabolic energy, but the metabolic energy needed for the CE is higher than the mechanical work calculated. This is because in isometric contraction the mechanical energy generated by the CE is zero when the muscle length is kept constant, whilst in reality the muscle needs a lot of metabolic energy to keep the muscle tension.
The maximum metabolic efficiency with which a muscle may transfer chemical energy from the oxidation of food into mechanical work is about 25 % [52]. The muscles need 209 % of the rigid body energy to lift the CM. The contribution of elastic energy to the muscle energy is 29% so that the CE has still to generate 149 % of the CM potential energy to lift the body. Together with the metabolic efficiency of maximal 25 % the muscle is found to be very inefficient in maximal height drop jumping.

By increasing the SEE compliance from 4.0 to 4.5 % on average 10 % more energy was stored in the SEE in all four drop jumps considered (fig. 5.8). The eccentric energy of the CE is reduced about 13 % so that less energy was dissipated in the CE element during downward movement. With the higher amount of elastic energy returned the CE does not produce less power in the concentric phase of all four drop jumps. For the slowest and the fastest drop jump number 1 and 4 respectively the concentric energy of the CE was almost the same as those with 4.0 % strain. For the other contact times, jump number 2 and 3, the energy was lower. On average 2 % less energy was generated by the CE with the 4.5 % maximum strain compared to the 4.0 % maximum strain.
As shown in section 4.5, the CM take-off velocities were higher for the more compliant SEE. This is a result of the higher amount of energy released from the SEE. The amount of concentric CE work remains almost the same for jump 1 and 4 and is reduced for jump 2 and 3.

So far the energy values of the muscles were averaged over four drop jumps with different contact times ranging from 212 (jump 1) to 160 ms (jump 4). Now the behavior with different contact times is discussed. It has to be remembered that the jumps 1,2 and 3 resulted in almost the same take-off velocity whereas jump 4 showed a considerable decrease (fig. 4.4). The over-

all muscle energy shown in fig. 5.6 shows the same behavior. It decreases for jump 4. For both simulations, the one with 4.0 % and the other with 4.5 % maximum strain, the CE energy in the concentric as well as in the eccentric phase shows a decrease with shorter contact times (fig. 5.8). The decrease of the CE energy can be explained by the smaller muscle length change due to smaller joint motion in the faster jumps. To obtain the same amount of muscle energy in the jumps 2 and 3 more series elastic energy has to be used in the concentric phase. The higher amount of series elastic energy storage in jumps 2 and 3 can be explained by higher maximum knee extensor forces in the jumps 2 and 3 of 4 % and 8 % respectively. Drop jumps 1 and 4 show nearly the same maximum force in the knee extensor muscles. This higher knee extensor force in jump 2 and 3 results from of a complex connection between the activation functions, the force-length properties, force-velocity properties and force enhancement following stretch for the muscles acting around the knee joint.

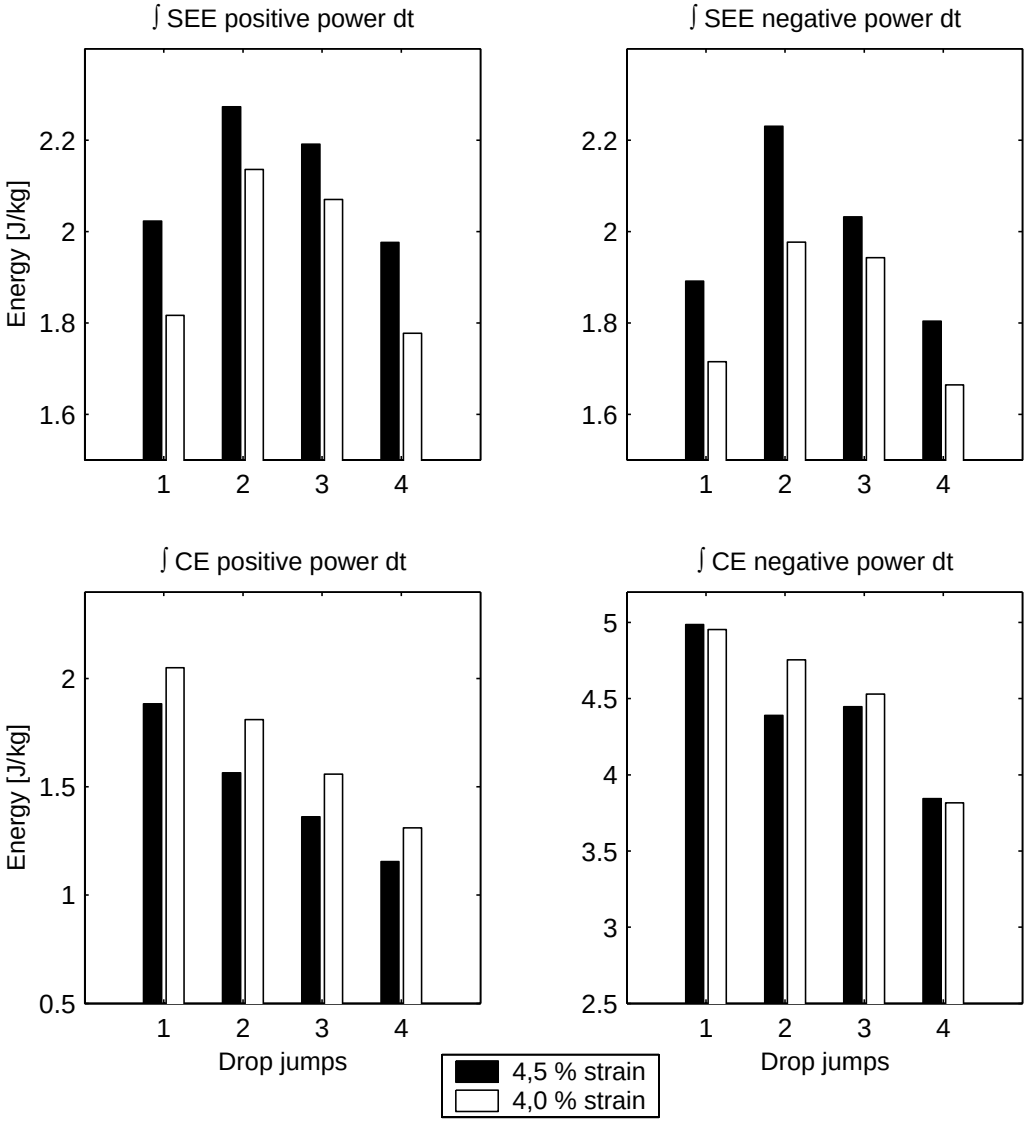

Figure 5.8: *Energy for drop jumps with different contact times ranging from 212 ms (drop jump 1) down to 160 ms (drop jump 4). The simulation was carried out with* 4.0% *and* 4.5% *maximum strain for all muscles. The energy is obtained by integrating the negative and the positive muscle power over time.*

5.3 Muscles force-velocity potentials

The calculations show that a considerable amount of series elastic energy is stored and released afterwards. In the following it is investigated how the recoil of the stored elastic energy influences the velocity of the CE in the concentric phase.
The MTU and CE velocities of four drop jumps from 20 cm with contact times between 160 and 212 ms are shown in fig. 5.9. All drop jumps show a similar characteristic, first after touch-down the MTU works eccentrical and then at take-off it has a high concentric shortening velocity. The velocity of the CE is smaller than that of the MTU in both the eccentric and the concentric phases. This behavior can bee seen for all muscles acting against gravity for all jumps shown. To demonstrate the force producing ability according to the CE force-velocity properties, the MTU and CE velocities are averaged over all four jumps and the force-velocity potential for the CE velocity is calculated. To discuss the function of series elasticity the elasticity of the SEE is neglected, which means it acts like a stiff cable. The CE velocity is then assumed to have the same velocity as the MTU. Both force potentials during ground contact are shown in fig. 5.10. Regarding the last 50 % of the ground contact, for all muscles the force potential of the CE velocity is higher than the force potential for the MTU velocity. The difference is high for the muscles at the ankle and knee joint and low for m. gluteus and m. hamstrings acting around the hip joint. The one joint muscles m. soleus, m. vasti and m. gluteus start to shorten earlier than the two joint muscles. According to the joint kinematics in drop jumping the two joint muscles remain longer at low shortening velocities which is advantageous for their force-velocity potential.

In conclusion for all muscles part of the MTU shortening distance is taken up by the shortening of the previously stretched SEE. Therefore the shortening velocity of the CE is lower than that of the MTU. A low shortening velocity is advantageous for the force-velocity properties, especially at high shortening velocities at the end of the ground contact the CE can still produce force. In contrast with a stiff SEE, when the CE velocity would follow the MTU velocity, the force would drop to zero. When the force is zero no segment accelerations can be obtained in the last phase and the body take-off velocity would be lower.
The second hypothesis stating that the stored mechanical energy can be used in producing a final velocity greater than that at which the contractile component itself can shorten is true for all muscles acting against gravity and

for all four drop jumps. The other important finding is that in drop jumping the CE of the two joint muscles m. gastrocnemius and m. rectus are in an advantageous situation according to their force velocity potential compared to the stronger one joint muscles m. soleus. and m. vasti.

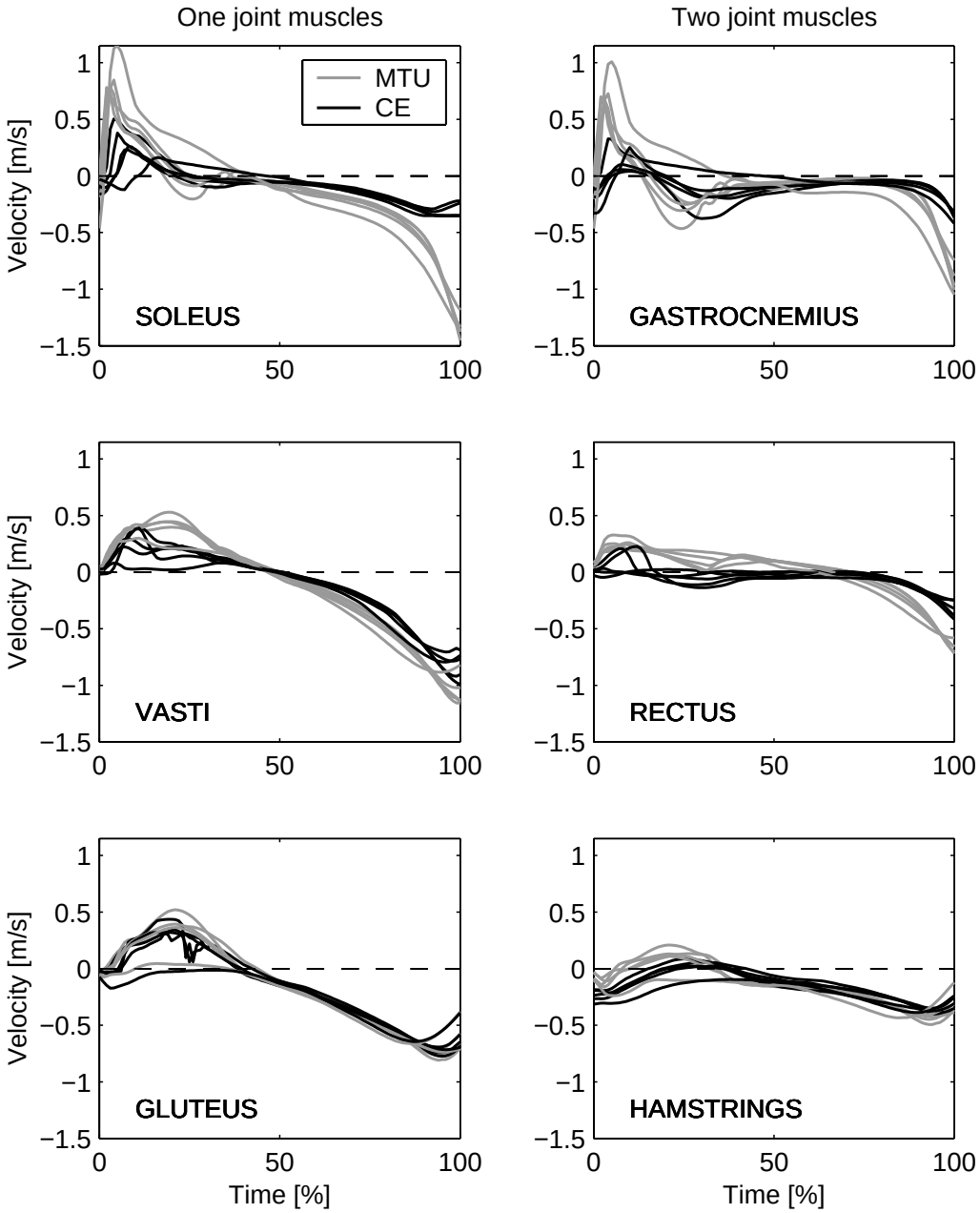

Figure 5.9: *Simulated CE and MTU velocity over time for drop jumps with different contact times ranging from 160 to 212 ms.*

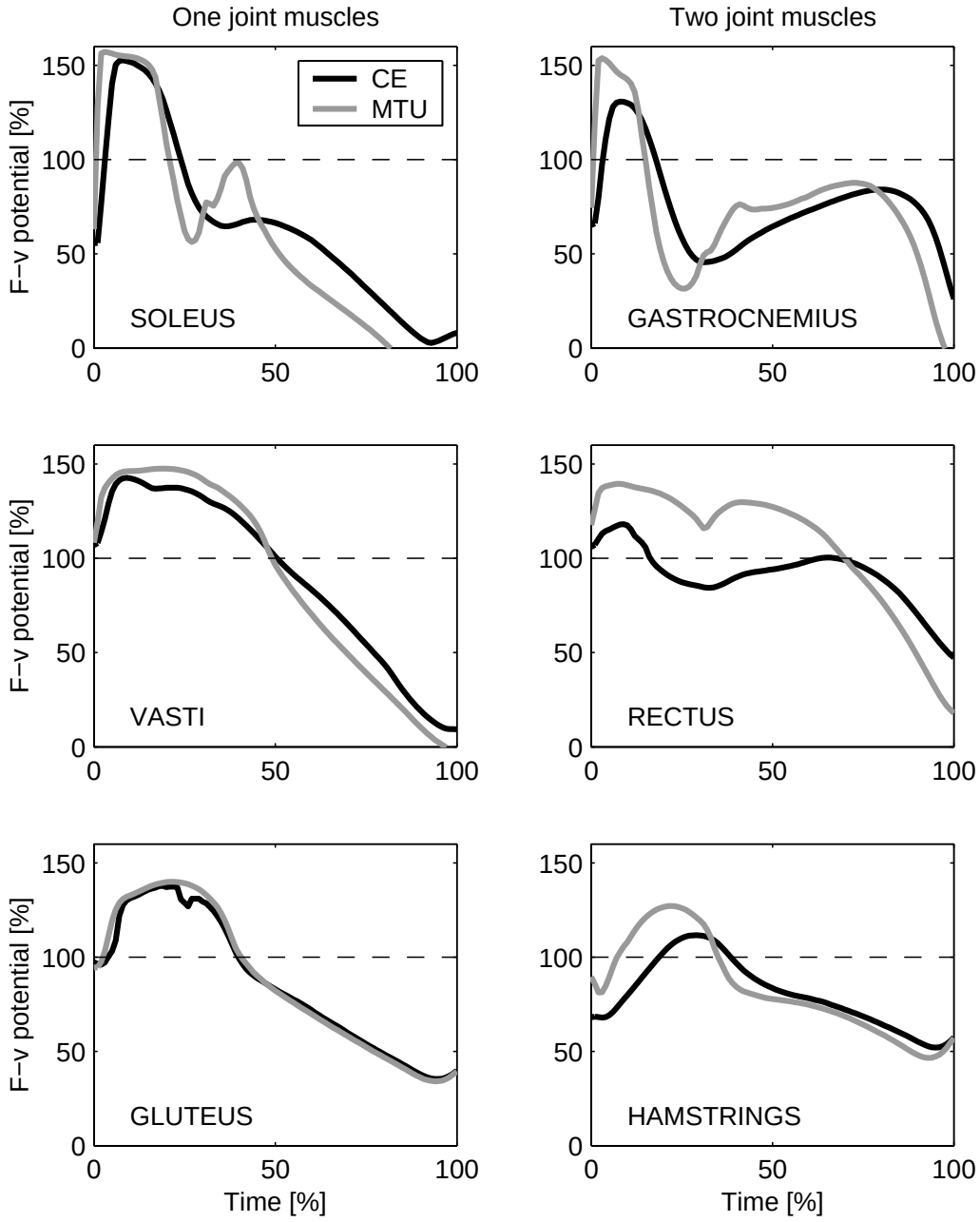

Figure 5.10: *Force potential according to the Hill force-velocity properties. The velocity for the different contact times shown in 5.9 are averaged*

5.4 Muscles force-length potentials

Along the same line as for the force-velocity properties, the effect of SEE elastic compliance on the length of the CE is discussed. The force-length potential according to the parabola described by equation 3.5 is calculated. The force-length potential is best when the length is close to the optimal length L_{CEopt}. In fig. 5.11 it can be seen that the only muscle which reaches optimal length of the CE is m. rectus, which start at a length longer than optimal. All other muscles acting against gravity starts at a CE length shorter than optimal. The CE length of m. soleus, m. gastrocnemius , m. vasti and m. gluteus are stretched up to 20 % from the beginning of ground contact and their force potential increases. At take-off all these muscles have a length shorter than optimal. In case of m. vasti the shortening from maximum stretch is about 40 %. It has to be remembered that in the simulation the CE length is not the fiber length, but the projection of the fibers with a certain angle of pennation on the muscle line of action. The change in length due to the increase in pennation angle is about 20 % of the overall length change measured in section 3.4.1. The CE length change in dynamic situations is difficult to measure on humans. Biewener et al. [6] measured the length change in pigeon's m. pectoralis and found a lengthening of 10-15 % in the beginning and then 30-40 % shortening in the end of the force producing phase. This behavior agrees well with those found for the one joint muscles in fig. 5.11. The CE length of the four different drop jumps vary because the overall muscle length change is greater in the longer jump where the vertical sinking of the body CM is lowest. This leads to greater joint angles, and therefore to longer MTU length and hence the CE length change is dependent on the movement performed.

Regarding the average force potential of the CE in four different drop jumps, its general behaviour is different for the one and two joint muscles. As already seen in the force-velocity potential the shortening velocity of the two joint muscles is lower than that in the one joint muscles. This leads to less length change for the two joint muscles. Especially m. rectus, the knee extensor, remained at about 100 % during the whole movement. With a stiffer tendon the CE stretch would be higher and would be more advantageous for all muscles except m. rectus. Therefore the third hypotheses that series elasticity leads to a higher force-length potential is only true for one muscle in the four drop jumps simulated. For all other muscles the opposite is true, a less compliant or stiff tendon would lead to a length closer to optimal and this leads to a higher force-length potential. Taking into account that the most important muscles which generate the highest energy in drop jumping are the knee

muscles and m. rectus being one of them, its force-length potential is essential for drop jumping performance and therefore tendon compliance serves its purpose in the drop jump excecution for the force-velocity properties as well as for the force-length potential.

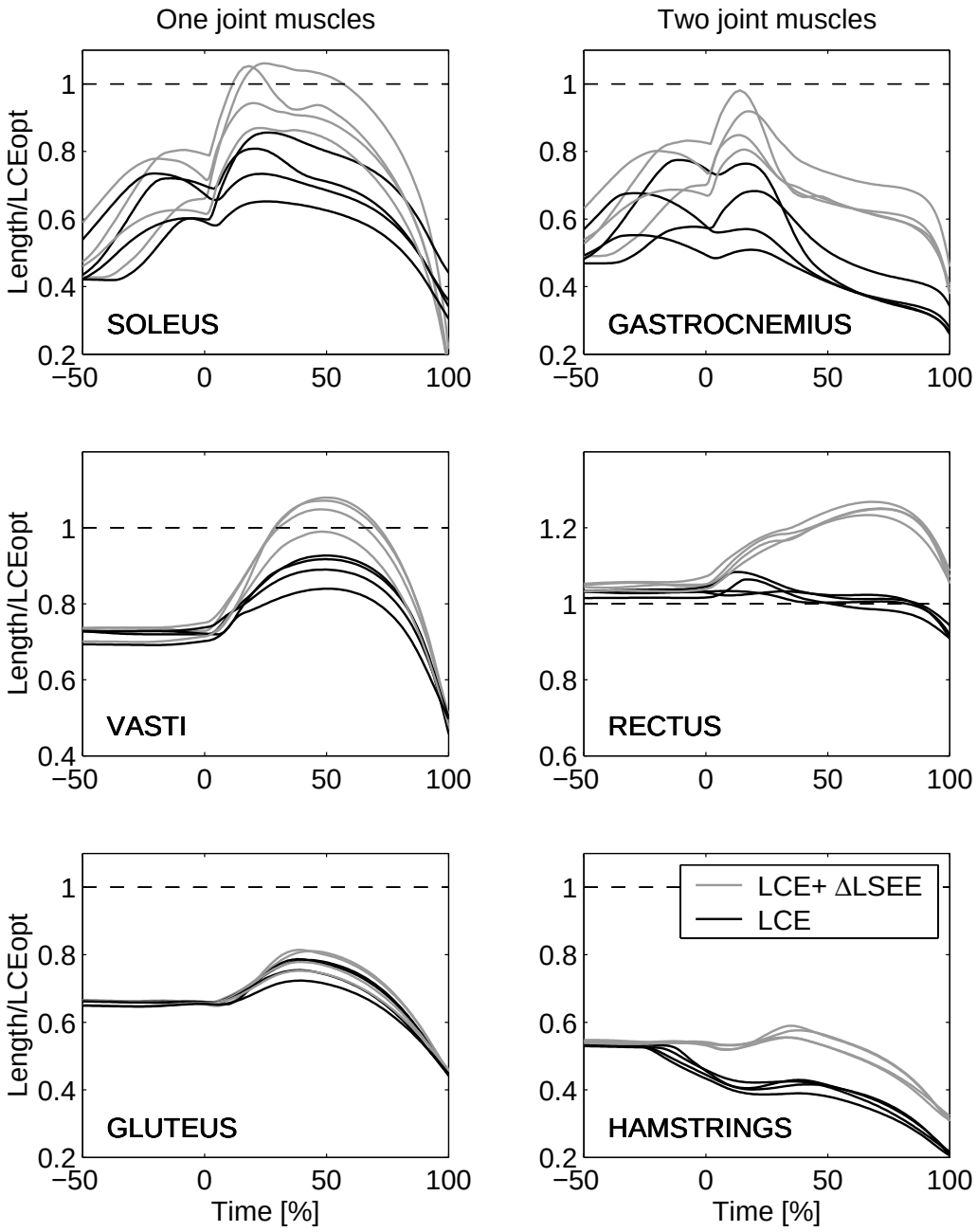

Figure 5.11: *Simulated CE length and CE length plus SEE elongation over time for drop jumps with different contact times ranging from 160 up to 212 ms. The length is normalized to the optimal CE length* L_{CEopt}

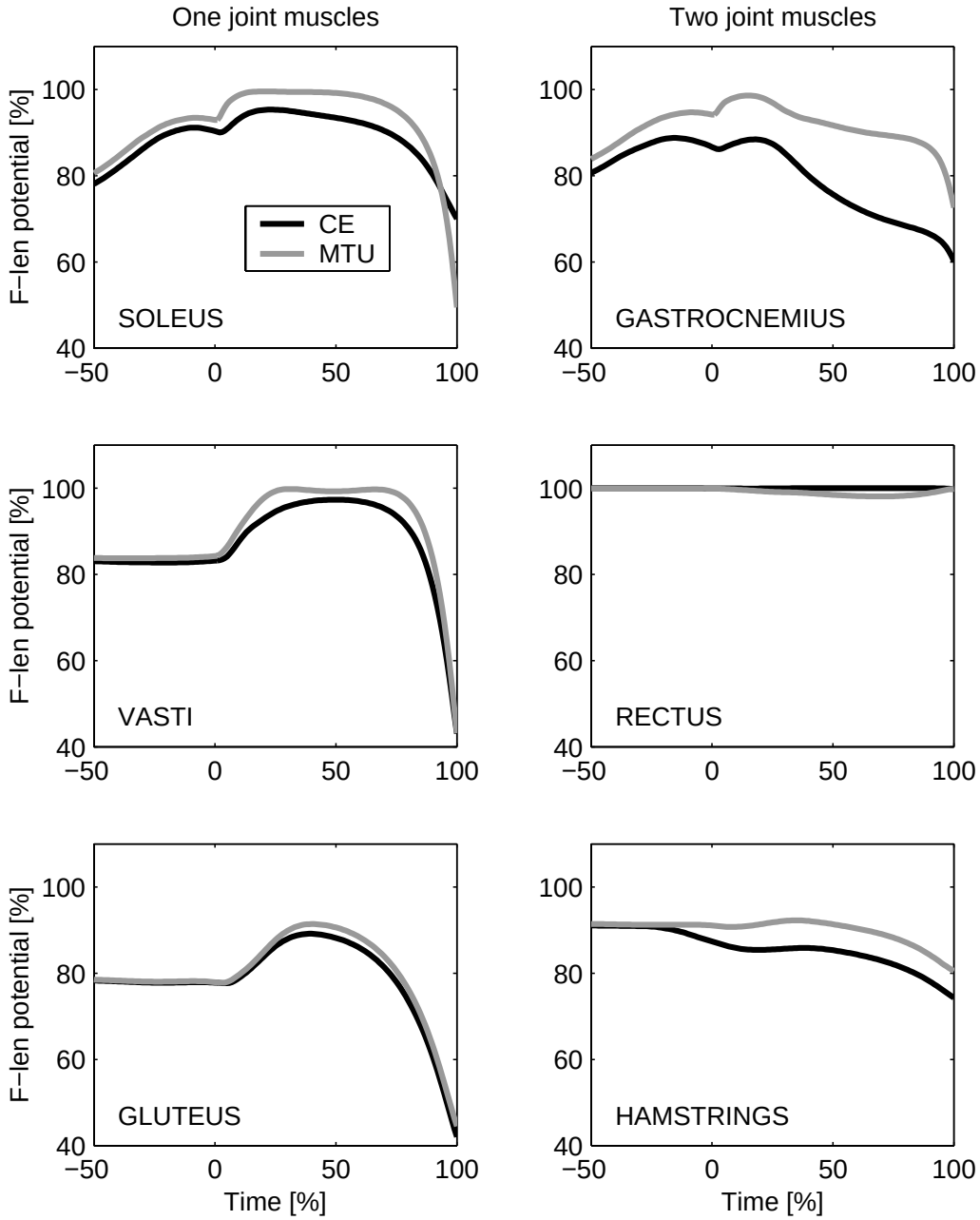

Figure 5.12: *Force potential according to the force-length properties. The length for the different contact times shown in 5.11 are averaged.*

Chapter 6

Summary and future directions

The purpose of this thesis was to develop a computer simulation model to prove the following three hypotheses of the function of series elastic strain energy in drop jumping.

1. A considerable amount of energy can be stored in the muscles SEE's.
2. The SEE's strain energy allows the CE's to reduce their shortening velocity to develop a higher force thanks to the force-velocity property.
3. The SEE's strain allows the CE's to work closer to their optimal length.

The rigid body model developed in this study is able to reproduce the measured drop jump characteristics within the standard deviation measured. This justifies the modelling of the rigid bodies and muscles. Compared to other authors simulating vertical jumping [73], [2], the flight phase after ground contact is also integrated. This requires a more complex muscle active state function, allowing muscles to be activated more than once and change their level of activation. This active state function agrees qualitatively well with the EMG measured in drop jumping.
The following answers to the three hypotheses about the function of SEE in drop jumping were proven with four drop jumps from 20 cm drop height and ground contact times ranging from 160 to 212 ms.

1. A considerable amount (29 %) of the concentric muscle energy is contributed by the SEE energy stored in the eccentric phase. The remaining amount (71 %) is produced by the contractile elements and requires metabolic energy.

The overall concentric muscle energy is about twice as much as the increase of potential energy when the body's CM is lifted from its lowest position. Therefore the amount of SEE energy expressed in percent of the potential energy is 63 %.

2. The SEE's strain energy allows the CE's to reduce their shortening velocity to develop a higher force. This is true for all muscles and all jumps calculated.

3. The SEE's strain allows only the CE of m. rectus to work closer to its optimum length. So that hypothesis 3 is not true for all muscles.

Investigating these hypotheses, differences between one and two joint muscles were found. Due to the joint kinematics in drop jumping all two joint muscles are favored because of their force-velocity potential, especially in the last 50 % of ground contact. According to data from Winters [78], the two joint muscles have smaller PCSA than the one joint muscles. If this ratio between one and two joint muscles measured in vitro is also true for trained athletes has not yet been studied. From the outcome of this study a greater PCSA for the two joint muscles would be advantageous. The second factor found which is important for muscle performance, is that increasing SEE compliance from 4.0 to 4.5 % maximal strain leads to increasing take-off velocities.
Summarized, the athletes abilities of muscle force generation can be be quantified by tendon compliance and by the ratio of the PCSA between the two joint compared to the one joint muscles.

The model is assembled together from different literature sources, not always matching the average trained athlete. The trained athletes themselves show quite different individual jumping techniques which can be seen in the high standard deviations in fig. 1.1. Individual parameters can be obtained and related with the help of the simulation model to the athletes jumping abilities and techniques. This can be done in a standard training situation such as drop jumping. The model can also be extended to competing movements such high or long jump.

Appendix A

List of muscle parameters

a	: Parameter describing the shape of the hyperbolic force-velocity function.
$a1, 2$	: Coefficients to calculate MTU length .
act	: Active state function.
af	: Asymptote factor for the eccentric force-velocity curve.
b	: Parameter describing the shape of the concentric hyperbolic force-velocity function.
c	: Parameter describing the shape of the parabolic force-length function $c = 1/width^2$.
$c1, 2, 3$	: Parameters describing the shape of the eccentric force-velocity function .
CE	: Contractile element.
cf, df	: Parameters describing force enhancement after stretch.
F	: Muscle force measured or simulated, specified in the text.
F_{CE}	: Force of the CE.
F_{fiber}	: Force along one muscle fiber.
F_{len}	: Force-length property of the CE.
F_m	: Muscle force equals F_{SEE}.
F_{max}	: Maximal isometric force of the muscle.
FTF_{muscle}	: Amount of fast type fibers in the muscle.
F_{vel}	: Force-velocity property of the CE.
K_{PEE}	: Factor describing passive PEE compliance.
K_{SEE}	: Factor describing passive SEE compliance.
L_{CE}	: Length of the CE.
L_{CEopt}	: Optimal length of the CE where the isometric force is maximal.
L_{fiber}	: Length of the muscle fiber.

L_{MTU} : Length of the muscle-tendon-unit.
L_{PEE} : Length of the PEE.
$L_{PEEslack}$: PEE slack-length.
L_{SEE} : Length of the SEE.
$L_{SEEslack}$: SEE slack-length.
MTU : Muscle-tendon-unit.
Pa : Angle of pennation.
$PCSA$: Physiological crossectional area.
PEE : Parallel elastic element.
pot : Force enhancement function after stretch.
SEE : Series elastic element.
sf : Slope factor for eccentric force-velocity curve.
$strain_{PEE}$: Strain in the PEE at maximal isometric force.
$strain_{SEE}$: Strain in the SEE at maximal isometric force.
V_{CE} : Velocity of the CE.
V_{max} : Maximal shortening velocity of the CE.
V_{MTU} : Velocity of the muscle tendon unit.
$width$: Width of the force-length curve.

Appendix B

Active state function

The active state function is given by control nodes j equally spaced in time, with the first and last control node of muscle i having the amplitude $anodes_{ij} = act_0 = 0.005$. The other amplitudes are ranging between act_0 and one. These nodes are connected with sinus functions on the interval $\frac{1}{2}pi$ to $\frac{3}{2}pi$. defined by

$$act_i = as_{ij} * sin(omega_{ij}\,(t - tnodes_{ij}) + phase_{ij}) + bs_{ij} \qquad \text{(B.1)}$$

To make the active state function smother when there are three or more nodes following in time with increasing or decreasing amplitude, the interval of the sinus functions is decreased. The overall active state function with the decreased interval is calculated so that it is still continuous and differentiable. The fortran subroutine 'interpsin' having the time of the nodes as well as the amplitudes stored in the arrays tnodes(i,j) and anodes(i,j) respectively, calculates the parameters as, bs omega and the phase. The function fzero(startval,vv) used is a standard program for finding zeros for a given function (fun(x,vv)) using parameter vv when the starting point (*startval*) is given. The function fzero is not listed here.

```
      subroutine interpsin(i)
c*****************************************************************
c* interpolates active state control nodes with sinus functions
c*****************************************************************
      INTEGER i,j,maxsinp
      DOUBLE PRECISION tges,yd,vv,slope,ydp1,startval,crmin,
     &                 ast,omegat,phaset,cr(maxsinp),pl(maxsinp)
      PARAMETER(crmin = pi/200, startval = pi/4, crconst = 0.2, maxsinp=10)

c set cr and pl to zero
```

```
      DO j = 1,maxsinp
         cr(j) = 0.0d0
         pl(j) = 0.0d0
      END DO
      tges = tnodes(i,2)-tnodes(i,1)

C build cr so that there is a solution for pl in the range [0..pi]

      DO j = 1,(np(i)-2)
        if ((anodes(i,j) .LT. anodes(i,j+1))
     &      .AND. (anodes(i,j+1) .LT. anodes(i,j+2)) ) then
            cr(j) = crconst
        elseif ((anodes(i,j).GT.anodes(i,j+1))
     &      .AND. (anodes(i,j+1).GT.anodes(i,j+2)) ) then
            cr(j) = crconst
        else
            cr(j) = 0.0d0
        endif

        if (cr(j).NE. 0.0d0) then

c slope next section

          ydp1 =(anodes(i,j+2)-anodes(i,j+1))/tges
          DO
             omegat = pi/(tges*(1.0d0+cr(j)))
             phaset = halfpi
             ast = (anodes(i,j)-anodes(i,j+1))/
     &            (1.0d0-dcos(omegat*tges))
             yd = ast * dcos(omegat*tges + phaset) * omegat
             if (dabs(yd).LT.dabs(ydp1)) exit
             cr(j) = cr(j) - crmin
             if (cr(j) .LT. crmin) then
                cr(j) = 0.0d0
                exit
             endif
          END DO
        endif
      END DO

C as,bs,omega,phase:
```

```
       phase(i,1) = halfpi
       omega(i,1) = pi/(tges*(1.0d0+cr(1)))
       as(i,1) = (anodes(i,1)-anodes(i,2))/
      &          (1.0d0- dcos(omega(i,1)*tges))
       bs(i,1) = anodes(i,1) - as(i,1)

       DO j = 2,np(i)-1
         if (cr(j-1).EQ.0.0d0) then
            pl(j)= 0.0d0
         else
            slope = as(i,j-1) * dcos( omega(i,j-1)*tges + phase(i,j-1) )
      &             * omega(i,j-1)
            vv = (anodes(i,j)-anodes(i,j+1))/(slope*tges)
            pl(j) = fzero(startval,vv)

            if (cr(j).NE. 0.0d0) then

c slope next section

              ydp1 = (anodes(i,j+2)-anodes(i,j+1))/tges

              DO
               omegat = (pi-pl(j))/(tges*(1.0d0+cr(j)))
               phaset = halfpi + pl(j)
               ast = (anodes(i,j)-anodes(i,j+1))/( dsin(phaset)
      &               - dsin(omegat*tges + phaset) )
               yd = ast * dcos(omegat*tges + phaset) * omegat

               if (dabs(yd).LT.dabs(ydp1)) exit

               cr(j) = cr(j) - crmin

               if (cr(j) .LT. crmin) then
                  cr(j) = 0.0d0
                  exit
               endif
              END DO
           endif
         endif

C calculate curve parameters

         omega(i,j) = (pi-pl(j))/(tges*(1.0d0+cr(j)))
```

```
        phase(i,j) = halfpi + pl(j)
        as(i,j) = (anodes(i,j)-anodes(i,j+1))/( dsin(phase(i,j))
     &            - dsin(omega(i,j)*tges + phase(i,j)))
        bs(i,j) = anodes(i,j) - as(i,j)*dsin(phase(i,j))

      END DO
      return
      end
c*********************************************************************

      DOUBLE PRECISION function fun(x,vv)
c*********************************************************************
c* PURPOSE: defines function used in fzero
c*********************************************************************
      DOUBLE PRECISION x,vs

      fun= vv * (pi-x) * dcos(halfpi+x) - dcos(x)-  1.0d0

      return
      end
c*********************************************************************
```

Appendix C

State equation

To actually calculate the muscle force the state equation 3.32 has to be solved. To obtain the state equation eq. 3.20 has to be resolved for V_{CE}. The state function is then not continuous at high eccentric velocities. To avoid numerical difficulties, the eccentric function 3.12 increases linearly with the slope ($slopelin = -10$) for eccentric forces $F_{CErel} = F_{CE}/F_{max}$ higher than F_{lin}

$$F_{lin} = F_{len}\,(-\sqrt{((-c1 - c2 * c3)/(slope_{lin}\,F_{len})} - c2). \tag{C.1}$$

The threshold F_{lin} is defined so that the state function is continuous and differentiable. The state equation is then defined for different situations depending on the contractile velocity of the muscle associated with a certain muscle force.

Concentric hyperbolic part ($F_{CErel} \leq F_{len}\,act$):

$$V_{CE} = b\,\frac{act - F_{CErel}/F_{len}}{F_{CErel}/F_{len} + a}. \tag{C.2}$$

Eccentric hyperbolic part ($F_{CErel} > F_{len}\,act$) and ($F_{CErel} \leq F_{lin}$):

$$V_{CE} = \frac{c1 - c3 * F_{CErel}/F_{len}}{F_{CErel}/F_{len} + c2}. \tag{C.3}$$

Eccentric linear part ($F_{CErel} > F_{len}\,act$) and ($F_{CErel} > F_{lin}$):

$$V_{CE} = slope_{lin}\,(F_{CErel} - F_{lin}) + (c1 - c3\,\frac{F_{lin}/F_{len}}{F_{lin}/F_{len} + c2}). \tag{C.4}$$

F_{len} is given by eq. 3.5 and F_{CE} is calculated from

$$F_{CE} = F_{SEE} - F_{PEE} \tag{C.5}$$

with F_{SEE} and F_{PEE} defined by eq. 3.24 and 3.22 respectively. Due to simplicity force enhancement due to stretch is not considered in the state equation but can be included by replacing F_{len} by $F_{len}(1 + pot)$.

Bibliography

[1] P. Aerts and D. de Clercq, *Deformation characteristics of the heel region of the shod foot during simulated heel strike: The effect of varying midsole hardness*, J. Biomech. **11** (1993), 449–461.

[2] F. C. Anderson and M. G. Pandy, *Storage and utilization of elastic strain energy during jumping*, J. Biomech. **26** (1993), 1413–1427.

[3] D. Arampatzis, F. Schade, M. Walsh, and G. P. Brüggemann, *Influence of leg stiffness and its effect on myodynamic jumping performance*, J. of Electromyography and Kinesiology **11** (2001), 355–364.

[4] E. Asmussen and F. Bonde-Petersen, *Storage of elastic energy in sceletal muscles in man*, Acta Physiologica Scandinavica **92** (1974), 385–392.

[5] A. S. Bahler, *The series elastic element of mammalian skeletal muscle*, American J. Physiol. **213** (1967), 1560–1564.

[6] A. A. Biewener, W. R. Corning, and B.W. Tobalske, *In vivo pectoralis muscle force-length behavior during level flight in pigeons*, J. Exp. Biol. **201** (1998), 3293–3307.

[7] M. F. Bobbert, G. C. Ettema, and P. A. Huijing, *The force-length relationship of a muscle tendon complex experimental results and model calculations*, American J. Physiol. **213** (1990), 1560–1564.

[8] M. F. Bobbert, P. A. Huijing, and G. J. van Ingen Schenau, *An estimation of power output and work done by the human triceps surae muscle-tendon complex in jumping*, J. Biomech. **19** (1986), 899–906.

[9] _____, *Drop jumping. II. the influence of dropping height on the biomechanics of drop jumping*, Med. Sci. in Sports and Exerc. **19** (1987), 339–346.

[10] M. F. Bobbert and G. J. van Ingen Schenau, *Mechanical output about the ankle joint in isokinetic plantar flexion and jumping*, Med. Sci. in Sports and Exerc. **22** (1989), 660–668.

[11] H. Böhm, *Dynamik der Riesenfelge am Reck im Rahmen von Mehrkoerpersystemen*, Master's thesis, University of Tübingen, 1997.

[12] C. Bosco and P. V. Komi, *Potentiation of the mechanical behavior of human skeletal muscle through prestretching*, Acta Physiologica Scandinavica **106** (1979), 467–472.

[13] G. A. Cavagna, B. Dusman, and R. Margaria, *Positive work done by a previously stretched muscle*, J. Appl. Physiol. **24** (1968), 21–32.

[14] P. R. Cavanagh and P. V. Komi, *Electromechanical delay in human sceletal muscle under concentric and eccentric contractions*, Eur. J. Appl. Physiol. **45** (1979), 159–163.

[15] J. W. Chow and W. G. Darling, *The maximum shortening velocity of muscle should be scaled with activation*, J. Appl. Physiol. **11** (1999), 1–24.

[16] R. Close, *Dynamic properties of fast and slow skeletal musclesof the rat during development*, J. Physiol. **173** (1964), 74–95.

[17] _____, *Force-velocity properties of mouse muscle*, Nature **206** (1965), 718–719.

[18] C. S. Cook and M. J. N. McDonach, *Force responses to controlled stretches of electrically stimulated human muscle-tendon complex*, exp. Physiol. **80** (1995), 447–490.

[19] A. Corana, M. Marchesi, C. Martini, and S. Ridella, *Minimizing multimodal functions of continuous variables with the simulated annealing algorithm*, ACM Trans. Math. Software. **13** (1987), 262–280.

[20] R. D. Crowninshield, *Use of optimization techniques to predict muscle forces*, J. Biomech. Eng. **100** (1978), 88–92.

[21] S. L. Delp, *Surgery simulation: A computer graphics system to analyse and design musculosceletal reconstructions of the lower limb*, Ph.D. thesis, Stanford University, Department of Mechanical Engineering, 1990.

[22] S. Ebashi and M. Endo, *Calcium ion and molecular contraction*, Progr. Biophys. Mol. Biol. **18** (1968), 125–183.

[23] R. M. Enoka, *Neuromechanical basis of kinesiology*, Human Kinetics, Leeds, England, 1988.

[24] M. Epstein and W. Herzog, *Theoretical models of sceletal muscle*, Wiley, New York, 1998.

[25] G. J. C. Ettema and P. A. Huijing, *Properties of the tendinous structures and series elastic component of edl muscle-tendon complex of the rat*, J. Biomech. **22** (1989), 1209–1215.

[26] J.A Faulkner, D.R. Claflin, and K.K. McCully, *Power autput of fast and slow fibers from human skeletal muscles*, in Human Muscle Power **Human Kinetics Publisher** (1986), 81–94.

[27] J. A. Friedrich and R. A. Brand, *Muscle fiber architecture in the human lower limb*, J. Biomech **23** (1990), 91–95.

[28] S. Fukashiro, P. V. Komi, and M. Järvinen, *In vivo achilles tendon loading during jumping in humans*, Eur. J. Appl. Physiol. **71** (1995), 453–458.

[29] S. Fukashiro, M.Itoh, Y. Ichinose, Y. Kawakami, and T. Fukanaga, *Ultrasonography gives directly but noninvasively elastic characteristic of human tendon in vivo*, Eur. J. Appl. Physiol. **11** (1995), 1–24.

[30] K. Gerritsen, *Computer Simulation of FES-Assisted Locomotion*, Ph.D. thesis, University of Calgary, Calgary, Canada, 1997.

[31] G. L. Gottlieb and G. C. Agarwal, *Dynamic relationship between isometric muscle tension and the electromyogram in man*, J. Appl. Physiol. **3** (1971), 345–351.

[32] K. Gruber, H. Ruder, J. Denoth, and K. Schneider, *A comparative study of impact dynamics: wobbling mass versus rigid body models*, J. Biomech. **31** (1998), 439–444.

[33] R. W. Guelch, P. Fuchs, A. Geist, M. Eisold, and H. C. Heitkamp, *Eccentric and posteccentric contractile behavious of sceletal muscle: a comparative study in frog single fibres and in humans*, Eur. J. Appl. Physiol. **63** (1991), 323–329.

[34] H. Hatze, *Myocybernetic control models of sceletal muscle*, University of South Africa Press, Pretoria, 1998.

[35] W. Herzog, W. leonard, T. R. Renaud, J. M. Wallace, and J. Chaki, *Force-length properties and functional demands of cat gastrocnemius soleus and plantaris muscle*, J. Biomech. **25** (1992), 1329–1335.

[36] W. Herzog, L. J. Read, and H. E. D. J. ter Keurs, *Experimental determination of force-length relations of intact human gastrocnemius muscles*, Clin. Biomech. **6** (1991), 230–238.

[37] W. Herzog and H. E. D. J. ter Keurs, *Force-length relation of in vivo human rectus femoris muscles*, Eur. J. Physiol. **411** (1988), 642–647.

[38] A. V. Hill, *The heat of shortening and the dynamic constants of muscle*, Proc. R. Soc. London **126** (1938), 136–195.

[39] _____, *The series elastic component of muscle*, Proc. R. Soc. London **Ser. B 137** (1950), 273–280.

[40] A. L. Hof, *In vivo measurement of the elasticity release curve of human triceps surae muscle*, J. Biomech. **31** (1998), 793–800.

[41] P. A. Huijing, *Muscle as a collagen fiber reinforced composite: a review of force transmission in muscle and whole limb*, J. Biomech. **32** (1999), 329–345.

[42] B. Katz, *The relation between force and speed in muscular contraction*, J. Physiol. **96** (1939), 45–64.

[43] Y. Kawakami and R. L. Lieber, *Interaction between series compliance and sarcomere kinetics determines internal sarcomere shortening during fixed-end contraction*, J. Biomech. **33** (2000), 1249–1255.

[44] P. V. Komi and C. Bosco, *Utilization of stored elastic energy in leg extensor muscles by men and woman*, Med. Sci. in Sport and Exerc. **10** (1978), 261–265.

[45] S. Kurokawa, T. Funkunaga, and S. Fukashiro, *Behavior of fascicles and tendinous structures of human gastrocnemius during vertical jumping*, J. Appl Physiol. **90** (2001), 1349–1358.

[46] O. Lindahl, A. Movin, and I. Ringquist, *Knee extension*, Acta orthop. Scandinav. **40** (1969), 79–85.

[47] V. Lombardi and G. Piazzesi, *Muscular contraction*, vol. 313, ch. Force response in steady lengthening of active single muscle fibres, pp. 237–255, Cambridge University press, Cambridge and New York, 1992.

[48] A.R. Luff, *Dynamic properties of the inferior rectus, extensor digitorum longus, diphragm and soleus muscle of the mouse*, J. Physiol **313** (1981), 161–171.

[49] B. R. MacIntosh, W. Herzog, E. Suther, P. Wiley, and J. Sokolosky, *Human skeletal muscle fibre types and force: velocity properties*, Eur. J. Appl. Physiol. **67** (1993), 499–506.

[50] C. N. Maganaris and J. P. Paul, *In vivo human tendon mechanical properties*, J. Physiol. **521.1** (1999), 307–313.

[51] S. P. Magnusson, P. Aagaard, S. Rosager, and P. D. Poulsen, *Load displacement properties of the human triceps surae aponeuroseis in vivo*, J. Physiol. **531.1** (2001), 277–288.

[52] R. Margaria, *Biomechanics and energetics of muscular excercise*, Clarendon, Oxford, 1976.

[53] NASA Reference Publication, *Anthropometric Source Book*, Tech. Report 1024, NASA Scientific and Technical Information Office, Springfield, 1978.

[54] G. Nemeth, *In vivo moment arm lengths for hip extensor muscles at different angles of hip flexion*, J. Biomech. **18** (1985), 129–140.

[55] G. Nemeth, U.Arborelius, K. Ringdahl, and K. Schueldt, *Influence of knee flexion on isometric hip extension strength*, Scand. J. Rehab. Med. **15** (1983), 97–101.

[56] R. R. Neptune, *Optimization algorithm performance in determining optimal control in human movement analysis*, J. Biomech. Eng. **121** (1985), 249–252.

[57] S. J. Olney and D. A. Winter, *Predictions of knee and ankle moments of force in walking from emg and kinematic data*, J. Biomech. **18** (1985), 9–20.

[58] M. G. Pandy, F. E. Zajac, E. Sim, and W.S. Levine, *An optimal control model for maximum height human jumping*, J. Biomech. **23** (1990), 1185–1198.

[59] K. W. Ranatunga, *Temperature dependence of shortening velocity and rate of isometric tension development in rat skeletal muscle*, J. Physiol. **329** (1981), 465–483.

[60] K. Roeleveld, R.V. Baratta, M. Solomonow, A. G. van Soest, and P.A. Huijing, *Role of tendon properties on the dynamic performance of different isometric muscles*, The American Physiological Society (1993), 1348–1355.

[61] S. G. Rugg, R. J. Gregor, B. R. Mandelbaum, and L. Chius, *In vivo moment arm calculations at the ankle using mri*, J. Biomech. **23** (1990), 495–501.

[62] D. Sale, J. Quinlan, E. Marsh, and A. J. McComas, *Influence of joint positions on ankle plantarflexion in humans*, J. Appl. Physiol. **52** (1982), 1636–1642.

[63] H. Schechtman and D. L. Bader, *In vitro fatigue of human tendons*, J. Biomech. **30** (1997), 829–835.

[64] G. J. Schenau, M. F. Bobbert, and A. Haan, *Does ellastic energy enhance work and efficiency in the stretch shortening cycle*, J. Appl. Biomech **13** (1997), 389–415.

[65] G. L. Smidt, *Biomechanical analysis of knee flexion and extension*, J. Biomech. **6** (1973), 79–92.

[66] C. W. Smith, I. S. Young, and J. N. Kearney, *Mechanical properties of tendons: changes with sterilization and preservation*, J. Biomech. Eng. **118** (1996), 56–60.

[67] K. Sogaard, *Motor unit activation patterns during concentric wrist flexion in humans with different muscle fibre composition*, Eur. J. Appl. Physiol. 78 (1998), 411–416.

[68] C. W. Spoor and J. L. Van Leeuwen, *Knee muscle moment arms from mri and from tendon travel*, J. Biomech. **25** (1992), 201–206.

[69] E. Suter, W. Herzog, J. Solosky, J. P. Wiley, and B. R. MacIntosh, *Muscle fiber type distribution as estimated by cybex testing and by muscle biopsy*, Med. Sci. Sport. Exerc. **25** (1993), 363–370.

[70] H. E. D. J. ter Keurs, T. Iwazumi, and G. H. Pollak, *The sarcomere length-tension relation in skeletal muscle*, J. Gen. Physiol. **72** (1978), 565–592.

[71] J. Tihanyi, P. Apor, and G. Y. Fekete, *Force-velocity-power characteristics and fiber composition in human knee extensor muscles*, Eur. J. Appl. Physiol. **82** (1982), 331–348.

[72] T. M. G. J. van Eijden, W. A. Weijs, and J. Verburg, *Forces acting on the patella during maximal voluntary contraction of the quadiceps femoris muscle at different knee flexion / extension angles*, Acta Anat. **129** (1987), 310–314.

[73] A. G. van Soest, *Jumping from structure to control. a simulation study of explosive movements*, Ph.D. thesis, Vrije Universiteit, Amsterdam, Netherlands, 1992.

[74] A. G. van Soest and M. F. Bobbert, *The contribution of muscle properties in the control of explosive movements*, Biol. Cybern. **69** (1993), 195–204.

[75] J. J. Visser, J. E. Hoogkamer, M. F. Bobbert, and P. A. Huijing, *Length and moment arm of human leg muscles as a function of knee and hip-joint angles*, Eur. J. Appl. Physiol. **61** (1990), 453–460.

[76] R. L. Waters, J. Perry, J. M. McDaniels, and K. House, *The relative strength of the hamstrings during hip extension*, J. of Bone and Joint Surgery **56-A** (1974), 1592–1597.

[77] D. R. Wilkie, *Muscle, Studies in Biology, No. 11*, Edward Arnold, London, 1988.

[78] J. M. Winters and S. L. Y. Woo, *Biomechanics and movement organisation*, Springer-Verlag, New York, 1990.

[79] S. L. Y. Woo, *Mechanical properties of tendons and ligaments*, Biorheology **19** (1982), 385–396.

[80] I. C. Wright, R. R. Neptune, A. J. van den Bogert, and B. M. Nigg, *Passive regulation of impact forces in heel-toe running*, Clin. Biomech. **13** (1998), 521–531.

[81] J. A. Zagzebski, *Essentials of ultrasound physics*, Mosby, St. Louis, Missouri, 1997.